POLITECNICO DI TORINO

Corso di Laurea in Ingegneria Biomedica

Tesi di Laurea Magistrale

Quantification and reduction of crosstalk in the electromyograms of flexor carpi radialis and pronator teres

Relatore:
Prof. Luca Mesin

Candidato:
Matteo Raggi

Correlatore:
Prof. Gennaro Boccia

Luglio 2022

Ai miei Nonni

Contents

List of Figures

Chapter 1

Introduction to Muscular System

Human body is a complex system capable of making several movements, from walking to dancing. All are the result of interaction and coordination of many biological systems, one of them is the muscular system. In this chapter will be described how muscles are is made up and their interaction with the nervous system, mainly referring to [1, 2].

1.1 Structure and physiology

Muscles are made up of fibres, containing thousands of individual contracting units, named *sarcomeres*. Those structures, delimited by Z lines, are contained into a cylinder called *myofibril*, while a membrane, known as *sarcolemma*, surrounds groups of myofibrils. In Fig. 1.1 it is possible to appreciate a graphical representation of the previous description.

More specifically, in the sarcomere there are two contractile proteins that play an important role in this muscular contraction: *actin* and *myosin* (see Fig. 1.2). The first is attached to the Z lines, whereas the latter is placed in the centre of sarcomere. Their interaction produces the muscle contraction according to *sliding filament theory*, for which bridges on the myosin pull actin filaments toward the centre, thus making sarcomere shorter. In the actin filaments there are two inhibitory proteins: *troponin* and *tropomyosin*, whose role is to prevent the sliding movement when the muscle is not contracted. In this system, ions calcium (Ca^{2+}) are fundamentals, indeed, without them it is not possible to produce a muscular contraction. When the concentration of calcium ions in the cytoplasm of muscle fibre changes, because of a stimulus, other Ca^{2+} are released by the *sarcoplasmic reticulum*, a structure that surrounds the sarcomere, according to *calcium induced calcium release mechanism* (CICR) [3]. By doing so, the contraction of a muscle can be obtained.

Muscles are not stand alone entities, they are connected to the nervous central

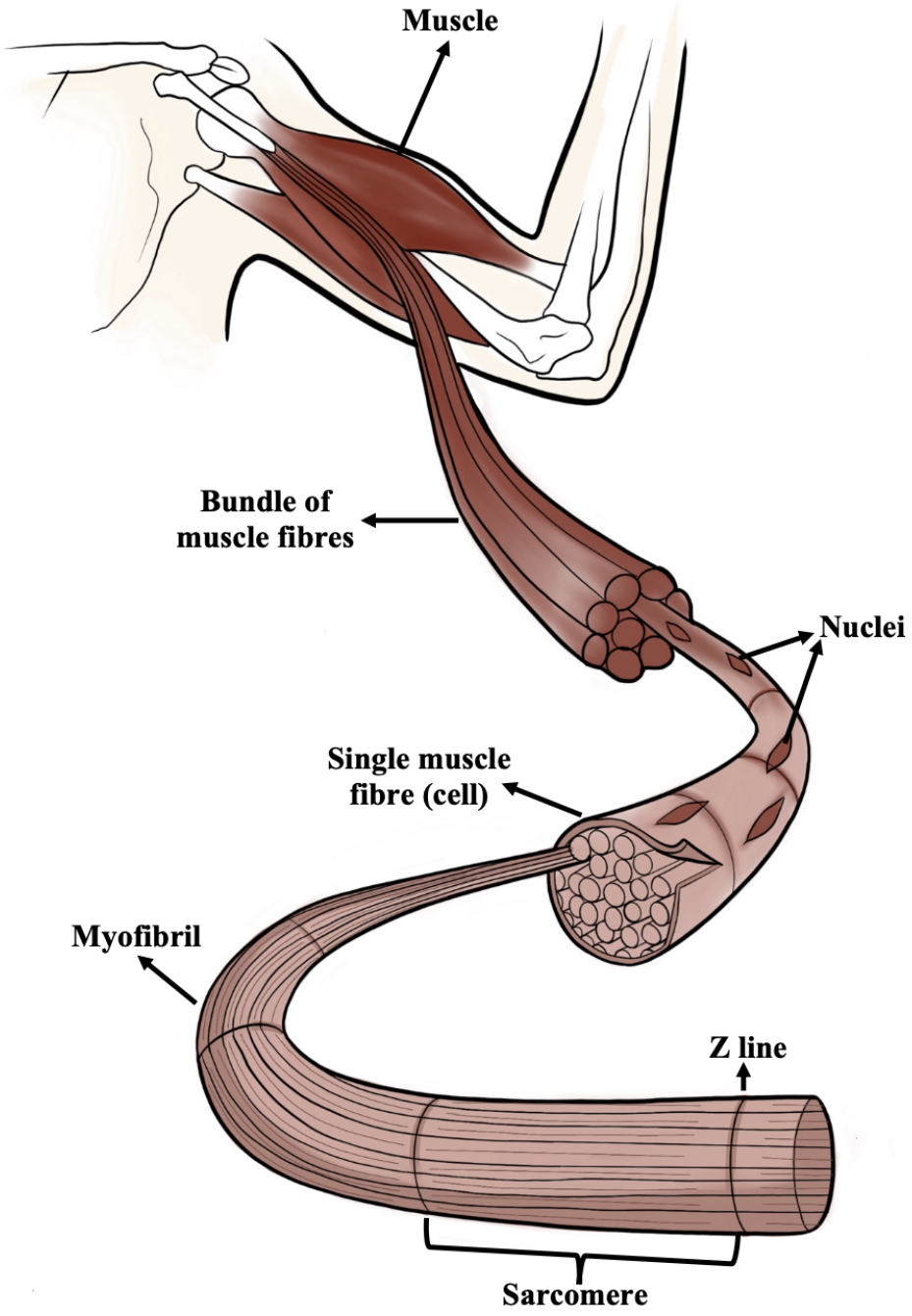

Figure 1.1: *Structure of a striated muscle at different dimensional scales: from the muscle to myofibrils.*

system (NCS) through *efferent* and *afferent* pathways. More specifically, the first pathway carries information for a command to be executed and exit from ventral horn of the spinal cord, while the other, originated in the dorsal horn of the spinal cord, provide sensed information, so that fine tuning of a specific movement could be achieved. Therefore, the control of a muscles is obtained through neurons, called *motor neurons*. In couple with interneurons, entities that enable the communications between sensing and motor neurons, provide the *reflex response*: a phenomena does not requires a complex process in the brain, being elaborated in the spinal cord.

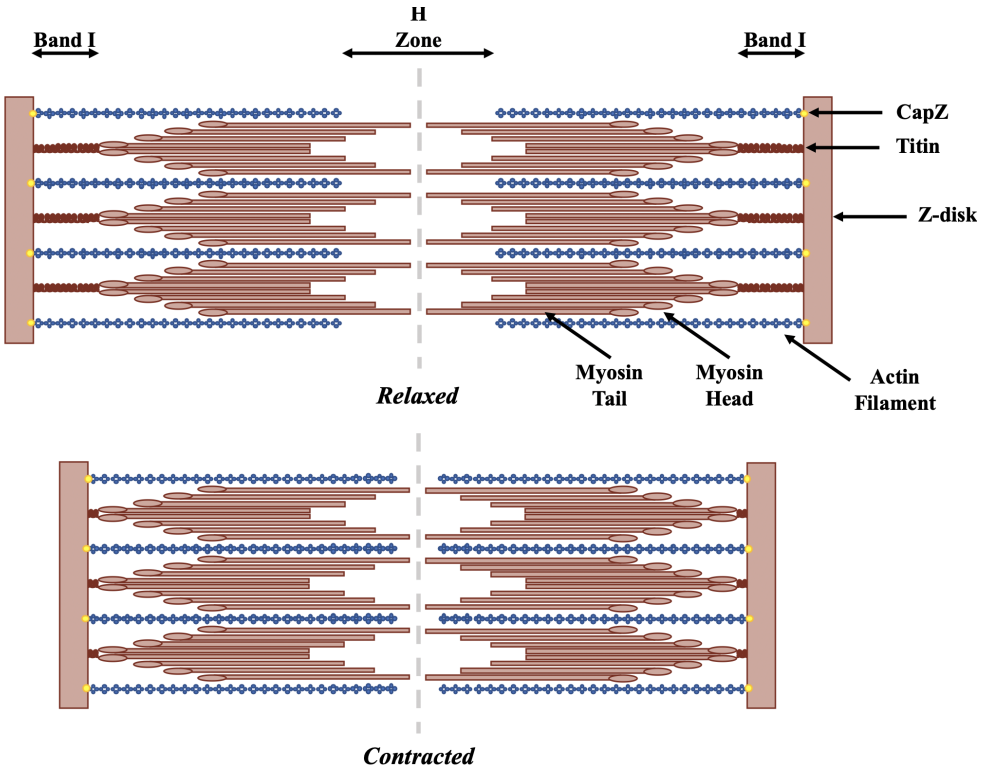

Figure 1.2: *Scheme of sarcomere's structure in two conditions: relaxed (top) and contracted (bottom).*

A muscle reflex is obtained if an external stimulus is provided. Specific sensor detect them and send informations to an integration module, in the form of electrical signals, through afferent pathways. Those signals are elaborated and the produced response is then sent to the effector through efferent pathways (motoneurons). More specifically, motor neurons α send efferent stimuli to muscles and simulate the Renshaw cells, which provide a negative feedback, so that a tune in the muscle contraction can be archived. The sensors cited before belong to the group of *sensory receptors* that are connected to nervous system through sensory neurons. They are localized in different zones of the muscular system, such as skeletal muscles,

ligament and joint capsules.

Muscles have their own system of proprioception, defined as the sense of relative position of body segments in the space and strength of the efforts. This system is made up of three components: the *muscle spindles*, that measure the contraction velocity, the *Golgi tendon organs* (GTO), which detects the strain and force produced by the muscles, and the capsule in joints. The afferent nerves recruited for the previous quantifications are: type *Ia*, for the velocity measure, type *II*, for the sense of position and type *Ib* for muscle tension.

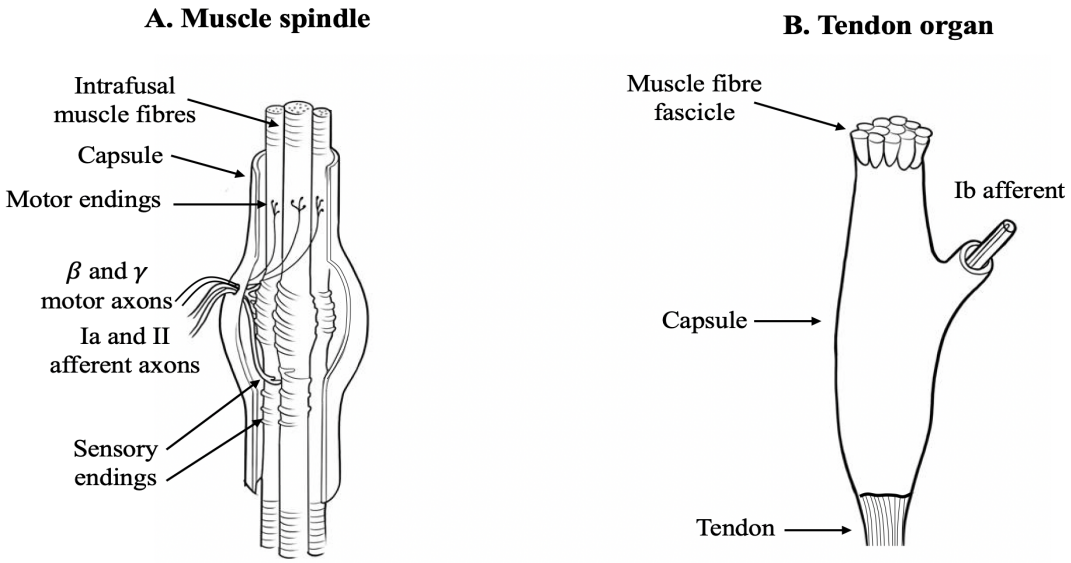

Figure 1.3: *Anatomy of muscle spindle and Golgi tendon organ.*

As showed in Fig. 1.3 A, muscle spindles are place anatomically in within the muscle, parallel to their fibres. Tension is controlled by the γ efferent, that are motor neurons γ with a smaller diameter an higher threshold of activation rather than α motor neurons. When a muscle stretches, an elongation of those sensors occurs, determining an excitatory feedback to α motor neurons of agonist muscle and an inhibitory stimulus to the antagonist. Changes in stretch and velocity of contraction are reflected on a different firing rate of *Ia* afferent nerve fibres. The Golgi tendon organ, is involved in the measure of force. It is coated by capsules of connective tissue and it is placed anatomically between the muscle fibre fascicle and the tendon, as reported in Fig. 1.3 B. Type *Ib* provides the connection with NCS, while through *Ib* interneurons is possible to inhibit the activity of α motor neurons.

In rest condition, the sarcolemma is polarized, which means that there are different electrical charges between cytoplasm and the external environment. This

difference is due to sodium (Na^+) and potassium (K^+) ions. In rest conditions, sodium is mainly concentrated outside the fibres, while potassium inside. Because of the different concentrations, sodium ions tend to diffuse into the fibres and potassium in the opposite direction. In this condition the resting potential can be obtained as the weighted average of the Nerst potential of the ions inside and outside the membrane, with weight depending on their permeabilities. Indeed, under the assumption of a linear model for the channels, the reversal voltage can be obtained as

$$V_r = \frac{g_{Na} V_{Na} + g_k V_k}{g_{Na} + g_K} \tag{1}$$

where g_{Na} and g_K are the permeabilities of sodium and potassium and V_{Na} with V_K are the Nerst potentials of sodium and potassium, respectively. Moreover, sodium and potassium channels are voltage-depend, so their permeability to the respective ions changes with the membrane potential.

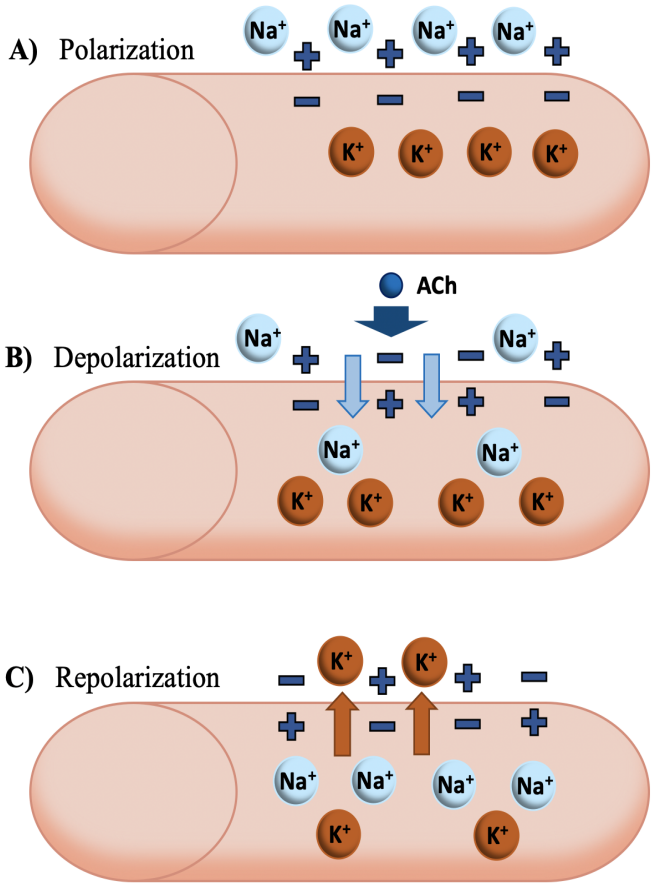

Figure 1.4: *Polarization, depolarization and repolarization phases.*

When a nervous impulse reaches a neuromuscular joint, defined as point of contact between the axon terminal and the fibres that it innervates, *acetylcholine* (Ach) is released in the small space between them, known as *synaptic cleft*. The result is a change of permeability to (Na^+) ions in sarcolemma, which rapidly enter into the cells changing their membrane potential from -70 up to +40 mV. This phenomena is known as *depolarization*, at which follows a change in the permeability of cell membranes to (K^+), enabling the exit of those ions from inner (*repolarization*). Because of the different activation kinetics of sodium and potassium channels, the number of outgoing (K^+) ions is higher than entering (Na^+) ions, so a *hyper-polarization* of the membrane occurs. During this phase, the potential is more negative than the one measured before neural stimuli and will return to the potential in rest condition slowly.

The sequence of depolarization, repolarization and hyper-polarization defines the three main phases of the *action potential* (AP), a electrical signal that propagates through sarcolemma to tendons, where it extinguishes. In depolarization phase there is an "all or nothing" mechanism, so if the neural stimulus exceed a threshold of activation, at approximately -55 mV, an AP is generated and propagates. In order to obtain a propagating wave an adequate ions concentration is fundamental. Indeed, the proper ions distribution is kept by the sodium-potassium pump, consuming adenosine triphosphate (ATP).

Since sodium channels can have three different states (active, inactive and close) while potassium channels only two (active or close), a new action potential can be summed to others if the stimulus occurs during the *relative refractory period*, an interval of time in which the sodium channels are inactivated, but can be activated if the stimulus has enough energy. On the other hand, during the *absolute refractory period* sodium channels are closed, so the action potential can not be generated.

1.2 Motor units

The combination of a motor neuron and the muscular fibres at which it is attached is known as *motor unit* (MU), that is the minimal functional unit of neuromuscular system.

The manner in which MU are recruited depends on two factors: *spatial* and *temporal* recruitment. The first defines the order in which MU are activated: from small to big ones, following the Henneman principle [4][5]. Especially, each MU has a threshold, expressed as level of force, above which it is recruited and then activated to contrast the external load. This phenomena can be simulated with an exponential distribution of the thresholds (expressed in percentage of the maximal voluntary contraction (MVC)), with several small MU activated at low levels of force and few lager MU recruited at higher thresholds [6].

On the other hand, temporal recruitment defines how a specific MU fires when

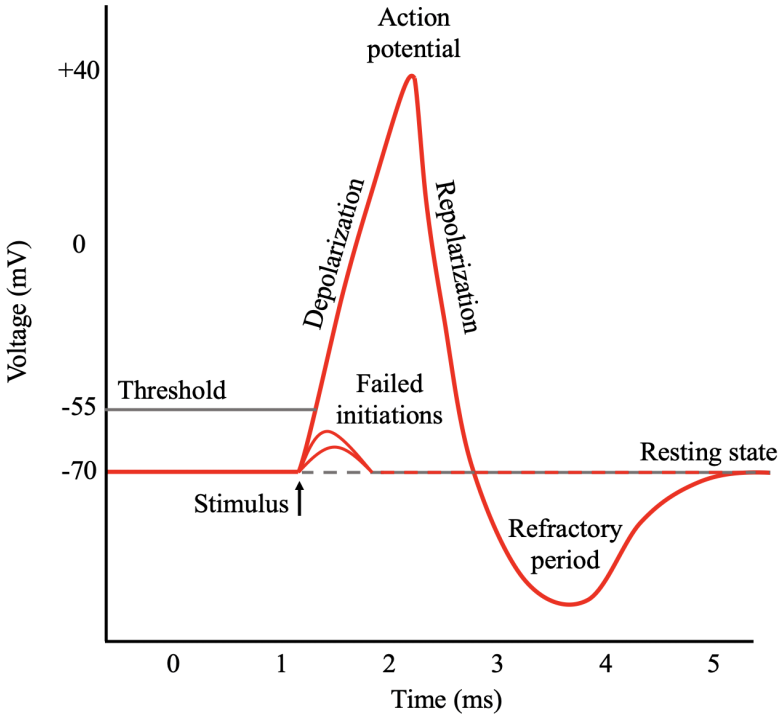

Figure 1.5: *Phases of the action potential and voltage (mV) reached.*

its recruitment threshold is reached. Indeed, MU start firing at a low firing rate, that raises if the force level is increases until its maximum firing rate is reached. That pattern is not regular, indeed, there is a random variability of delays between the impulsed observed [7].

The MU's firing rate plays an important role in force production, indeed, if the discharge rate raises, the force generated increases. This phenomena is due to the twitch of muscle fibres, which duration is longer than the single AP. For this reason, even though there is no AP superimposing of the same MU, forces twitches could be summed. This event, obtained only if the firing frequency of a MU is higher enough to stimulate muscle fibres, produces a *tetanic contraction*, which results in a great amount of tension.

In addition, is fundament to distinguish two type of contraction: *unfused* and *fused* tetanus. The difference between them depends on the firing rate of the MU, indeed, if the maximum firing rate is reached, a fused tetanus is obtained, if not the result is unfused tetanus, as reported in Fig. 1.6.

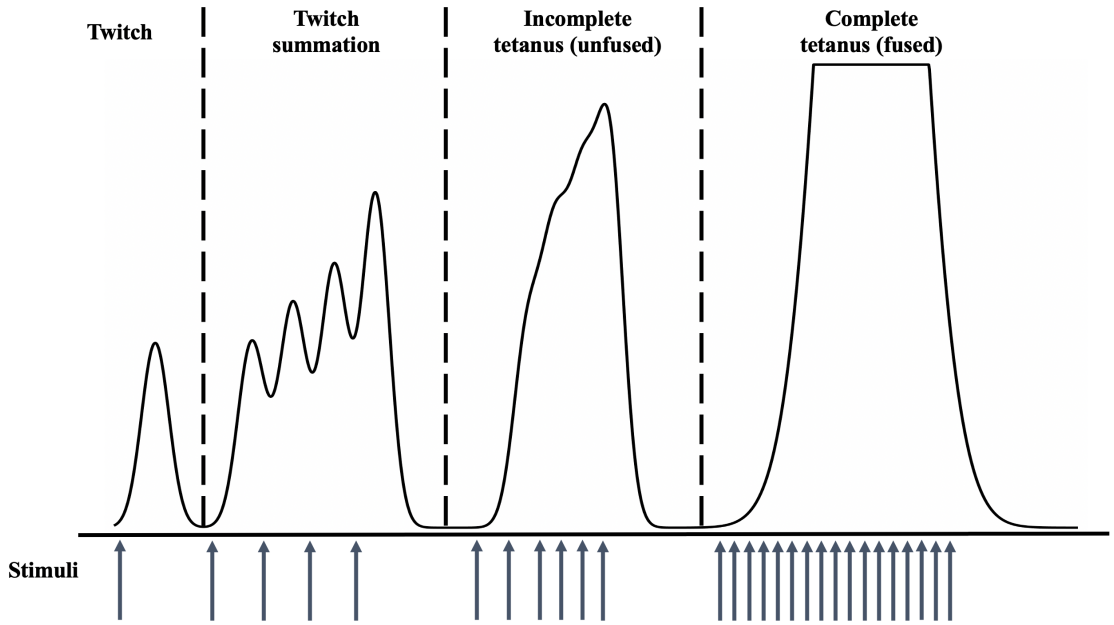

Figure 1.6: *Force produced at different firing rates: from single twitch to fused tetanus contraction.*

1.3 Muscular fibres

Muscular fibres can be distinguished three categories: *I*, *IIa* and *IIb*. Type *I*, also know as red fibres, are slow, resistant and have an aerobic metabolism. Type *IIb*, also know as white fibres, are fast and have a glycolytic metabolism. Type *IIa* have an intermediate behaviour between fast and slow, being resistant and fast. The sources of energy used for the two metabolisms are triglycerides and glycogen, respectively. Each human being has a different amount ot those fibres, indeed, who has a huge number of type I fibres is genetically compatible to endurance sport such as long-distance running. On the other hand, subjects with a great number of type *IIb* fibres, could be a good athlete in sport where is required an high amount of energy in a rapid period of time, for example weightlifting. Moreover, type *IIa* fibres can be converted into *I* or *IIb* type with training [8].

In addition, muscle fibres orientation determinate differences in terms of force production an speed of contraction. Muscles with parallel fibres, for example the biceps, have more sarcomeres in series, so they can contract their fibres more quickly, but the produced force is limited. On the other hand, pennate muscles, for example the gastrocnemius, are designed for strength, but their fibre contraction is lower than parallel fibres muscles [9].

1.4 Role of muscles

In human body there are more then 600 muscles, most attached to the bones. They can be classified in two main categories: *smooth* or *striated*. Smooth muscles are involved into involuntary functions, such as: breathing or blood pumping into the arterial system, the latter includes muscles that can be activated voluntary by the subject, producing, for example, the motion of a specific segment of the body through generation of tension. More specifically, striated muscles can produce different types of contractions. If during the phase of shortening a constant tension is produced, an *isotonic* contraction is obtained. If a muscle keeps its length during the production of tension, the result is an *isometric* contraction. In addition, if a muscle has been contracted keeping a constant speed an *isokinetic* contraction occurs.

In body segments motion, an important roles is played by *joints*, which enable the relative movement of bones and keep their surfaces in contact. In the following discussion joints and their classifications will not be treated, however a brief classification of the muscles involved in those bio-mechanical structures will be presented. Indeed, in order to control the movement of a joint at least two muscles are present:

- *Agonist*: the muscle that contrast the external load,
- *Antagonist*: a muscle that with its shortening opposes the agonist contraction, providing modulation.

An example of agonist and antagonist muscles could be biceps brachii and triceps. In addition to the previous classification, a more detailed muscles distinction can be reported [10]. Indeed, there are also

- *Synergist muscles*: not mainly involved in the movement of a body segment, but collaborate with the agonists,
- *Fixator muscles*: which contraction, stabilize one part of the body during movement of another,
- *Neutralizer muscles*: whose contraction neutralize the action of agonist that is anatomically connected to different joints. Without their activation the movement of another body segments could occur.

Chapter 2

Electromyogram

The propagation of each AP from IZ to tendons generates currents in the surrounding tissues with electrical conductive properties, determining a potential that could be recorded through electrodes, producing the electromyogram (EMG). The previous signal could be obtained into two conditions: *invasive* or *non-invasive*. The first uses electrodes placed on the skin, while in the latter needle electrodes. Since in this thesis project the surface EMG is has been studied, from now on, it will be simply referred to EMG.

The EMG signal is used in several applications: from research to medical purpose, for example in study gait analysis [11]. Indeed, in order to detect a walk disorder, is fundamental to know how much a specific muscle is involved and when it is activated during phases of gait cycle [12]. So, with electromyogram, is possible to collect all those information with a unique signal.

In this chapter a brief introduction to electromyography will be provided, including a presentation of the main indexes obtained from EMG recording used in the biomedical signal processing and clinics fields. The main source used are [13, 14].

2.1 Electrodes and skin

In order to record the EMG signal is necessary to use electrodes. Nowadays, several types of them are available, mainly classified in two categories: invasive and non-invasive. The first can detect the activity of a small number of motor units (MUs) close to tip's sensor. The detection volume is really small, in the order of 1-2 mm^3, so is possible to study small MUs and their internal structure. The potential recorded has a range of 0.1-5 mV and a frequency band of 0-10 kHz. The other electrodes, used in the non-invasive recording, are commonly made of Ag-AgCl and are placed on skin's subject. The signal produced has a range of 50-3000 μV and frequency band of 0.1-350 Hz.

The interaction between skin and electrodes is intricate. Indeed, two systems

with different conductivity are interfaced: the skin, fairly conductive, and the electrode, made of metal, a conductive material by definition. In order to reduce those differences a conductive gel is used before placing the electrodes. Metallic materials have electrons weakly linked to their nuclei, making them free to move in the interatomic space. This behaviour is typical of conducting material and is fundamental that electrodes used for EMG acquisition have this property. When metallic atoms get in touch with electrolyte solution, e.g NaCl, electrons release occurs. During this process, cations (ions with positive charge) take electrons from metal, becoming neutral, whereas anions (ions with negative charge) give their extra electrodes to metal becoming neutral particles. These continuous change of charges determinate micro-fluctuations, that generate noise during the acquisition.

The reaction that takes place can be summarized as

$$M \Leftrightarrow M^{n^+} + ne^- \tag{2}$$

Assuming an electrode embedded into a electrolyte solution, the reaction that occurs from left to right is known as *oxidation*. Metallic atoms (M) release n electrons and cations M^{n^+} into solution. By doing that, electrode's charge is negative in respect to the solution, generating a current that enter in the electrode. A reaction that occurs in the opposite direction is called *reduction*. In this chemical reaction solution ions acquire n electrons from electrode and deposit it as form of metallic atoms, determining a change of charge and a current that comes out from the electrode (anodic current).

Moreover, because of charge distribution, a voltage between electrode and electrolyte occurs. The previous potential is present until an equilibrium between oxidation and reduction reactions is reached. This voltage is know with the name of *half-cell potential* and it can be quantified through Nerst equation:

$$E_{eq} = E_0 + \frac{RT}{nF} ln \left[\frac{a_0}{a_r}\right] \tag{3}$$

where E_0 is the standard half-cell potential (referring to standard hydrogen electrode), R is the universal constant of gases, n is the number of electrons that are present during the reaction, T is the absolute temperature (expressed in K), while $a_{0,r}$ is the activity of oxidized and reduced ionic species.

Assuming now an electrolyte solution interfaced to an electrode, with ions having valence values either +1 or -1, their motion could be analysed through the following equations

$$\begin{cases} \nabla^2 V = -\dfrac{q}{\epsilon}(n_+ - n_-) \\ \dfrac{dn_\pm}{dt} = -\nabla \cdot \mathbf{j}_\pm \end{cases} \tag{4}$$

where V is the potential that satisfies Poisson equation, ϵ is the dielectric constant of the gel, q is proton's charge and $n_\pm$ are the densities of cation and anions embedded in the gel. Their flux is obtainable as

$$\mathbf{j}_\pm = -D_\pm \nabla n_\pm \mp \mu_\pm n_\pm \nabla V \tag{5}$$

where $D_\pm$ refers to diffusion coefficients of the two ions, $\mu_\pm = \frac{qD_\pm}{K_B T}$ is the ionic mobility and K_B is the Boltzmann constant.

In addition to electrodes classification reported above, those sensors can be divided in two other categories: *polarizable* and *nonpolarizable*. The first avoid charges motion in electrode-electrolyte interface ($\mathbf{j} \cdot n = 0$ on the boundary, being n the normal vector), the latter allow charges to move without restrictions across the interface. Real electrodes have physical properties between perfectly polarizabile and nonpolarizable extremes. However, the most common sensors for EMG belong to nonpolarizable class, for example the ones made of silver/silver chloride (Ag/AgCl) .

When potential is applied to an electrode, ions with opposite charge (positive if the potential applied is negative and vice versa) are attracted to the metal forming a layer of charges on its surface. If an high ions concentration occurs a half cell potential is produced. Moreover, the superficial charge attract ions of opposite sign, forming a double layer, that could be model with a parallel-plate capacitor. In addition, ions at interface are free to move because of electrostatic and diffusive forces, known as polarization effect. This phenomena could be represented adding a leakage resistor in parallel to the previous capacitor. Finally, the bulk resistance of the gel could be modelled by a resistor connected in series with the previous components. A complete model could be observed in Fig. 2.1 A.

Skin is the first physical barrier that could be found in EMG acquisition. It consists of three main layers, each with different electrical properties, listed in the following lines according to their depth: *epidermis*, *dermis* and *subcutaneous layer*.

- *Epidermis* is the most superficial layer, in which epithelial cells, known as *keratinocytes*, are present. In turn, this layers could be subdivided into other levels which represent keratinocytes life cycle: a slow motion from deep epidermis layer to superficial ones. Indeed, newborn cells could be find with major concentration in the deepest part of the present layer, while mature ones in the superficial side. Epidermis could be modelled with an electric scheme as reported in Fig. 2.1 C, including: a voltage source (E_{se}), a resistor (R_e) and a capacitor (C_e). In presence of sweating the tissue conductivity changes. In order to consider this phenomena a parallel circuit, included in the light grey ellipse in Fig. 2.1.

- *Dermis* is located anatomically below epidermis and is conductive tissue, made up of collagen and elastic fibres; elements that give flexibility to skin.

- *Subcutaneous layer*, made up of connective tissue and adipocytes is the last and deeper layer. In term of conductivity, its behaviour could be represented with dermis layer through a bulk resistor (R_u).

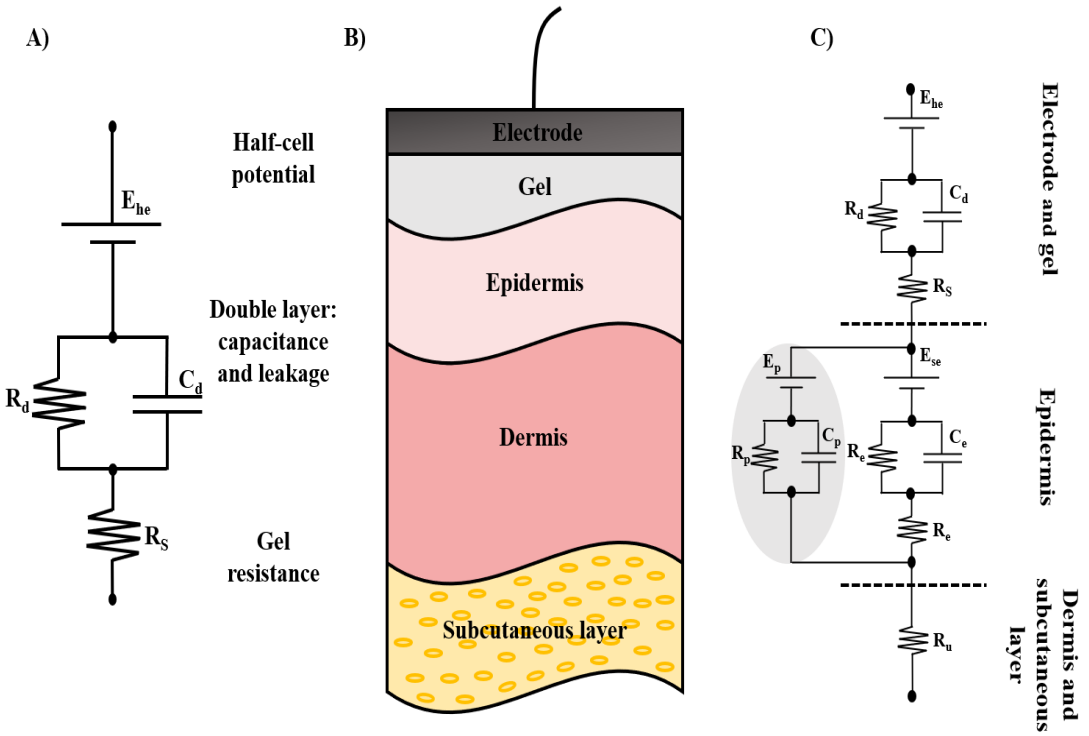

Figure 2.1: *A) Model of electrode/electrolyte interface (electrical scheme). B) Skin's main layers with electrode and gel for EMG. C) Complete electrical scheme taking in consideration all the layers included in part B. Components in light grey ellipse model the sweat glands and ducts.*

2.2 Sources of noise

As reported in the previous section, electrode-skin interface is intricate. In addition, different forms of noise could detected by electrodes during an EMG acquisition.

Electrode's half-cell potential is unstable because of motion. This phenomena generates a form of noise, known as *movement artefact*. In order to reduce it, non-polarizable electrodes should be used because ions are mostly absorbed on electrode's surface. Moreover, small and random voltage fluctuations, due to the continuous transfer of charge across the interfaces, could be detected. This form of noise is always present in EMG recordings, indeed, voltage fluctuations in the order of few μV_{RMS} could be recorded even when EMG sensors are placed on a soaked

cloth. Usually, a couple of electrodes produce a noise of 2-4 μV_{RMS} at which are summed other 1-2 μV_{RMS} due to noise generated by the amplifier. In order to obtain an informative EMG it is important to reduce the impedance of electrode-skin contact. This archived cleaning the skin in a proper manner, that is rubbing the surface with a solvent or with a slightly abrasive cloth soaked in water. This process is important because dead cells from epidermis are removed.

In addition to the previous forms of noise, there is another source of interference could be detected by EMG sensors: the power-line interference. This noise is due to parasitic coupling that connects the power-line to EMG amplifier, generating an intense noise in recordings. To avoid this issue, shielded cables connected either to the common mode or to the earth are used, then short-circuiting most of the parasitic connections.
However, further interference could be detected by electrodes, such as:

- Electromagnetic sources generated from other electronic devices (radio, mobile-phones or fluorescent lamps flickering). Since EMG amplifier are made up of millions of transistor, it is possible that electromagnetic radiation can be collected by the p-n junction and then rectified, producing noise during the acquisition.

- Variable electromagnetic field. Indeed, being the patient with electrodes cables a closed loop, if the presented field has a flux across the loop, a current is induced into the cables. To avoid this condition, the loop area should be reduced, twisting the cables.

- Artefact due to electrical stimulation.

- Ground loop. A phenomena that occurs if the patient is connected to different equipments not referenced to the same potential. Indeed, in this condition a current could flow through the patient being source of noise.

- Movement of the electrodes, determining a continue change in the electrode-skin interface.

- Disconnection of one or more cable.

Therefore a good quality EMG is obtained if most of the presented source of interference are restrained. However, a proper electrodes placing is fundamental. In the following lines an example of experimental is summarized:

- Choose the optimal EMG sensors for the aim. Electrodes used for EMG acquisitions could be in form of array or matrix.

- Prepare the skin properly (cleaning).

- Subject's movement must be reduced, so that artefact due to movements could not occur.

- Determinate, if possible, the IZ through a "dry" probe placed on target muscles. Considering an electrode array, it should be placed between IZ and the most distal tendon. If the estimation of conduction velocity (CV) is desired, an appropriate electrode placing is reached if the amplitude of SD signals is large enough and if DD signals are similar with a delay in physiological range.

- Place and then fix either the matrix or electrodes array to skin. The EMG sensors are included in a flexible system and is kept in contact with skin through disposable double-sided foam, whereas electrodes with the conductive gel, filling the holes present in the foam under each electrode.

- Test the connection.

2.3 Amplification chain for bio-potentials

Once the flexible system containing electrodes has been placed, the bio-potential detected need to be amplified, filtered and then sampled. Some features of an adequate amplifier for bio-potentials are: safe for the patient, differential type (in order to reduce noise as much as possible), with high gain (since the signal has a small amplitude), with high input impedance (so that the impedance of electrode-skin interface could be minimized) and with *high common mode rejection ratio* (CMRR). This last parameter is defined as $20 \log_{10} A_d/A_c$, where A_d and A_c are the differential and common mode gain of the amplifier. In most of amplification chair for bio-potentials an *instrumentation amplifier* is present. In addition, two other electronic system are used: an high pass filter to remove the movement artefact and a low pass filter with function of anti-aliasing, connected in cascade mode. The cut-off frequency could be, for example, 10 and 500 Hz, respectively. Moreover, in order to remove the common mode, a circuit know as *driven right leg* (DRL) could be used. Through this system, common mode is measured and re-injected to patient with opposite phase. Therefore, choosing properly the feedback resistance (R_f in Fig. 2.2) this form of interference it could be strongly attenuated. Therefore through a combination of filters at specific bandwidth is imposed, in order to empathize the frequencies in which most of the energy is present.

At the end of the chain an optoisolator and ADC converter is present. The first isolates the patient from acquisition circuit, while the latter samples data recorded from electrodes. The resolution of an ADC can be expressed in number of bit, usually an acquisition with ADC having a resolution of 16 bit can be considered as good quality; however, nowadays systems with more than 20 bit are available. An example of acquisition chain is represented in Fig. 2.2.

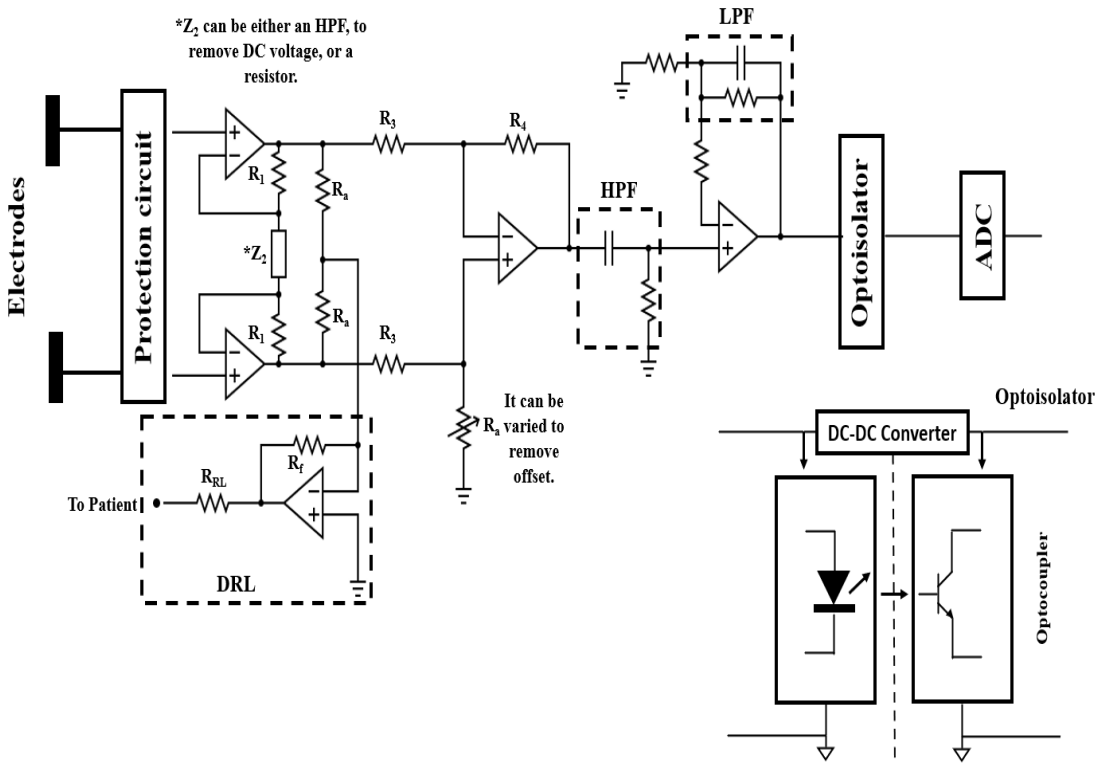

Figure 2.2: *Electrical scheme of an amplification chain for electromyography. The electronic components between the protection circuit and HPF, excluded the DRL, define the instrumentation amplifier.*

In conclusion, an appropriate amplification chain is fundamental to reduce noise and use properly all the levels available of ADC, paying attention to avoid saturation of previous amplifiers. Nowadays, it is possible to find systems that include all the electronic components described in a unique device enabling the acquisition of different types of bio-potential with an high number of channels.

2.4 Amplitude indexes

The amplitude of recorded EMG can provide important information such as its activation and force produced. The EMG can be considered as spatial and temporal interference pattern result of MU's activity that are present under the detection zone [15]. More specifically, it can be modelled as a stochastic process with standard deviation proportional to the amount of MUs recruited and activation rate as

$$s(k) = \sum_{i=1}^{R} \sum_{l=-\infty}^{+\infty} x_{il}(k - \phi_{i,l}) + v(k) \tag{6}$$

where $s(k)$ represents the k^{th} sample of EMG signal, R defines the number of recruited MUs, x_{il} is the l^{th} MUAP of the i^{th} MU, $\phi_{i,l}$ describes the occurrence time of x_{il} and v the source of additive noise.

The most common indexes used for amplitude estimation are *average rectified value* (ARV) and the *root mean square* (RMS), defined respectively as

$$ARV = \frac{1}{N} \sum_{i=1}^{N} |EMG_{ch}(i)| \tag{7}$$

$$RMS = \sqrt{\frac{1}{N} \sum_{i=1}^{N} [EMG_{ch}(i)]^2} \tag{8}$$

where N identifies the number of samples in the considered epoch. Indeed, those indexes should be used on epochs of signals with temporal length in the range of 100 - 500 ms.

2.5 Power Spectral Density and frequency indexes

The power spectral density (PSD) is a common tool through which is possible to represent the spectral energy distribution per unit of time of a signal. It is an important tool applied in different engineering fields. For example, referring to bio-medical field, the power spectral density of EMG signals can provide important information regarding MUs activated during the muscle contraction [16][17][18][19]. There are different strategies to estimate the PSD of an epoch of signal [20]. Assuming epochs as wide sense stationary (WSS), there are two techniques for PSD estimation: the *direct* and *indirect* method, both belonging to the classic non parametric group. The first is based on signal's Fourier transform, while the latter on it's autocorrelation. More specifically, a PSD estimation through the direct method, known also as *periodogram*, could be obtained computing the absolute square of signal's discrete Fourier transform. On the other hand, the indirect method requires to compute the Fourier transform of an estimate of signal's autocorrelation. This last method is know with name of *correlogram*.
Since the PSD estimation is a statistical problem that is not consistent, a smoothing is necessary. Through the following techniques, belonging to the class of direct methods, is possible to obtain a more robust estimations:

- The method of Daniell involves a moving average of sample spectrum, with the aim to smooth it.

- The method of Barlett divide the time series in numerous sub-series (M) of N/M samples. Then their spectra is averaged.
- The method of Welch is similar to Barlett, indeed an average of periodograms is computed. However, the sub-series are windowed with the possibility of overlapping. In this manner a better resolution is obtained, since the same periodograms can be computed with longer sub-series.
- The Blackman and Tukey method involves the windowed autocorrelation time series, minimizing the estimations with large delay.

From the obtained PSD some important EMG index could be extracted, such as:

- *Median Frequency (MDF)*: the value of frequency that divides the spectrum into two parts having the same power

$$\sum_{j=0}^{N_{MDF}} P_j = \sum_{j=N_{MDF}}^{M} P_j = \frac{1}{2}\sum_{j=0}^{M} P_j \tag{9}$$

  where P_j is PSD of EMG signal at a frequency bin j, M indicates the number of frequency bins while N_{MDF} is the bin at which corresponds the MDF.

- *Mean Frequency (MNF)*: defined as the barycentre of the spectrum

$$MNF = \frac{\sum_{j=0}^{M} f_j P_j}{\sum_{j=0}^{M} P_j} \tag{10}$$

2.6 Conduction velocity

As reported in chapter 1, the AP generates in the IZ and propagates through the muscle fibres to tendons where it extinguishes. The speed with which this waveform travels in the fibres is called conduction velocity (CV). It is an important physiological parameter that is used in several application. Indeed, either the type of fibre or the fatigue or pathological disorders could be analysed through this electromyographic index. The CV estimation is not trivial, indeed, the *multi-unit action potentials* (MUAP) detected from electrodes do not propagate all in the same direction having a constant shape, so the ratio between IED and the waves delay is not always possible, except in ideal conditions. Many factors impact the shape of AP, and as a consequence the CV estimation.

- Because of noise, the waveform changes its shape randomly.
- Electrodes could be placed not perfectly aligned with muscle fibres.
- If other AP travel in the opposite direction, a perturbation in the waveform could occur.
- Non propagating components, such as end-fibre effect due to AP extinction generate a distortion in MUAP.
- Non homogeneity of tissues may produce a change in waveform, due to the different conductivity around the propagating source.
- If pinnate muscles are studied, their fibres go deep determining a more complex CV estimation.

Moreover, only a global estimation of muscle's fibres CV could be obtained, since each MU has its own CV. As proposed in [21] a weighted average of CVs could be used, with weights as function of MUs dimension and location. Due to the previous non-idealities, the CV estimation is quite complex and several methods has been proposed in literature [22]. In the following lines some of them are presented. They can be classified into three categories, according on how many channels are used for the estimation: one, two or multichannel.

Scaling of the spectrum

It is a technique that uses only one channel and its power spectral density [23], which could be written as

$$P(f) = \frac{1}{v_2} G\left(\frac{f}{v}\right) \tag{11}$$

where v is the conduction velocity, while G is the shape of the spectrum. Therefore, the MNF is proportional to CV, through a parameter, α, that depends of the volume conductor

$$MNF = \frac{\int_0^{+\infty} fG\left(\frac{f}{v}\right) df}{\int_0^{+\infty} G\left(\frac{f}{v}\right) df} = v\frac{\int_0^{+\infty} sG(s) ds}{\int_0^{+\infty} G(s) ds} = \alpha v \tag{12}$$

Reference points

Its a method based on two channels in which two reference points are detected and their delay is computed. Since the IED is known, the CV can be estimated. As reference points could be used either points of zero crossing or local maxima or minima. However, reference points can not be detected easily in noisy signals. Furthermore this method can not be applied in multichannel condition and with interference signals.

Cross-correlation function method

This technique is based on the maximum of cross-correlation function, with which the delay between input signals can be obtained. It is a method stable to additive noise, since all the information included in the signals is considered. The estimation of CV depends on the resolution of time sampling. Oversampling data or a local interpolation of cross-correlation maximum could overcome this issue.

Spectral matching

The spectral matching belongs to methods which use two signals as input. The lag at which the cross-correlation functions has its maximum is the one that minimize the mean square error of target signals, defined as function of the delay (τ) between them. Therefore, minimizing the square error, the method is stable to noise, as cross-correlation technique, although both are sensitive to shape changes of waveforms, such as due to non propagating components.

$$\begin{aligned} &\int_{-\infty}^{+\infty} |x_1(t) - x_2(t-\tau)|^2 \, dt = \\ &\int_{-\infty}^{+\infty} |x_1(t)|^2 \, dt + \int_{-\infty}^{+\infty} |x_2(t)|^2 \, dt - 2 \int_{-\infty}^{+\infty} x_1(t) x_2(t-\tau) dt \end{aligned} \tag{13}$$

The first two terms of equation (13) are the energies of signals, whereas the last is the negative cross-correlation. The value of delay which reduce the mean square error can be obtained in the frequency domain, to overcome resolutions problems. Therefore, the error can be rewritten using the Parseval equity and the shift property:

$$e^2(\tau) = \sum_{n=0}^{N-1} [x_1(n+\tau) - x_2(n)]^2 = \frac{1}{N^2} \sum_{k=0}^{N-1} |X_1(k) e^{j\frac{2\pi k\tau}{N}} - X_2(k)|^2 \tag{14}$$

where N is the number of samples that define the signal. According to (14) the error depends continuously on τ, so it can be calculated without problems of resolution. The minimization of $e^2(\tau)$ is a non linear optimization problem and different strategies can be adopted to this aim. For example is possible to explore all the values of τ and determinate the best one for this purpose, but its a high time-consuming research. To overcome this issue, a different strategy could be adopted: the delay estimation may be updated going in opposite direction to gradient error, with a small step of update when the minimum of $e^2(\tau)$.

Alternatively, the Newton technique can be used. This method detects a root in the first derivative of the functional $f(\tau) = e^2(\tau)$. A set of x_n is created from an initial guess x_0 that have to converge to x^* for which $f^{'}(x^*) = 0$. Analysing the second-order Taylor expansion of the function around x_n

$$f_T(x) = f_T(x_n + \Delta x) \approx f(x_n) + f^{'}(x_n)\Delta x + \frac{1}{2} f^{''}(x_n)\Delta x^2 \tag{15}$$

In (15) the correction, defined as Δx, need to be chosen so that $x_n + \Delta x$ is a stationary point of the functional, for example using the minimum of quadratic Taylor approximation

$$\Delta x = -\frac{f^{'}(x_n)}{f^{''}(x_n)} \tag{16}$$

In conclusion, the estimation it is much more correct when the point x_n is close the zero of functional first derivative. Moreover, this method with Newton's one may converge to a local minimum, instead of a global one. For this reason, a good initialization of x_0 is fundamental to overcome this case. For example, the delay obtained through the cross-correlation method could be a good candidate as initial x_0.

Maximum likelihood estimation

It is a technique that uses more than two channels as input. The maximum likelihood estimation method is a generalization of spectral matching. It is applied at pairs of channels, with the vantage of a reduced estimation variance. Furthermore, it is less sensitive to noise, electrode's misalignment and non-homogeneity in tissues rather than the methods which use two channels as input. The signal obtained from one electrode could be defined as

$$x_k(n) = s(n - (k-1)\theta) + w_k(n) \tag{17}$$

where k is the number of channels considered, while $w_k n$ is an additive Gaussian noise. The error function could be obtained as follows

$$e_{MLE} = \sum_{k=1}^{K}\sum_{n=1}^{N}[x_k(n) - \frac{1}{K-1}\sum_{m=1,m\neq k} x_m(n+\theta_{m,k})]^2 \tag{18}$$

where the number of samples is represented by N and the delay between $x_m(t)$ and $x_k(t)$ through $\theta_{m,k}$. The functional reported in (18) assumes that the distance between channels is kept constant in all the electrode's array, determining a maximum likelihood estimation, with constraints. However, it can be rewritten into a functional without constraints defining $\theta_{m,k} = (m-k)\theta$.

$$e_{MLE} = \sum_{k=1}^{K}\sum_{n=1}^{N}[(x_k(n) - \frac{1}{K-1}\sum_{m=1,m\neq k} x_m(n+(m-k)\theta)]^2 \tag{19}$$

Chapter 3

Crosstalk and Optimal Spatio-Temporal Filter

As reported in the previous chapter, surface electromyogram is a measure of bio-potential with some differences from invasive electromyography. Nevertheless, the easiness of data acquisition can be considered as the principal. Indeed, for invasive recordings medical staff and needle electrodes are required, determining the acquisitions difficult to be replicated in most of the research laboratories. For this reason, surface EMG, is preferable. On the other hand, in surface electromyogram electrodes are far from the signal source, determining considerably bigger pick-up volume. For this reason, different forms of noise could corrupt the acquisition, one of them is *crosstalk*: defined as the signal produced by a muscle close to the one of interest, detected by the electrode on target muscle [24]. In this chapter a literature review of crosstalk phenomena will be given, mainly taking inspiration from [24] and the algorithm of *optimal spatio-temporal filter*, useful to avoid the problem of crosstalk, will be discussed [25].

3.1 State of the art and spatial filters

Crosstalk can be considered a significant concern in different applications: for example in neural control information used to command myoelectric prostheses with multiple degrees of freedom [26]. For this reason, different studies has been promoted to better analyse the effect of crosstalk and investigate how to quantify and then reduce it. In the following points, some results of crosstalk studies are reported:

1. According to experimental studies, an increase of crosstalk may occur in case of thick subcutaneous layer.
2. It can be reduced optimizing electrodes location on muscles of interest.

3. As reported above, crosstalk can be considered as noise produced by far muscles from recording electrodes. Initially, it was thought to be highly filtered by tissue in between, determining mainly low frequency components, easily removable through an high-pass filtering. However, this is not possible. Indeed, crosstalk is mainly due to non-propagating components concerning generation and extinction phenomena, characterized of short temporal duration and with high frequency components.

4. Surface EMG depends on the relative position of EMG electrodes and sources (within the active muscles). As direct consequence, crosstalk cannot be quantified by studying the cross-correlation between recoding over the two muscles of interest.

5. Spatial filter, better described in the following lines, can be used to reduce crosstalk. This effect is obtained reducing the detection volume. However, following this approach, an optimal configuration of the filter is not always reached. Indeed, it depends anatomical and physical parameters of the tissue studied.

In conclusion, the main strategy to reduce the effect of crosstalk is to apply spatial filters, with the compromise of a reduced detection volume and with the risk of a not optimized configuration for the subject.

A spatial filter can be defined as a linear combination of EMG channels to obtain a new signal from the input. In biomedical signal processing field there are different types of filters [27]: the most common are single and double differential filters (SD and DD, respectively). The first computes a difference between signals of two electrodes, approximating a spatial derivate, whereas the latter approximates a second derivate. Another important filter is the Laplacian or normal double differential filter (NDD), which approximates the Laplacian operator.
A spatial filter is different from another because of its selectivity, defined as a group of characteristics that each filter has, all described below

- *Longitudinal selectivity* is defined as the ability of a filter to distinguish short spikes produced by a singe source.

- *Transversal selectivity* is archived if with small transversal displacement the amplitude rapidly decreases.

- Selectivity with respect to depth is obtained if in presence of a source that goes deep, the potential recorded decreases rapidly.

- Selectivity with propagating components is archived if the filter suppress end-of-fibre contributions.

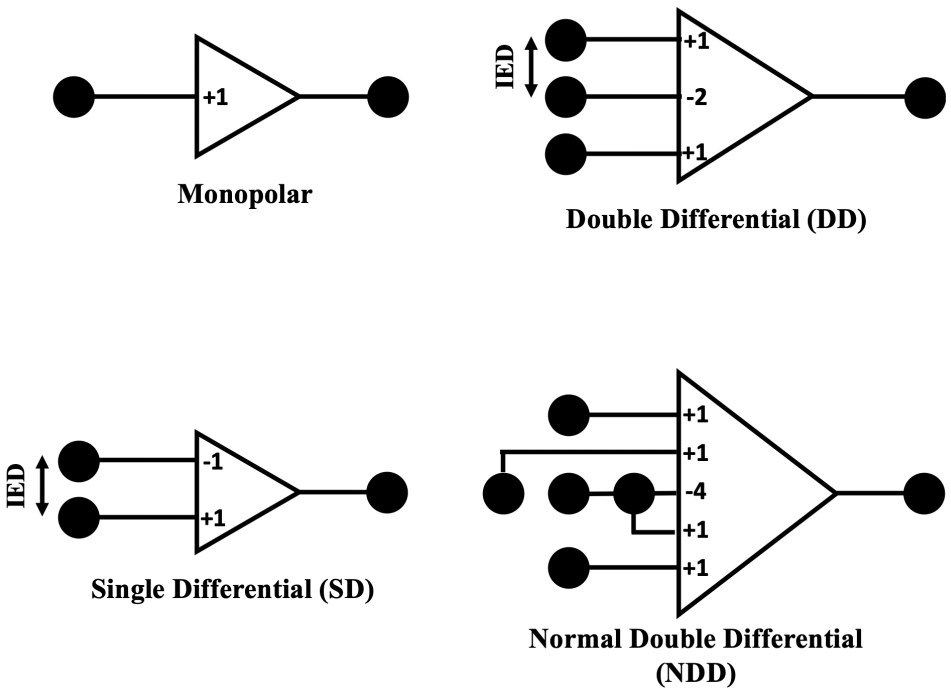

Figure 3.1: *Monopolar and common spatial filters used in biomedical signal processing field.*

Filter's selectivity is crucial if a specific muscle's region need to be studied, indeed through the use of those filters crosstalk can be reduced. On the other hand, a smaller region of analysis could provide a poor informative acquisition, in terms of muscle's activity, as other portions could behave differently [24].

In order to reduce crosstalk effect, some advanced signal processing techniques, presented in literature, could be used:

1. Assuming recorded data as linear instantaneous mixtures of independent signals produced by target muscles (sources) and, in addiction, that the number of muscles is lower than the detected signals, an advanced blind source separation technique could be used to data's time-frequency representations [28]. However, because of a mixing matrix that changes in time, real-time applications with this technique are not possible. In addiction, the previous assumptions restrict the application fields to small and superficial muscles with low gap between them and not synergic. [25]

2. Applying an inverse method to signals obtained with high-density system. However, this method still need to be tested in experimental conditions.

In conclusion, the most common technique to reduce crosstalk is applying spatial

filters, with the compromise of a small detection volume of target muscle, and so with the possibility that MUs activity detected are not representative of the whole muscle. In addiction, selective filters have not the same performances if larger electrodes are used.

3.2 Optimal spatio-temporal filter (OSTF)

The presented method has the objective to overcome the previous issues, with the following principles:

1. Filter coefficients are adapted and optimized to the subject, for example, taking in account the anatomy, physical properties of conductor volume and type of electrodes used.

2. The EMG of target muscle should be emphasized, while the signal produced from nearby muscle should be neglected as much as possible.

3. The presented algorithm is stable and simple, enabling real-time applications, for example, using few electrodes.

In order to obtain filter coefficients adapted to the subject, a portion of EMG acquisition is necessary. From now on, the recordings used to train the algorithm will be called training set. In this dataset, epochs of signals from target and crosstalk muscles are included, the first will be named as "signal" ($S_i(t)$), whereas the latter as "crosstalk" ($C_i(t)$). The index i = 1,2..., M indicates the ith EMG channel, while t the samples of concatenated epochs. According to [26] an *optimal spatial filter* (OSF) can be obtained combining a set of weights w_i that increase the *signal to crosstalk ratio* (SCR)

$$SCR = 10\log_{10}\frac{\left\|\sum_{i=1}^{M} w_i S_i(t)\right\|_2^2}{\left\|\sum_{i=1}^{M} w_i C_i(t)\right\|_2^2} \tag{20}$$

where the sum of w_i is equal to zero. The presented problem has been solved in [26], but according to [25] an analytical solution could be obtained as follows. If monopolar signals are used, common mode could be removed subtracting the mean over channels as first step, while if SD or DD signals are chosen, common mode has been removed yet. Since the functional in (20) is monotone increasing, it is possible to maximize its argument. More specificity, the problem could be defined rewritten as follows

$$J(\mathbf{w}_i) = \frac{\left\| \sum_{i=1}^{M} w_i S_i(t) \right\|_2^2}{\left\| \sum_{i=1}^{M} w_i C_i(t) \right\|_2^2} = \frac{\mathbf{w}^T \mathbf{S}^T \mathbf{S} \mathbf{w}}{\mathbf{w}^T \mathbf{C}^T \mathbf{C} \mathbf{w}} = \frac{\mathbf{w}^T R_S \mathbf{w}}{\mathbf{w}^T R_C \mathbf{w}} \tag{21}$$

where $J(\mathbf{w})$ is the functional to be optimized and R_S and R_C are signal and crosstalk's autocorrelation matrices. It is important to note that functional optimization in (21) is invariant if the $\mathbf{w}$ is scaled. That is why the previous relation is equivalent to the following constrained optimization problem

$$\begin{aligned} &\max_{\mathbf{w}} \ \frac{1}{2} \mathbf{w}^T R_S \mathbf{w} \\ &\text{such as } \mathbf{w}^T R_C \mathbf{w} = 1 \end{aligned} \tag{22}$$

that can be solved with the following Lagrangian

$$L_P = \frac{1}{2} \mathbf{w}^T R_S \mathbf{w} + \frac{1}{2} \lambda (1 - \mathbf{w}^T R_C \mathbf{w}) \tag{23}$$

where λ is the Lagrangian multiplier. According to Karush-Kuhn-Tucker (KKT) conditions [29], the following relation must be satisfied

$$R_C \mathbf{w} = \lambda R_C \mathbf{w} \rightarrow R_C^{-1} R_S \mathbf{w} = \lambda \mathbf{w} \tag{24}$$

Since the matrix R_C^{-1} R_S is not symmetric, the present eigenvalue can be solved analytically with a change of variables. The vector $\mathbf{v} = R_S^{1/2} \mathbf{w}$ is introduced, being R_S symmetric and positive, obtaining

$$R_S^{1/2} R_C^{-1} R_S^{1/2} \mathbf{v} = \lambda \mathbf{v} \tag{25}$$

The matrix $R_S^{1/2} R_C^{-1} R_S^{1/2}$ is symmetric and positive definite, so its eigenvectors ($\mathbf{v}_k$) are orthogonal and its eigenvalues (λ_k) are positive. More specifically, eigenvectors represent the directions of projections $\mathbf{w}_k = R_S^{-1/2} \mathbf{v}_k$. Taking into account the previous considerations, the functional $J(\mathbf{w}_k)$ becomes

$$J(\mathbf{w}_k) = \frac{\mathbf{w}_k^T R_S \mathbf{w}_k}{\mathbf{w}_k^T R_C \mathbf{w}_k} = \lambda_k \tag{26}$$

because $\mathbf{w}_k^T R_S \mathbf{w}_k = 1$ and $\mathbf{w}_k^T R_C \mathbf{w}_k = 1/\lambda_k$.

In conclusion, the weights that maximize (20) are the ones that has associated the largest eigenvalue. In addition, is possible to consider past values of EMG data to increase further the SCR, creating a optimal spatio-temporal filter (OSTF). Therefore signals are both filtered in space and time. Delay between subsequent

samples is an aspect that should be considered as well. Indeed, with the order of temporal filter, they are two parameters that can be tuned. According to [25] a tuning on different sets of data (test or validation set) rather than training set and lower values of delay are preferable. Indeed, parameters optimization on a validation set could improve filter's efficacy, whereas higher delay could produce over-fitting to training data, so reducing performances on test and validation sets.

Delayed data have an high mutual correlation which implies an high condition number of autocorrelation matrices R_S and R_C, specially if the delay is small and the length of the temporal filter is large. To avoid this problem, the autocorrelation matrices are regularized as follow

$$\widehat{R_S} = R_S + 10^{-4}\lambda^S_{max} I \qquad \widehat{R_C} = R_C + 10^{-4}\lambda^C_{max} I \tag{27}$$

where λ^S_{max} and λ^C_{max} are the maximum eigenvalues of the matrices R_S and R_C, respectively and I is the identity matrix. According to (27), the maximum conditional number is in the order of 10^4.

Chapter 4

Instrumentation Design and Experimental Protocol

In order to evaluate the efficacy of OSTF algorithm, two muscles has been studied: *flexor carpi radialis* (FCR) and *pronator teres* (PT). According to a literature review, this is not the first time that those muscles are analysed in EMG studies, an example is the research conducted in [28]. The cited study has been taken as inspiration for the experimental protocol and for the instrumentation design.

4.1 Target muscles

Target muscles are placed anatomically in the proximal part of the arm and their contraction produce different wrist movements. More specifically, the first enable wrist rotation, while the latter its flexion. Those muscles, placed anatomically one close to the other, have small dimensions and because of this configuration, the issue of crosstalk is more relevant, determining a bias in estimation of EMG indexes such as CV, MNF and MDF. An accurate estimation of the previous indexes could be useful, for example, in myo-electrical prosthesis, enabling a simpler and faster signal processing.

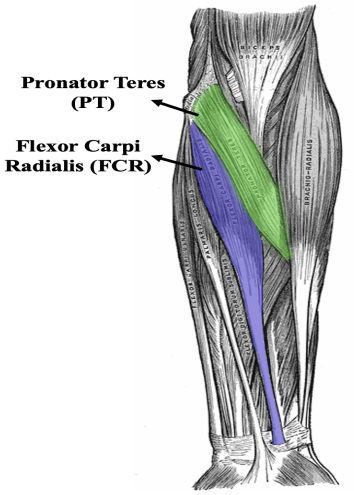

Figure 4.1: *Forearm anatomic table: pronator teres (PT) and flexor carpi radialis (FCR).*

4.2 Instrumentation design

A specific instrument has been designed and realized for this study, as reported in Fig. 4.3. It consists of a forearm support at which two plates are connected, forming an "handle" in which the hand of a subject can be inserted. The physical connection between the elements has been obtained through two load cell, with which was possible to quantify the forces applied to the handle. Analogue signals produced were amplified, sampled and digitalized through two *HX711*, a common device dedicated to load cells, one for each sensor. This system converts the analogue signal into a digital format, that will be processed through an *Arduino® Uno* board, an inexpensive and versatile device based on ATmega328P microcontroller [30].

Signals obtained from the sensors are then sent through an USB cable to a personal computer (PC), that process the acquired data with *MATLAB®* [31]. Indeed, with a specific add-on, available online at [32], it is possible to calibrate the sensors and acquire in real-time the forces applied to load cells. The trasductors used in this study are not expensive and have a good resolution. On the other hand, their capacity load is limited, so their application is restricted to few task. For this project load cells with capacity of 20 *kg* has been used.

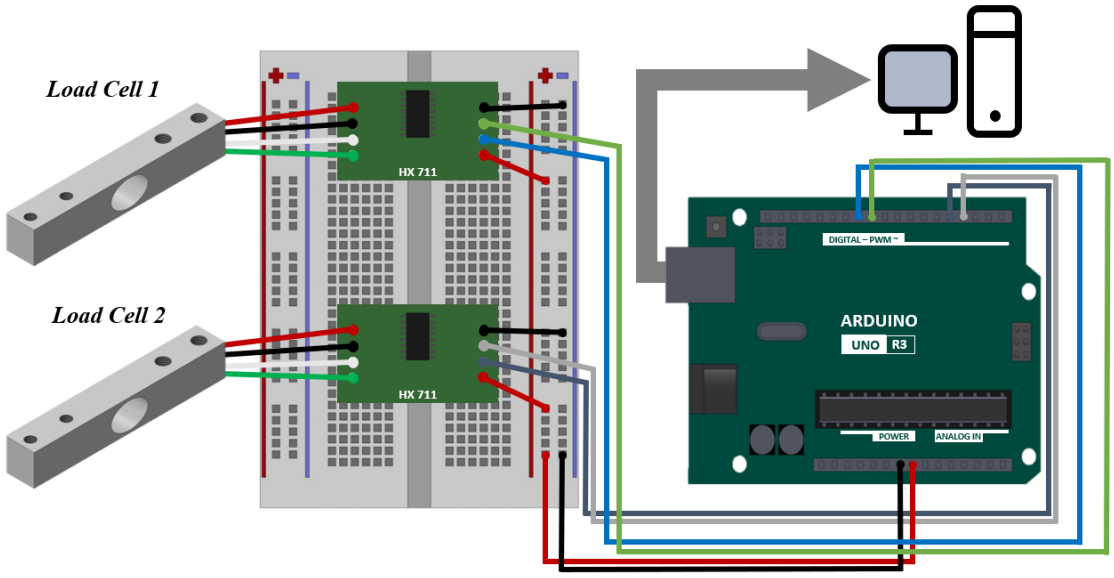

Figure 4.2: *Scheme of Arduino® Uno connection to amplifiers HX711 (on breadboard) and load cells.*

Since each load cell produces a signal depending on its deformation, with this set-up, showed in Fig. 4.2, is possible to distinguish flexion and pronation of the wrist analysing the phase of signals produced. Indeed, when a flexion occurs their phase is 0, whereas during a twist the phase is 180 *deg*.

ITEM NUM.	ITEM DESCRIPTION	QUANTITY
1	Arm Support (Base)	1
2	Soft Support (Latex)	1
3	Load Cell	2
4	Connector Base - Load Cell	2
5	Connector Load Cell - Handle	2
6	Upper Handle	1
7	Lower Handle	1
8	String Support	4
9	Bolt M4x40 mm	4
10	Screw M5x14 mm	4
11	Bolt M5x40 mm	4
12	Bolt M6x30 mm	2
13	Bolt M6x100 mm	4
14	Bolt M8x35 mm	2
15	Nut M6	4
16	Wingnut M6	4
17	Nut M8	2

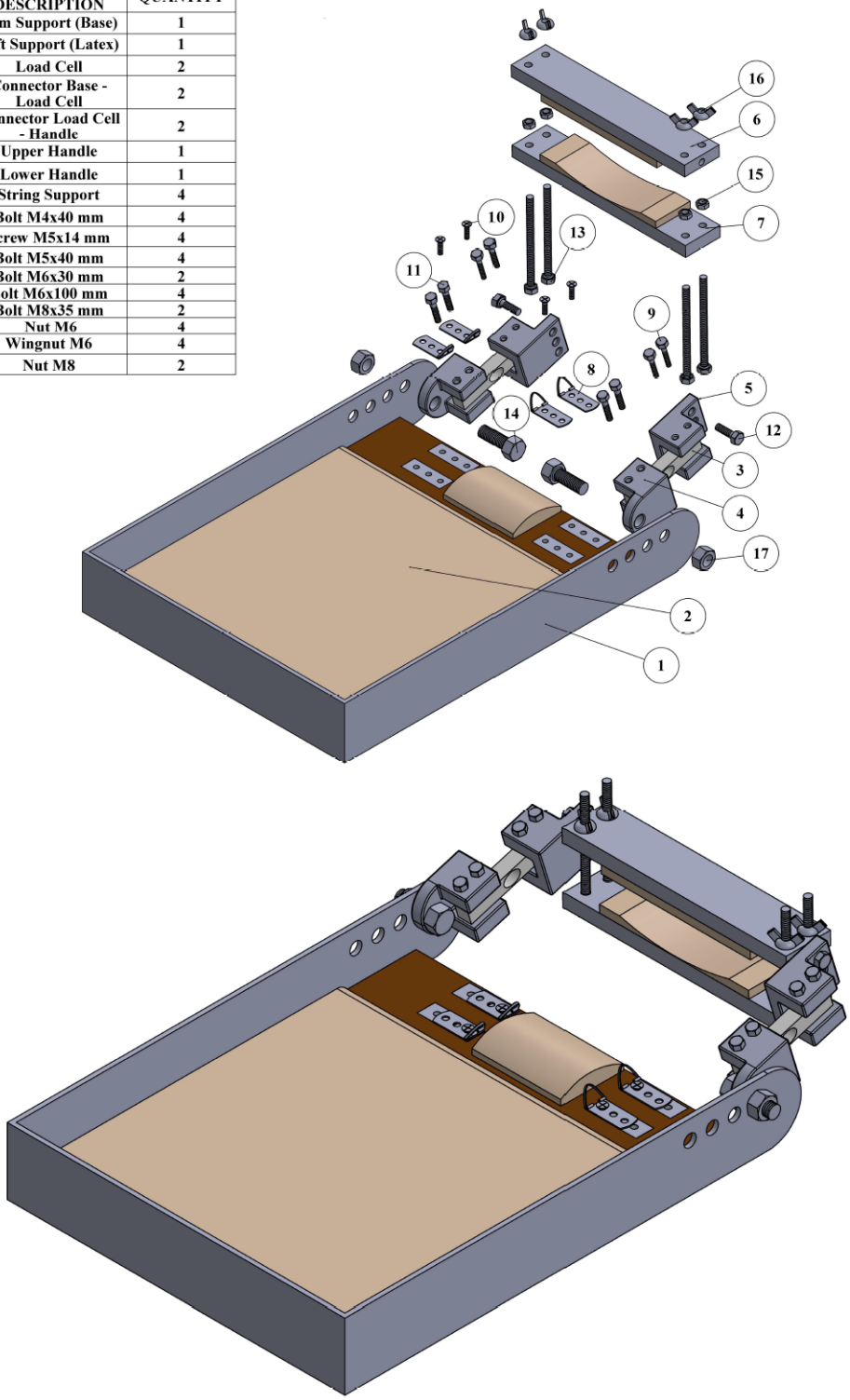

Figure 4.3: *Instrumentation's exploded view with table of components and 3D representation.*

During the acquisition it was fundamental to know when the subjects reached a force level, expressed as percentage of its *maximal voluntary contraction* (MVC), in order to have an EMG effectively informative. For this reason, the signal produced by load cell were used as additional input to EMG amplifier (Quattrocento, *OT Bioelettronica, Turin, Italy*). Since this system requires signals in analogue format, a new conversion from digital to analogue was executed.

Driving a digital pin of Arduino® Uno board, a *pulse-width modulation* (PWM) signal has been produced. It consists of a square wave with *duty cycle* (DC) that changes according to a variable value normalized between 0 and 1. A DC of 0 provides 0 V as output, while a DC of 100, a voltage of 5 V, indicating that the maximum value is reached. In this study the force signal (obtained as average of the absolute values of the two readings) was 0 V when no force was applied to the handle, while the output was equal to 5 V when the cells maximum load capacity is reached (20 kg). The analogue signal is then reconstructed filtering the square wave with a second order low pass filter, with cut off frequency of 10 Hz, and then sent to the EMG amplifier.

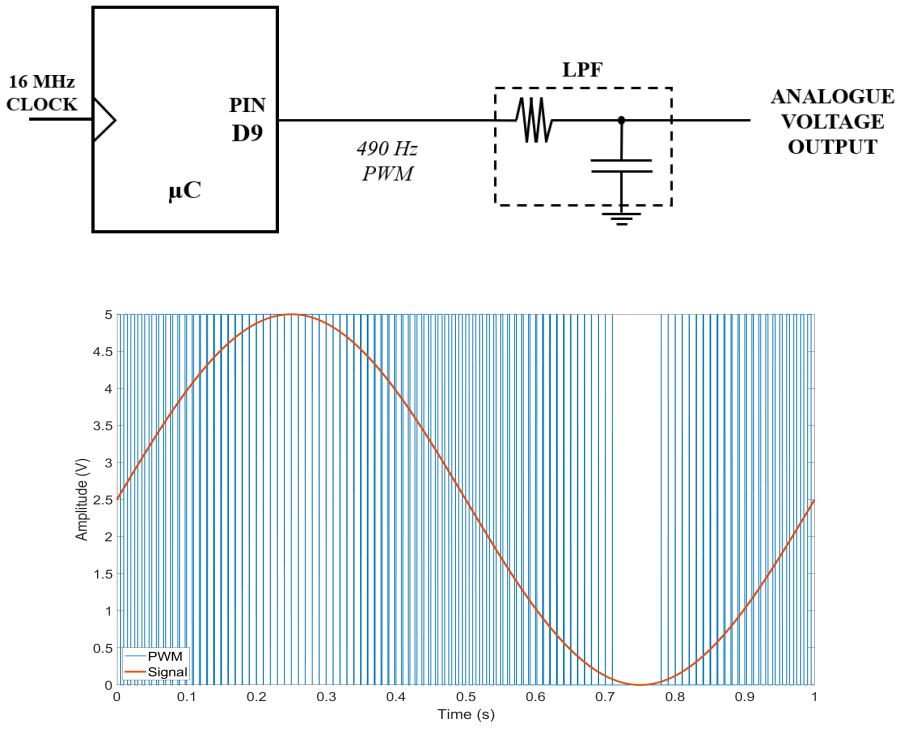

Figure 4.4: *Example of electrical connection between Arduino® Uno's µC and a low-pass filter (LPF) to obtain an analogue voltage from PWM signal (Top). A sine curve, with frequency 1 Hz reconstructed through a PWM signal at 490 Hz (Bottom).*

4.3 Experimental protocol

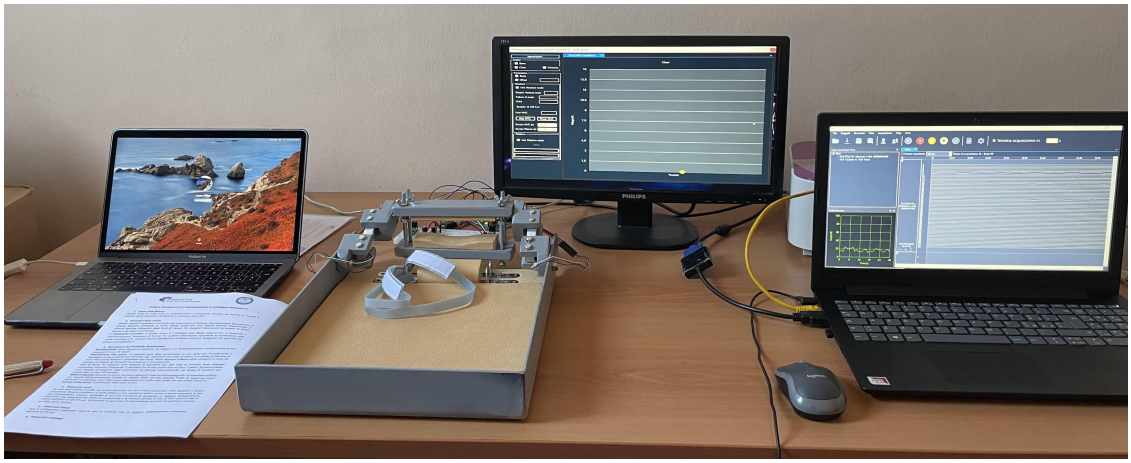

Figure 4.5: *Experimental setup: PC connected to Arduino board (left), instrumentation and support screen for force visualization as feedback (centre) and control monitor for EMG signals (right).*

In this study 8 subjects (6 men and 2 women, with 28.1 ± 7.5 years old) were involved as voluntaries. The experiments were conducted at *Neuro Muscular Function Laboratory, Turin, Italy* where each subject signed a informed consent document before the trials. Each volunteer seated on a chair and kept his forearm in contact with the instrumentation, forming a 90° angle with the arm. In order to obtain more selective contractions, a brief training made of instructions and free-trials were provided to each subject. Before electrodes placement, the muscles of interest were identified by palpation during a selective contraction. The skin was then slightly abraded with abrasive paste and a matrix of electrodes with IED of 8 mm was placed transversally to the muscle fibres, assuming that two columns are on PT, two on FCR and the last in between. During the acquisitions, a visual force feedback was given to the subject through a screen placed in front the instrumentation, as showed in 4.5.

In order to evaluate the performances of OSTF, it was necessary to acquire EMG at different force levels, expressed in function of subject's MVCs. Therefore, the MVCs of target muscles were acquired, with a pause of 2 min between each acquisition. Then, two sets of exercises were requested to the subjects, made up of 5 tasks at different force levels (10, 20, 30, 40 and 50 % MVC of the respective muscle), each lasting 20 s. Between the acquisitions a rest of 60 s has been fixed. The tasks were conducted with force levels chosen randomly between the set described before. An acquisition was considered valid if the subject can keep a dot-marker, representing the force produced to the upper handle (yellow in Fig. 4.6), between two lines that define ± 5 % MVC of target muscle as much as possible.

Figure 4.6: *Acquisition phase: a subject has the lower palm of dominant hand in contact with the upper side of the handle. Two reference electrodes are used: the first on the elbow, the latter on the acromion.*

Chapter 5

OSTF Application

In the present chapter, an experimental validation of OSTF algorithm will be provided. More specifically the method will be applied to one subject with the aim to demonstrate that results obtained in simulation can be archived in experimental conditions. The steps necessary to apply this method, the parameters used and the output will be described in this chapter starting with the training phase.

5.1 Training phase

The training phase can be considered as the most important step in the OSTF algorithm. As reported in the previous chapter, EMG has been recorded through a matrix of five columns of electrodes, but only three of them (external and central ones) and eight rows of the matrix are considered in this study, assuming that activities recorded under the chosen sensors are due to target muscles, while electrodes in the central column provide informations to border fibres. A scheme of the two configurations can be summarized in Fig. 5.1.

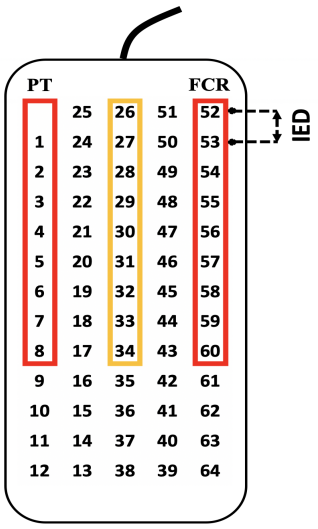

Figure 5.1: *"External" (red and yellow columns) and "No Middle" (red columns only) configurations.*

As first step, EMG data has been divided into *training*, *test* and *validation set*, through which, the filter could be trained (training set)

and tested (test set), in order to evaluate its effectiveness in crosstalk reduction in "new" recordings. The ability to generalize this effect has been analysed thorough the validation set. In order to simulate corrupted acquisitions, a noisy dataset was obtained summing the EMG of target muscle to recording of the other one, assuming it as crosstalk muscle, with the aim to simulate its co-contraction. Datasets was obtained concatenating epochs of muscles contractions, wrist's pronator and flexor respectively, at different force levels. The length of concatenated signals used as training and test set are kept constant and equal to 2 seconds. According to [25], sample's delay and temporal filter's order are parameters that should be tuned during training phase, so a tuning on test set has been conducted. The optimized parameter combination has been chosen as the one that produce an output, named *surrogate*, with the highest SCR on test set.

5.2 Surrogate signal

In order to better understand the output of OSFT, an example is provided in Fig. 5.2. PSD of EMG recorded on two channels (2 and 54) are obtained through Welch periodogram and then they are compared to surrogate. As reported in the figure, channels 2 and 54 are placed on PT and FCR respectively.

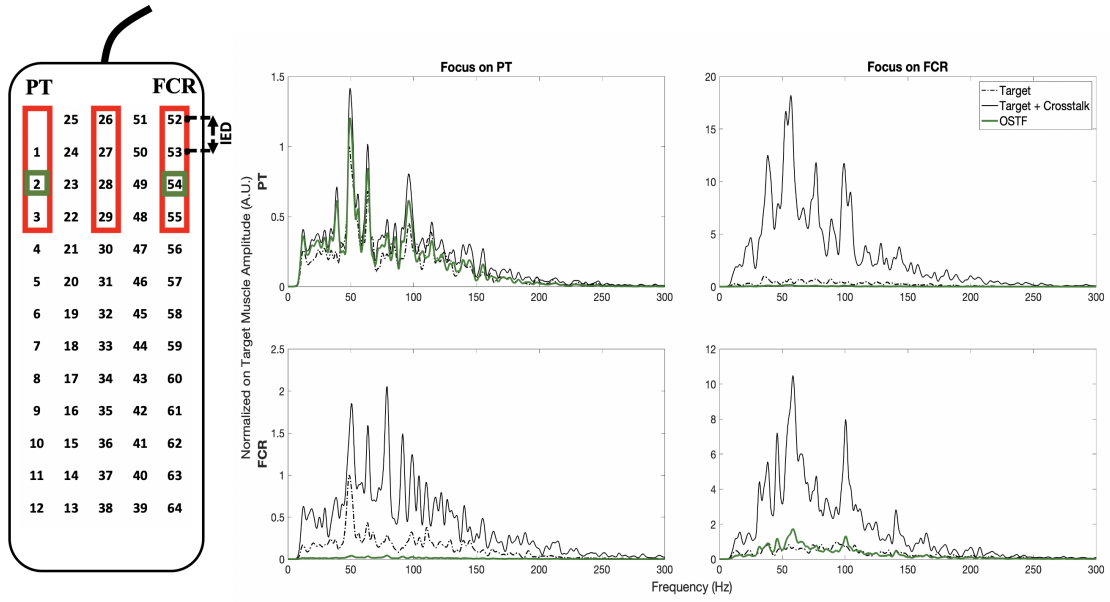

Figure 5.2: *PSD of PT and FCR compared with surrogate. Comparison at different trainings: focus on PT (left) and on FCR (right). The spectra are normalized to the PSD of target muscle.*

Since data given as input to the filter is filtered both in time and space, is possible

to extract the coefficients of temporal filter applied to each channel and observe how each input is filtered by the OSTF. In this example, spectra are normalized to the PSD of target muscle and two different trainings are analysed: the first empathize PT's activity, the latter FCR's one. When the focus is on PT and channel 2 is analysed (left part of Fig. 5.2), the green curve is almost overlapped with the dashed one, so the signal due to crosstalk is not considered, being the activity of FCR in the opposite channel (number 54). On the other hand, if the training is focused on FCR (right part of the Fig. 5.2), a reverse response could be observed.

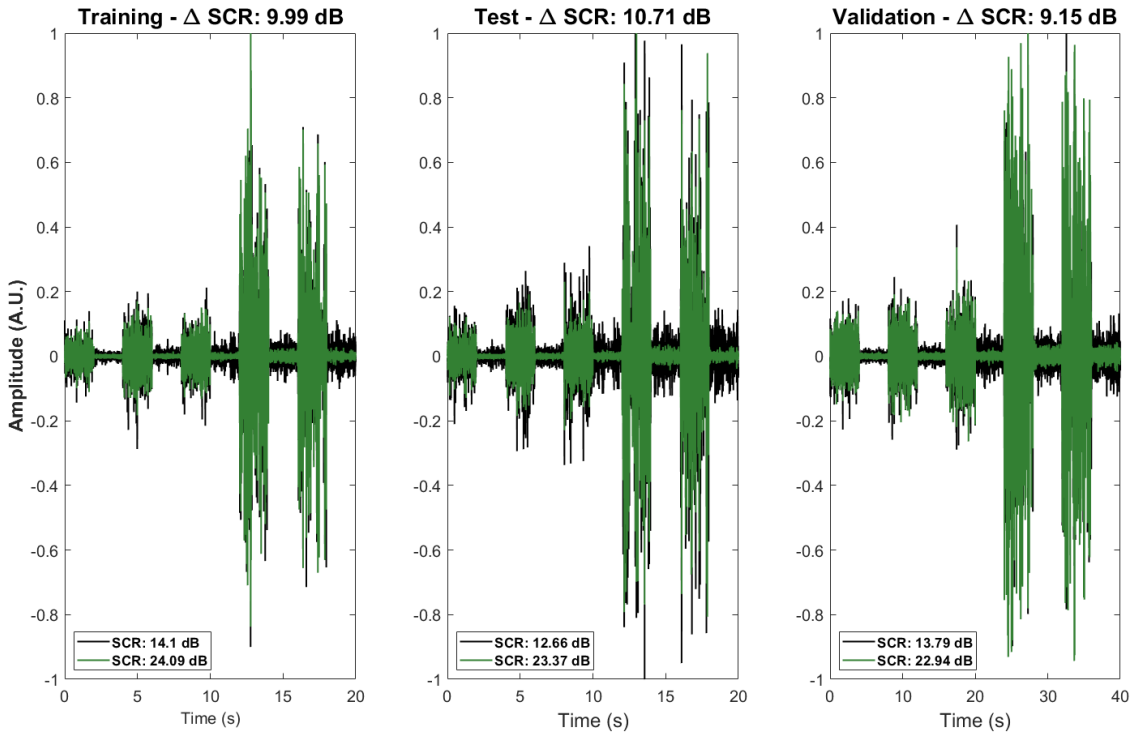

Figure 5.3: *Surrogates from clean dataset compared with the average signals on target muscles (PT) used as in training phase. SCR gain reported on top of each plot.*

Considering again a training focused on PT, in Fig. 5.3 it possible to observe the OSTF's ability of discard the activity of FCR in clean dataset. In order to compare the goodness of this method, each surrogate (green signal) has been compared with the average of signals given as input to OSTF, that has been obtained concatenating EMGs at different force levels of PT and FCR recorded on PT (black signals). It is possible observed that although SCR in training set is relatively good (more than 14 dB), the output of OSTF has an higher SCR with a gain of almost 10 dB. A similar behaviour could be appreciated for test and validation set.

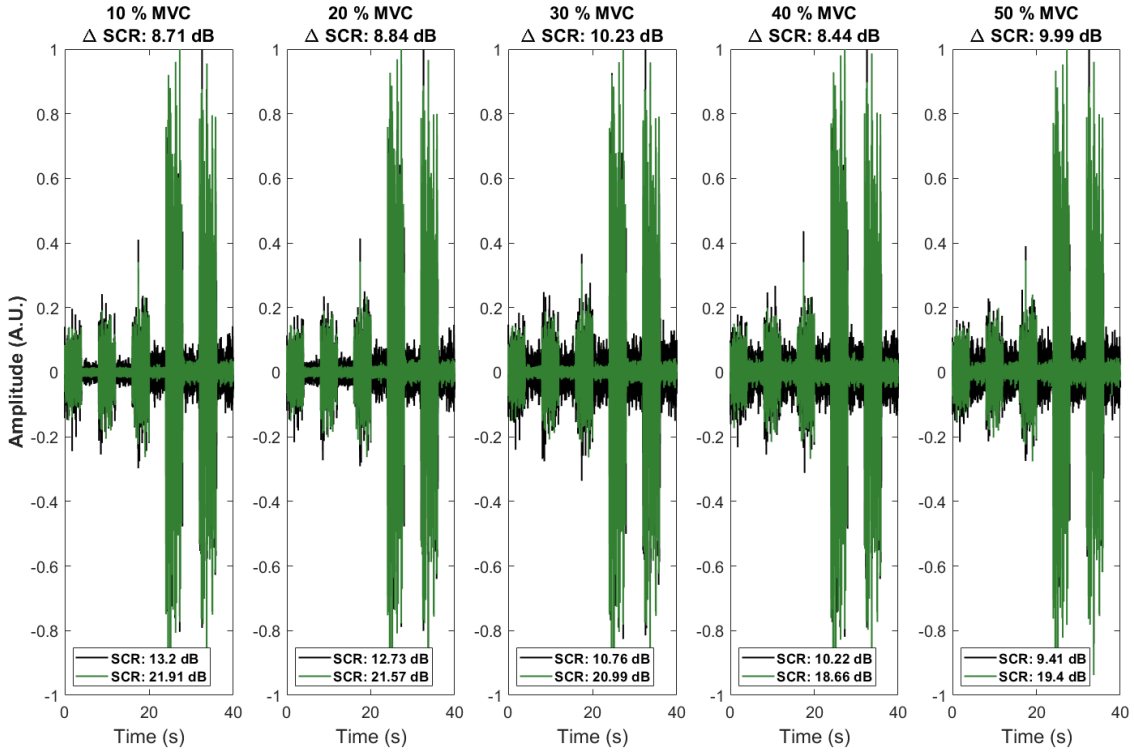

Figure 5.4: *Surrogates from noisy validation set compared with the average of signals on target muscles (PT) used as input to OSTF. The SCR gain are reported on top of each plot.*

In order to evaluate the ability of OSTF to reduce crosstalk the trained filter has been tested on noisy validation set. The surrogates obtained could be observed in Fig. 5.4 (green signals). Results demonstrate that even when co-contractions at different % MVC are added to clean data, the OSTF is capable to reduce crosstalk with a considerable gain in terms of SCR.

5.3 Comparison with traditional spatial filters

As reported in the previous lines, OSTF seems capable to reduce crosstalk in significant manner even in particularly noisy conditions. In this section the error in PSD and ARV estimation when noisy conditions are given as input to the filter will be presented. Signals of length equal to 4 seconds has been studied and the EMG parameters are calculated on epochs of 500 ms. The error in ARV estimation, expressed as percentage, has been obtained as

$$Error(\%) = 100 * \frac{|NoisySignal - CleanSignal|}{CleanSignal} \tag{28}$$

whereas the error in PSD estimation could be calculated as

$$Error(\%) = 100 * \frac{\sum |NoisyPSD - CleanPSD|}{\sum CleanPSD} \tag{29}$$

In order to have a preliminary evaluation of OSTF's performances, the estimation errors measured in different epochs has been averaged and then compared with the averaged errors obtained from signals of different type (raw monopolar, SD and DD) recorded on an electrode upon target muscle. In Fig. 5.5 it is possible to observe the differences between errors produced by traditional filters and OSTF for a single subject.

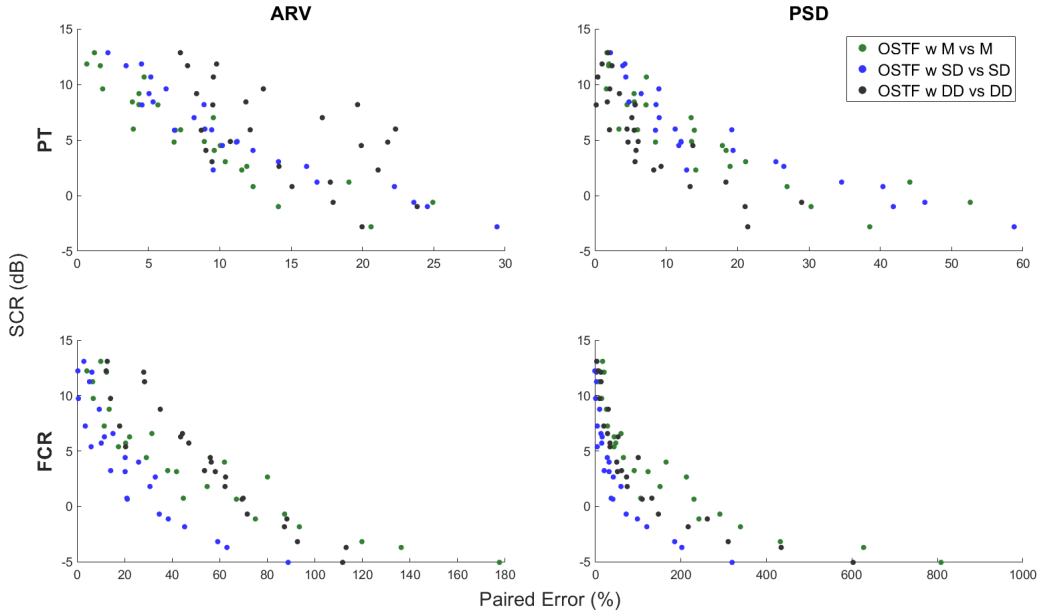

Figure 5.5: *Paired comparison between OSTF and traditional filters. The SCR, expressed in dB, and the percentage error are arranged on ordinate and abscissa, respectively.*

The OSTF trained with monopolar, SD and DD signals produce an estimation error always lower than traditional filters and monopolar recordings, being the difference major than zero. This effect could be appreciated both in signals with high SCR and, especially, in EMG corrupted with a lot of crosstalk; indeed, in those conditions, traditional filters produce considerable estimation error for the indexes studied. Since the presented method combines linearly a certain number of

signals from different muscles, the performances of OSTF trained with monopolar signals has been compared with traditional spatial filters, as reported in Fig. 5.6.

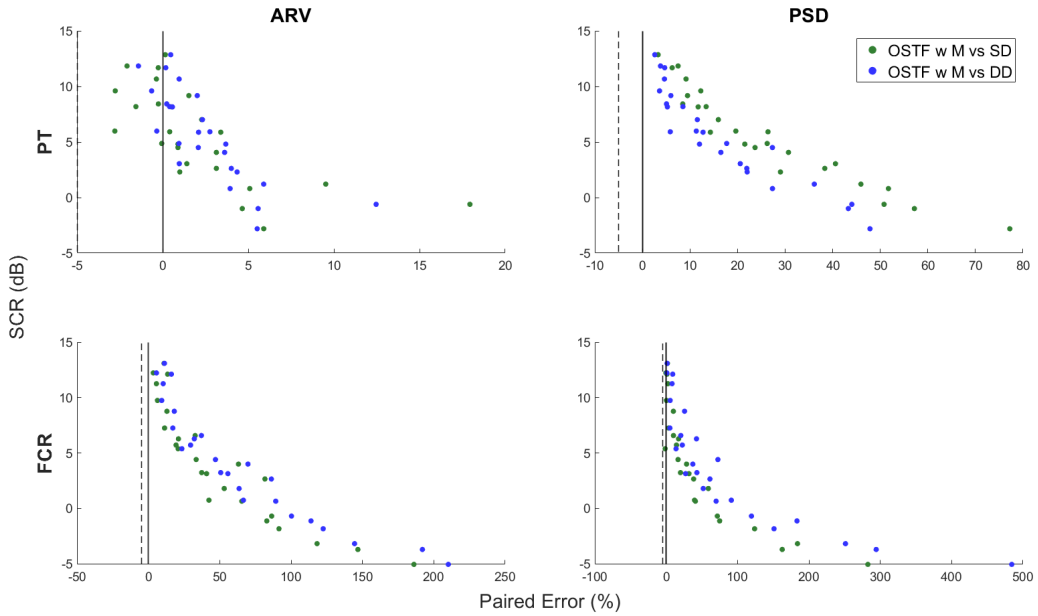

Figure 5.6: *Paired comparison between OSTF trained with monopolar signals and traditional filters. The SCR, expressed in dB, and the percentage error are arranged on ordinate and abscissa, respectively.*

Results show a similar behaviour as Fig. 5.5 for particularly noisy signals, indeed, the difference between errors is always major than zero. On the other hand, when the SCR increases, the OSTF performances could decrease, as the case of ARV estimation in PT recordings. However, the negative differences are always higher than -5 % (threshold delimited with a dashed line in plots of Fig. 5.6). In conclusion, for the analysed subject, OSTF seems to work better than traditional filters. From now on, the analysis will extended to remaining subjects considering different boundary conditions. More specifically, the tests that will be conducted include changes in:

- Number of electrodes used as input (longitudinal direction),
- Type of electrodes (square with a bigger dimension).
- Temporal length of the signals used for training phase,
- Signals used in training phase.

Those tests has as the objective to verify if the presented method keeps the previous performances in other subjects recordings and to determinate which parameter influences majorly filter's the behaviour.

Chapter 6

Statistics

Statistic is a branch of mathematics that deals with collection, organization, presentation and analysis of data with different purposes [33]. More generally, statistic can be divided into two main categories: *descriptive* and *inference* statistic. The first has as objective the analysis of samples by some index (mean, median, mode, variance, ecc), while the latter provides informations about a population from small samples. The aim of this chapter is to introduce some methods belonging to previous category, that will be used for a better analysis of results.

6.1 Distributions

A function that describes values for a specific variable and how often their occur is known as *distribution* [34]. In statistic branch there are several distributions [35], the most important ones are reported below

- *chi square* with k degrees of freedom

$$\chi_k^2 = Z_1^2 + ... + Z_k^2 \tag{30}$$

  where Z_j^2, with $j = 1, ..., k$, are independent and $Z_j \sim N(0,1)$.

- *t-Student* with a number of degrees of freedom equal to k

$$T_k = \frac{Z}{\sqrt{V/k}} \tag{31}$$

  with the independent distribution Z and V described as $Z \sim N(0,1)$ and $\sim \chi_k^2$.

- *F distribution* with two different degrees of freedom: u at the numerator and v at the denominator

$$F = \frac{W/u}{Y/v} \tag{32}$$

assuming W and Y as independent distributions such that $W \sim \chi^2_u$ and $Y \sim \chi^2_v$.

6.2 Hypothesis tests

An hypothesis test can be considered as a statistical tool with which is possible to take decisions from samples. More specifically, there are two choices: the null hypothesis (H_0), formulated with the aim to reject it, and the alternative one (H_1), opposite to (H_0). It may happen that either the null hypothesis is reject when it should be accept or that the alternative hypothesis is accepted when it should be rejected. If the previous situation happen, two types of errors are produced, the *type I error* and *type II error*, respectively. The probability with which a *type I error* can occur is known with *level of significance* α, while the probability of making the other type of error is defined by β. On the other hand, the probability of accepting the null hypothesis when is true is called *specificity*, while the rejecting probability is *sensitivity*.

The common hypotheses that are tested regard either the mean or variance of a sample's group that should be compared with other samples populations. It is important to underline that a significant statistically difference depends on size of samples population (N), influencing both the choice of test and confidence intervals [36].

6.3 P-value

The *p-value* is an important parameter that is used to find out if the difference between samples of populations are either due to randomness introduced by sampling or to significant statistically differences. In order to evaluate the previous possibilities a comparison with the level of significance is executed. The α value is traditionally set equal to 5 % or 1 %, so if the p-value is lower than the previous threshold, it is possible to reject the H_0 hypothesis with confidence equal to $1 - \alpha$ [37].

6.4 Analysis of variance (ANOVA)

The *analysis of variance* (ANOVA) is a statistical technique that is used when two or more groups are need to be studied. More specifically, with this method is possible analyse the effect of one or more factors in groups of data. In the following lines a brief introduction to a particular type of ANOVA (*one way test*) will be provided, mainly referring to [38].

Let a and b two groups of observation. Each member can be defines as X_{ki}, with $k = 1, \ldots, a$ and $i = 1, \ldots, b$. Those two observations represent, for example, data recorded from subjects to which a different treatment has been applied. The mean of k^{th} groups can be obtained as

$$\bar{X}_k = \frac{1}{b}\sum_{i=1}^{b} X_{ki} \tag{33}$$

whereas the overall mean

$$\bar{X} = \frac{1}{ab}\sum_{i=1}^{b}\sum_{k=1}^{a} X_{ki} \tag{34}$$

In addition, is necessary to define the variation within a group, between groups and total, obtained as sum of the previous variations:

$$V = \sum_{i=1}^{b}\sum_{k=1}^{a}(X_{ki} - \bar{X})^2 \tag{35}$$

The variation within an between groups can be defined with V_W and V_B

$$V_W = \sum_{i=1}^{b}\sum_{k=1}^{a}(X_{ki} - \bar{X}_k)^2 \tag{36}$$

$$V_B = \sum_{i=1}^{b}\sum_{k=1}^{a}(\bar{X}_k - \bar{X})^2 \tag{37}$$

summing (36) and (36) an explicit form of (35) is obtained

$$\begin{aligned} V &= \sum_{i=1}^{b}\sum_{k=1}^{a}(X_{ki} - \bar{X})^2 = \sum_{i=1}^{b}\sum_{k=1}^{a}(X_{ki} - \bar{X}_k + \bar{X}_k - \bar{X})^2 \\ &= \sum_{i=1}^{b}\sum_{k=1}^{a}(X_{ki} - \bar{X}_k)^2 + \sum_{i=1}^{b}\sum_{k=1}^{a}(\bar{X}_k - \bar{X})^2 + 2\sum_{k=1}^{a}(\bar{X}_k - \bar{X})\sum_{i=1}^{b}(\bar{X}_{ki} - \bar{X}_k) \\ &= V_W + V_B + 2\sum_{k=1}^{a}(\bar{X}_k - \bar{X})\sum_{i=1}^{b}(\bar{X}_{ki} - \bar{X}_k) \end{aligned} \tag{38}$$

where the mist contribute is equal to zero. Moreover, data can be interpreted after fitting with a linear model. Indeed, X_{ki} can be modelled as

$$X_{ki} = \mu + \alpha_k + \epsilon_{ki} \tag{39}$$

where the linear random deviation from mean μ is represented through α_k, the treatment's effect, and ϵ_{ki}, a Gaussian noise. The previous parameters can be estimated through a minimization of the residual random noise

$$\begin{aligned} L(\mu, \alpha_i) = \sum_{i=1}^{b}\sum_{k=1}^{a} \epsilon_{ki}^2 = \sum_{i=1}^{b}\sum_{k=1}^{a} (X_{ki} - \mu - \alpha_i)^2 \\ \rightarrow [\mu, \alpha_i] = \underset{\hat{\mu},\hat{\alpha_i}}{\operatorname{argmin}} L(\hat{\mu}, \hat{\alpha_i}) \end{aligned} \tag{40}$$

that with the imposition of gradient L equal to zero produce

$$\mu = \bar{X} \qquad \alpha_i = \bar{X}_i - \bar{X} \tag{41}$$

If there are no significant variation between treatments the means $\mu_k = \mu + \alpha_k$ are all equal to population means μ, so the null hypothesis could not be rejected. If ϵ_{ki} is normally distributed with mean equal to zero and σ^2, the expected values of the variations can be obtained as follows

$$D_{it} = \begin{cases} E[V_K] = a(b-1)\sigma^2 \\ E[V_K] = (a-1)\sigma^2 + b\sum_{k=1}^{a} \alpha_k^2 \\ E[V] = (ab-1)\sigma^2 + b\sum_{k=1}^{a} \alpha_k^2 \end{cases} \tag{42}$$

while the distributions of the variations V, V_B and V_W can be defined by *chi square* distributions

$$\begin{aligned} \frac{V_W}{\sigma^2} &\sim \chi^2_{a(b-1)} \\ \frac{V_B}{\sigma^2} &\sim \chi^2_{a-1} \\ \frac{V}{\sigma^2} &\sim \chi^2_{ab-1} \end{aligned} \tag{43}$$

Supposing that the null hypothesis is false, it plausible to expect that from the second equation in (42) the estimation of variance between groups

$$\hat{S}_B^2 = \frac{V_B}{a-1} \tag{44}$$

has a mean equal to

$$E[\hat{S}_B^2] = \sigma^2 + \frac{b}{a-1}\sum_k \alpha_k^2 \tag{45}$$

that becomes more noticeable as the difference between groups increases. On the other hand, the estimated variance within groups (obtained from the first equation of (42)

$$\hat{S}_W^2 = \frac{V_W}{a(b-1)} \tag{46}$$

is a biased estimator of σ^2, independently if the means are equal. In conclusion, to evaluate if the null hypothesis can be accepted of rejected the *F distribution* is analysed

$$F_0 = \frac{\hat{S}_B^2/(a-1)}{\hat{S}_W^2/a(b-1)} \sim F_{a-1,a(b-1)} \tag{47}$$

In case of no differences between treatments, F_0 the α_k values are equal to zero otherwise $F > 1$. The null hypothesis is rejected if $F_0 > F_{\alpha,a-1,a(b-1)}$

When a number of groups is studied it may happen that ANOVA lead the researcher to reject that hypothesis, with an important leak of information: it is unknown which pair of groups has a significant statistically difference. In order to avoid this problem *post-hoc* tests are used, with which is possible to detect which couple of sub-groups produce those differences. For example, in a *t-test* (not treated in this chapter) the significance level α determinates the probability above which there are not incorrect findings, if the null hypothesis is true. On the other hand, that is correct if only two couples of distributions are studied. Indeed, if more groups are considered, there are $n = k(k\text{-}1)/2$ pairs to be studied, with a probability of accepting correctly the H_0 hypothesis equal to $P{=}(1\text{-}\alpha)^n$. As a consequence, if the number of pairs increases, the probability of accepting the null hypothesis (when it is true) decreases. So the high number of couples increases the probability of making type I error. A possible solution is use the *Bonferroni correction*. This method decreases the level of significance of the test in each comparison to α/n, then reducing the probability of making a type I error. This is possible since the first order approximation of P is

$$P = (1-\alpha)^n \approx 1 - n\alpha \tag{48}$$

6.5 Kruskal–Wallis test

In inference statistic there are two categories of tests: *parametric* and non-*parametric* methods. Parametric methods are a group of statistic technique that used data with

normal distribution, same variance, randomly drawn from the population and with observations within the groups that are independent from each other. Another class of methods include the non-parametric techniques, which do not require stringent requirements on data, as parametric ones. Indeed, data can be not have normal distributions, small samples can be used, outliers can be considered and do not require limited assumption on data format [39]. Since data to be analysed does not have a Guassian distribution, a different form of ANOVA is necessary to study the results of the experiment. So in the following lines a non parametric alternative to ANOVA and will be presented and then used for the analysis of results: the *Kruskal-Wallis test*.

This method, known also as Kruskal–Wallis H test, is a non-parametric technique used to analyse whether samples originate from the same distribution [40, 41]. It can be considered as an equivalent test to one-way analysis of variance (ANOVA), where the medians of the groups are compared. The test do not uses numeric values to compute the statistic, since ranks of the data are considered. More specifically, their are obtained sorting data from smallest to largest in the groups and then indexing with a number this order [42].

The H statistic is obtained with the following relation

$$H = \frac{12}{N(N+1)} \sum_{i=1}^{k} \frac{R_i^2}{n_i} - 3(N+1) \tag{49}$$

where k is the number of sample, n_i the quantity of observations in the i^{th} sample, N the total number of observations and R_i the sum of ranks in the i^{th} sample. The degrees of freedom, *df*, are determined by

$$df = k - 1 \tag{50}$$

Results of H statistic can be compared with a table of critical values to detect study groups for significant differences. If k or n_i exceed the limit of tables available, then a sample approximation may be performed using tables with χ^2 distributions.

It may happen that values studied have ties, so a correction in (49) is necessary. More specifically, the relation (49) should be divided by

$$C_H = 1 - \frac{\sum (T^3 - T)}{N^3 - N} \tag{51}$$

where C_H is the ties correction and T the number of values from a set of ties. So the general expression of the H test is

$$H = \frac{\frac{12}{N(N+1)} \sum_{i=1}^{k} \frac{R_i^2}{n_i} - 3(N+1)}{1 - \sum T / N^3 - N} \tag{52}$$

that could be rewritten as

$$H = \frac{N-1}{N} \sum_{i=1}^{k} \frac{n_i[\bar{R}_i - (N+1)/2]^2}{(N^2-1)/12} \tag{53}$$

where $\bar{R}_i$ is the mean of n_i ranks in i_{th} sample.

The previous statistic determinates significant differences if H value is high. On the other hand, if low values of H are registered, the researcher can accept the null hypothesis. As ANOVA method, a post-hoc test is necessary to detect which sample pairs are significantly different. So the Bonferrori correction could be used as well.

6.6 Wilcoxon signed rank test

The *Wilcoxon signed rank test* is a method that belongs to non parametric class used for for comparing two samples that are related [43]. This test is the non-parametric equivalent to Student's test. The formula for Wilcoxon T-test can be summarized as

$$T = \text{smaller of } \sum R_+ \text{and } \sum R_- \tag{54}$$

where the ranks with positive and negative differences are included in R_+ and R_-, respectively.

Once the T statistic is computed an analysis for significance should be done. For this aim either tables of critical values can be used or a large sample approximation can be performed if the pairs n exceeds available tables. In addition, for large samples, a z-score and tables with normal distribution should be used to obtain a critical region of z-scores. In order to find the z-score of Wilcoxon signed rank test in the case of large samples, the following formulas should be used

$$\bar{x}_T = \frac{n(n+1)}{4} \tag{55}$$

where $\bar{x}_T$ is the mean and n is the number of matched paired considered in the statistic,

$$s_T = \sqrt{\frac{n(n+1)(2n+1)}{24}} \tag{56}$$

defining s_T as the standard deviation, is now possible to obtain the z^* score for an approximation to normal distribution using the T statistic obtained with (54)

$$z^* = \frac{T - \bar{x}_T}{s_T} \tag{57}$$

Chapter 7

OSTF and Different Boundary Conditions

In this chapter the OSTF is applied to EMG data of remaining subjects. Performances are evaluated analysing 4 seconds of EMGs divided into epochs of 500 ms. Since OSTF can be trained and then used with different sources (monopolar, SD and DD signals), each case has been considered. Temporal order of the filter and delay between samples has been chosen through a tuning on test set. The performances of presented filter has been evaluated through the error in ARV and PSD estimation when crosstalk is summed to EMG. By doing so, each subject produces a set of errors, because five different levels of forces has been explored and multiple epochs are analysed. In order to summarize each subject with an unique number, the average error has been calculated averaging the errors obtained in different epochs and co-contractions conditions. In the following experiments *Kruskal and Wallis* tests (KW) with *Bonferrori* correction has been used to detect significant statistically differences in the samples studied. In abscissa axes of the following graphs is possible to observed labels describing which source has been used, while in ordinate labels a description of which parameter and set of columns used is reported.

7.1 Spatial filter dimension

In this test a different dimension of the spatial filter has been evaluated. More specifically, the OSTF has been tested with 3 to 5 rows of electrodes. In order to better understand the combinations used for the test a scheme in Fig. 7.1 is provided. During the training phases, OSTF has been trained with signal containing contractions of target muscles at different force levels, each lasting 2 seconds. KW tests on results (Fig. 7.1) does not show significant statistically differences.

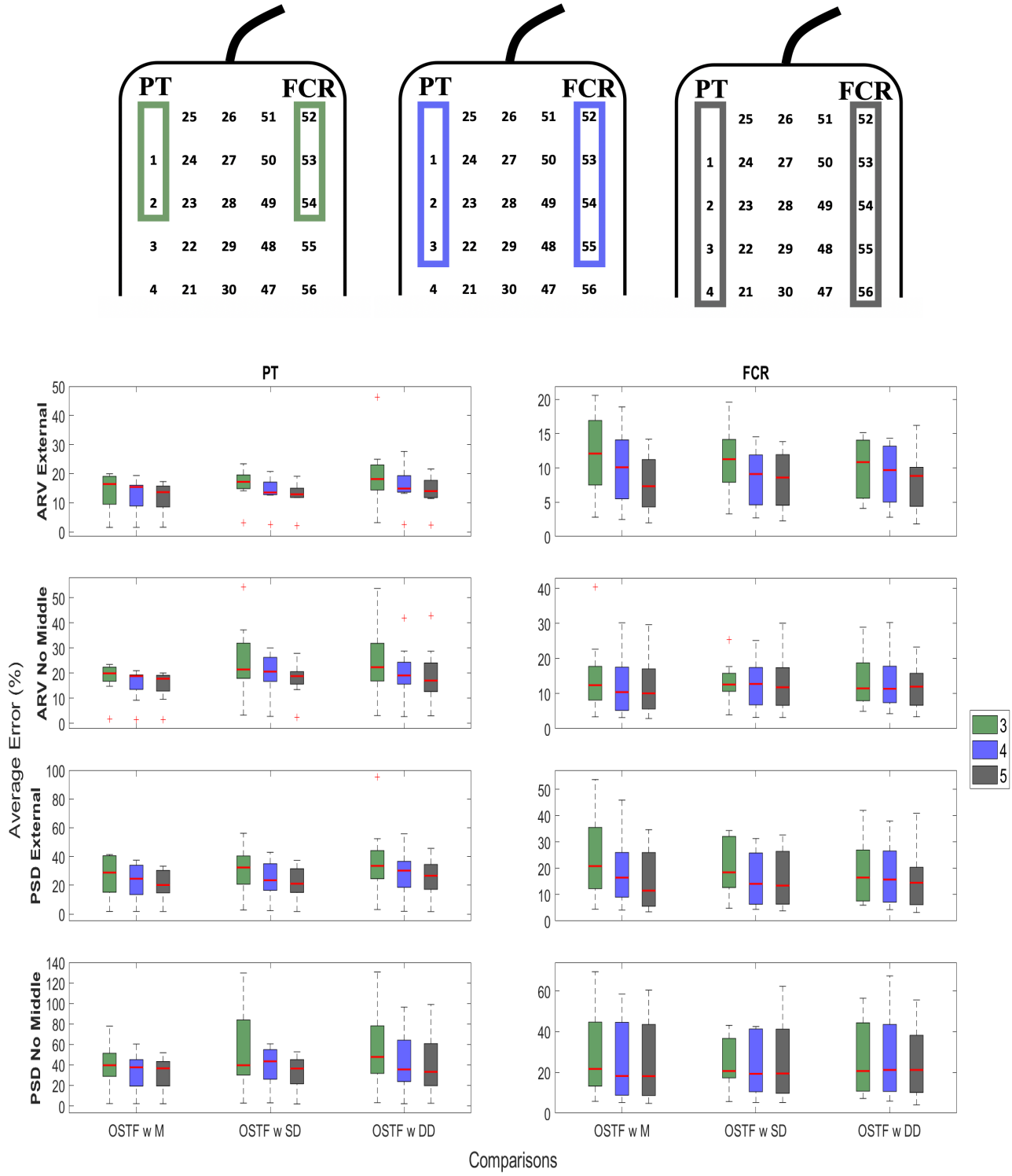

Figure 7.1: *Average error in ARV and PSD estimation with different number of electrodes included as input.*

7.2 Bigger electrodes

As reported in Chapter 2, electrodes used for electromyography can be of different type and shape. The aim of this tests is evaluate OSTF performances when bigger electrodes are used. Those sensors are used in several applications, such as gait cycle analysis [12].

In Fig. 7.2 is possible to observe how bigger electrodes has been simulated from a matrix of sensors. More specifically, each new electrode has been obtained summing the signals recorded on the channels included in the coloured squares in the previous figure. By doing that, the IED distance has changed, becoming two times the original one (from 8 to 16 mm). Since the matrix structure has been changed, from now on the configuration that includes only the "new" external electrodes will be called *"No Middle"*, whereas the configuration with external electrode an the central column (simulated through an array of rectangular electrodes) will be called *"All"*. OSTF has been trained with signal containing contractions of target muscles at different force levels, each lasting 2 seconds. A different number of electrodes as input has been evaluated. In Fig. 7.2, is possible to observe the configuration *"No Middle"* with two and three electrodes on each muscle. KW tests on results (Fig. 7.3) does not show significant statistically differences.

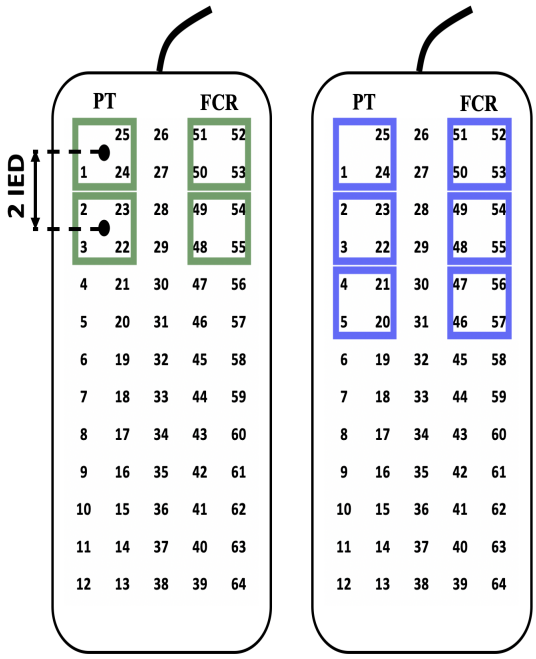

Figure 7.2: *Graphical representation of simulated bigger electrodes included in this test.*

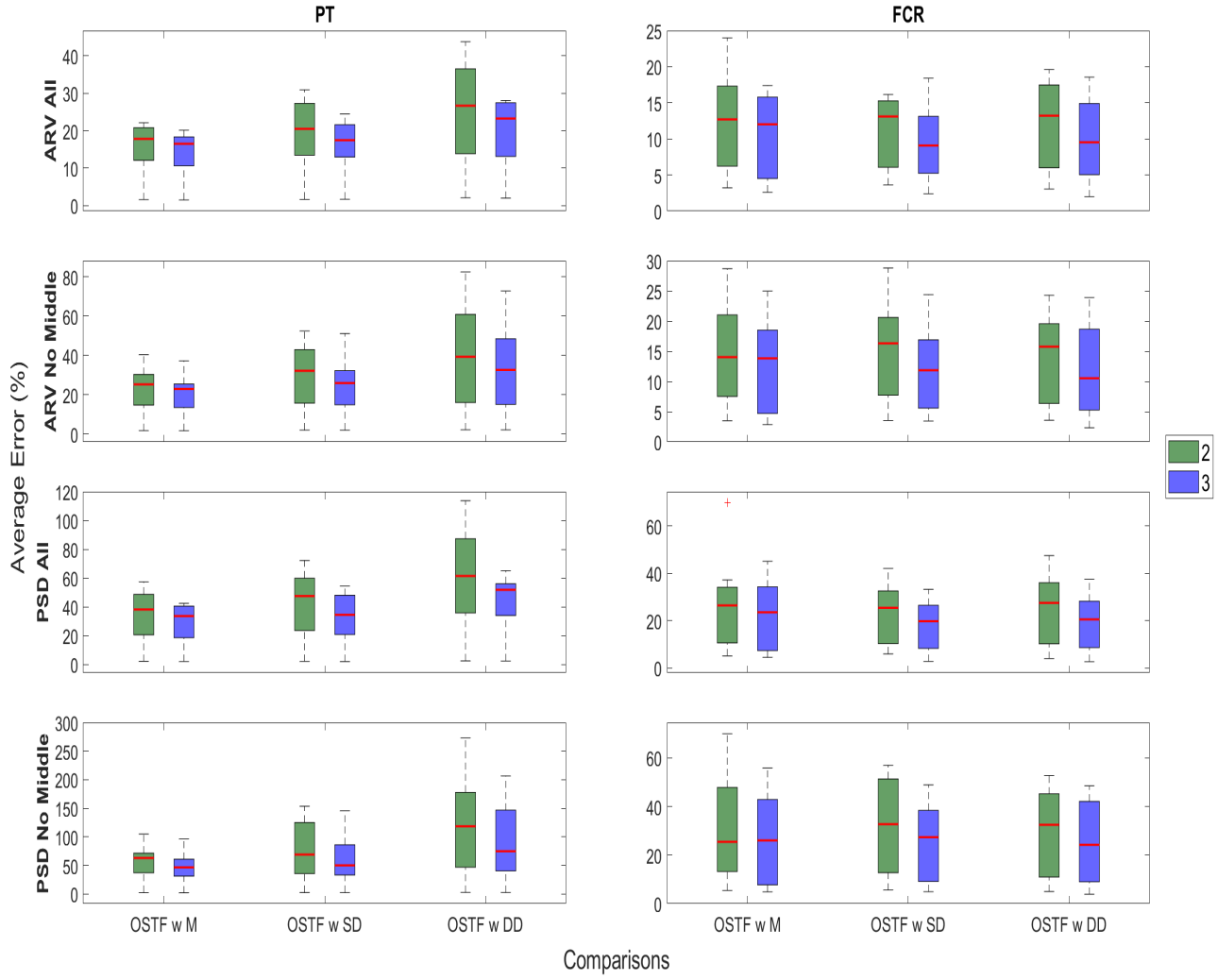

Figure 7.3: *Average error in ARV and PSD estimation with different number of bigger electrodes included as input.*

7.3 Training with selective contractions of different temporal length

The training phase in previous tests has been execute with signals obtained concatenating contractions at different force levels, each lasting 2 seconds. In this experiment the length of each contraction has been changed.

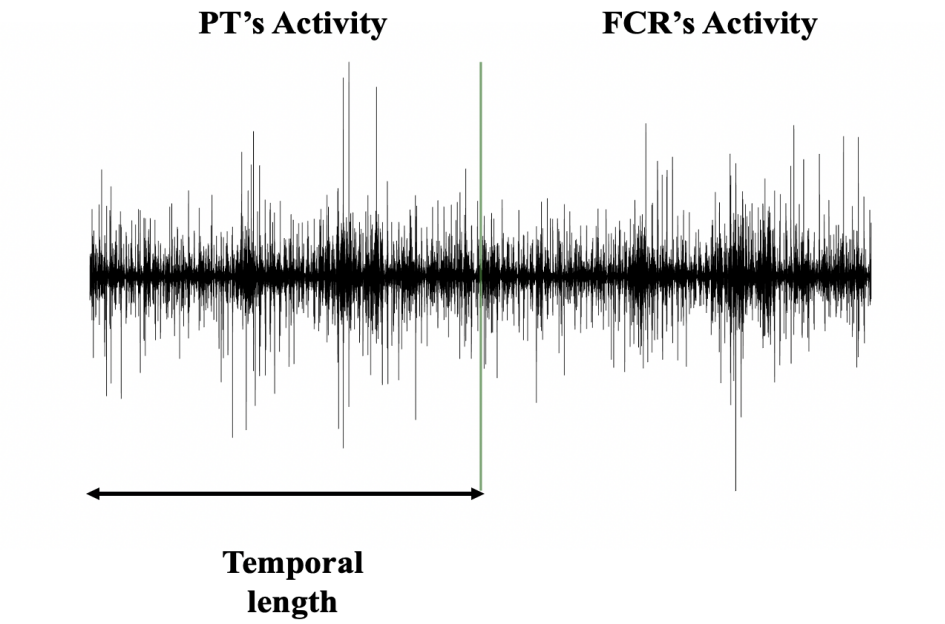

Figure 7.4: *Concatenated contractions at a specific force level.*

Signals with different lengths has been explored, more specifically, contractions of 125, 250, 500, 1000 and 2000 ms were used. This test has an important objective: verify if OSTF is capable to generalize crosstalk reduction on "new data" even when the training phase is really rapid. This aspect could be useful in clinical application, especially in EMG recording of patients that could not hold a muscular contraction for a long time, due to several factors and diseases.

In this test the number of electrodes included in longitudinal direction of the fibre are four. Temporal order and delay between samples are chosen through the optimization on test set, made up of concatenated contractions at different force levels each lasting 2 seconds. KW tests on results (Fig. 7.5) does not show significant statistically differences.

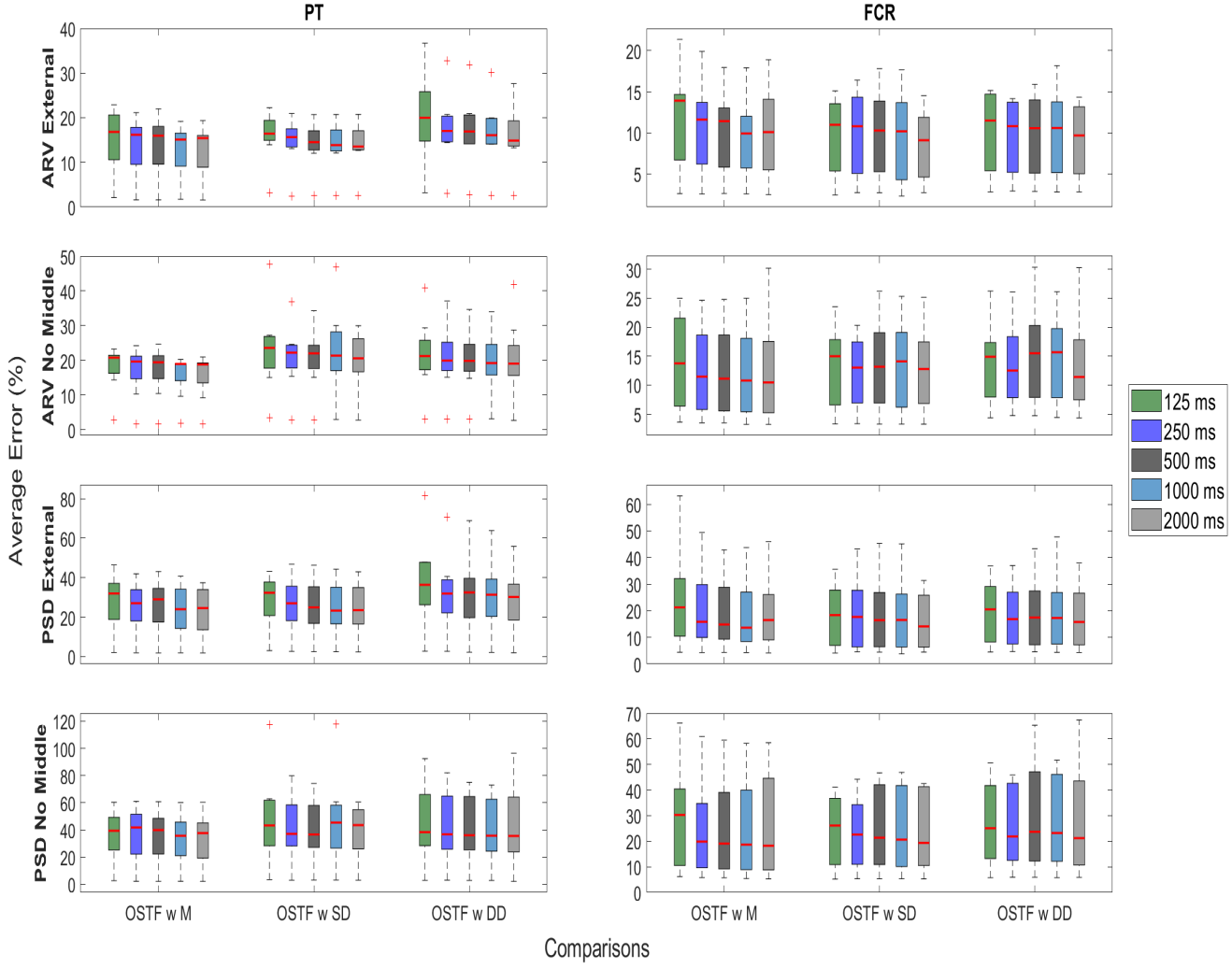

Figure 7.5: *Average error in ARV and PSD estimation with different training phase. The number of electrodes on each muscle is set equal to four.*

7.4 Training with two selective contractions

The presented test has the objective to evaluate method's performances using only two selective contractions for training phase, each lasting 2 seconds. The importance of this test is relevant, because it may happen that only one selective contraction per muscle can be produced by the subject.

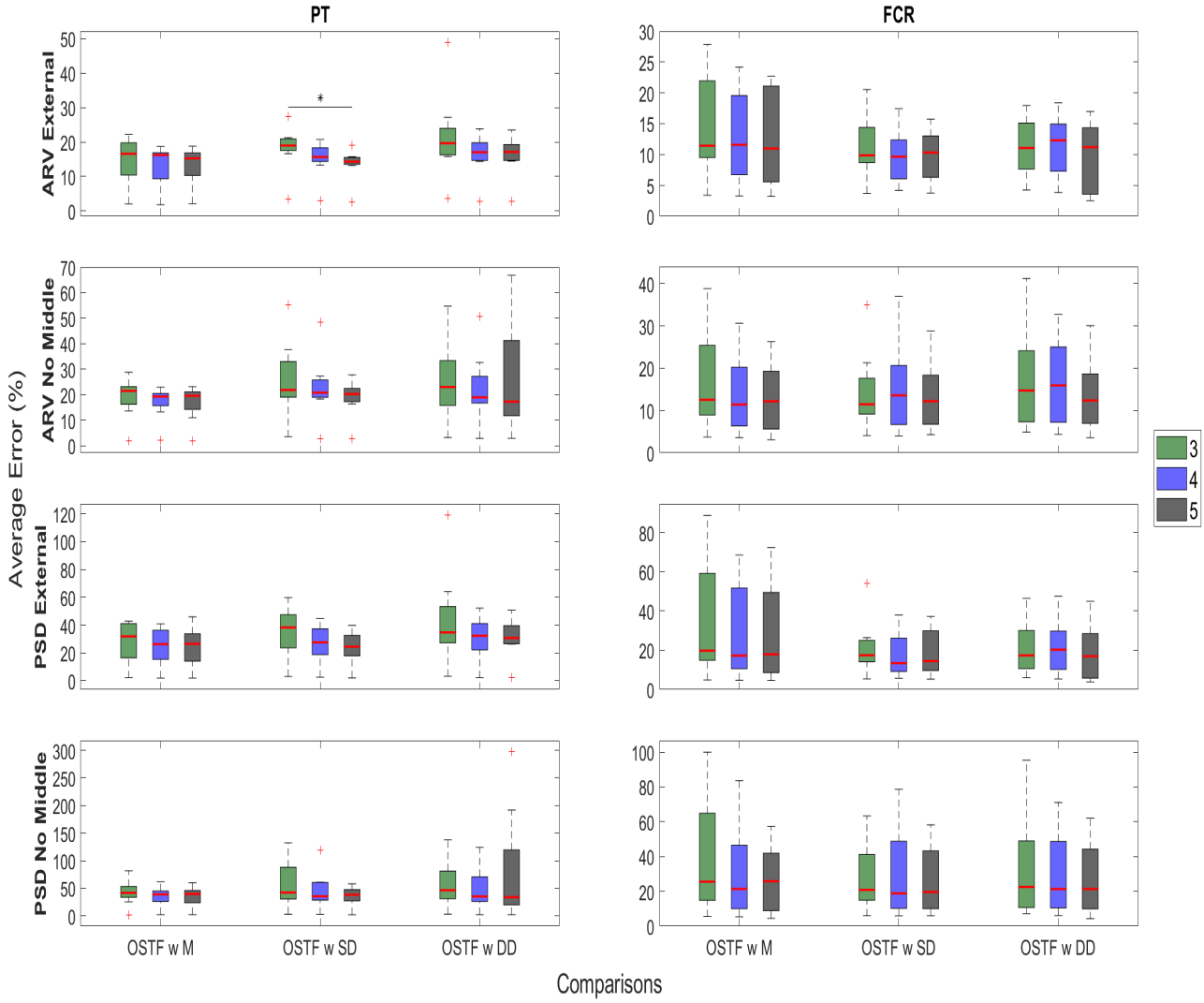

Figure 7.6: *Average error in ARV and PSD estimation with two concatenated contractions as training and different number of electrodes included as input. (* $p < 0.05$, ** $p < 0.01$)*

Since signals used in the previous tests include a certain number of concatenated contractions, for each muscle has been chosen the ones with highest SCR. More specifically, the test set includes contractions with all the force levels. In addition, four different channels for electrodes has been used as input.

Results show that the method works properly even in this "restricted" training conditions. There is only one statistically difference that has been recorded: in ARV External condition, OSTF w SD between 3 and 5 electrodes on each muscle.

7.5 CV estimation

As reported in Chapter 2, the velocity with which the AP travels from IZ is an important EMG index, used in several clinical applications. The estimation of this parameter is not trivial, indeed it is strongly dependent on how the EMG signals has been recorded; for example, if electrodes are not perfectly aligned with fibres of target muscles, it is not possible to estimate that parameter. Moreover, the issue of crosstalk generate bias in CV estimation. In order to avoid this problem, the OSTF has been tested as solution to reduce crosstalk in CV estimation.

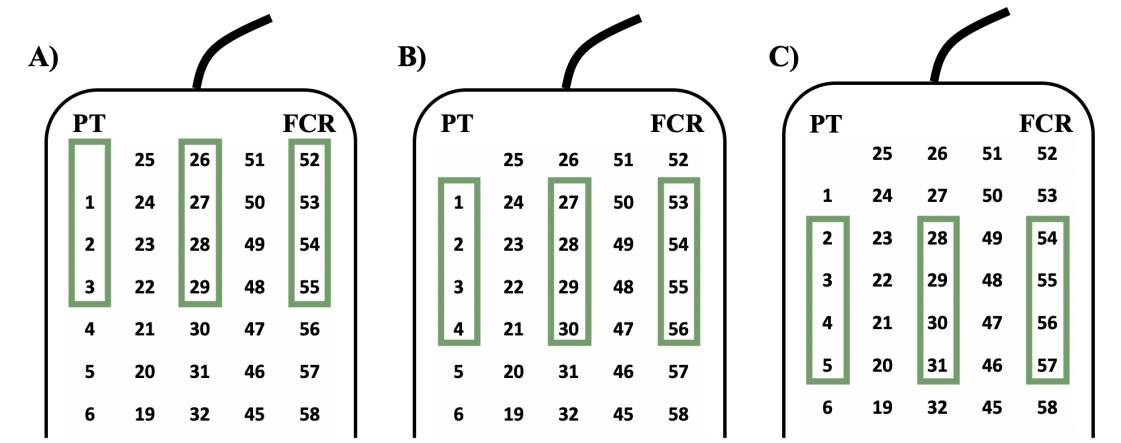

Figure 7.7: *CV estimation from surrogates. Each electrodes configuration in the figure represents a condition from which the OSTF produce a surrogate. The CV is then calculated from the obtained OSTF outputs.*

Since the OSTF produce a single output from a certain number of channels, the signals used to estimate this EMG index are obtained applying the OSTF to channels one IED away from the initial "block" of electrodes, assuming that the previous outputs are copies of the same signal but delayed. In order to better understand this idea, Fig 7.7 is provided. Indeed, is possible to appreciate that the "block" of electrodes on part A is shifted by one IED in part B, and by two IED in part C. OSTF has been tested with different sources and number of channel

as input, while the training phase has been conducted in the same manner as the previous experiments: optimization of filter's parameters on test set. From the obtained surrogates CV has been calculated through maximum likelihood estimation, described in Chapter 2.

Unfortunately the application of OSTF for CV estimation does not provide good results, indeed waveforms obtained does not keep a stable form preventing an appropriate estimation of the delay between them. Moreover, the presence of innervation zones under the electrodes chosen as input could produce surrogates propagating in opposite directions, determining the CV estimation very difficult.

Chapter 8

Analysis of Results and Conclusion

In this last chapter the analysis of results will be provided. All the graphics at which the following discussion refers are available in Appendix A.

The first experiment, in which a different dimension of spatial filter has been explored, demonstrates that OSTF, regardless by the muscle and parameter studied, has always lower average estimation error if compared with traditional filters (Wilcoxon signed rank test with $p < 0.01$ or $p < 0.05$ according to the cases), as showed in Fig. A.1. Paired comparison between distributions is reported in Fig. A.2. Results show that there are not always present a statistically significant differences, however in most of the cases is preferable to use an higher number of channels on each muscle for a lower average estimation error (Wilcoxon signed rank test with $p < 0.01$ or $p < 0.05$ according to the cases). In addition, as reported in Fig A.3, is possible to observe that in most of the cases using more columns of electrodes is preferable (Wilcoxon signed rank test with $p < 0.01$ or $p < 0.05$ according to the cases). Estimation errors using OSTF with different sources as input does not show statistically significant differences in the majority of the cases, as reported in Fig. A.4.

Results of the second test, in which the effect of bigger electrodes has been explored, demonstrate that OSTF provide an average error in ARV estimation, always lower than SD and DD filters (Wilcoxon signed rank test with $p < 0.01$); as reported in Fig. A.5. In PSD estimation for PT, when external electrodes and the central ones has been considered, OSTF seem to work better than SD and DD filters (Wilcoxon signed rank test with $p < 0.01$ or $p < 0.05$ according to the cases), with the exception of *No Middle* configuration where no statistically significant differences has been detected when OSTF w DD are studied and when OSTF w SD - 2 is compared with DD. When FCR has been chosen as target muscle, the estimation error obtained using OSTF is lower in most of the cases if compared with SD and

DD (Wilcoxon signed rank test with $p < 0.01$ or $p < 0.05$ according to the cases); the exceptions in which no statistically significant differences has been detected are: OSTF w DD - 2 compared with SD (*All* and *No Middle* configuration) and OSTF w SD - 2 compared with SD (*No Middle* configuration). A paired comparison between distributions of value obtained with two or three rows of electrodes on each muscle is available at Fig. A.6. Results show that in most of the cases OSTF's surrogate obtained with an higher number of electrodes on each muscle provides better performances (Wilcoxon signed rank test with $p < 0.01$ or $p < 0.05$ according to the cases), as the previous experiment. Moreover, for PT is always preferable to use more columns of electrodes to obtain lower average estimation error (Wilcoxon signed rank test with $p < 0.01$ or $p < 0.05$ according to the cases), as reported in Fig. A.7. FCR show a similar behaviour, with the exception OSTF w M - 2 and OSTF w DD - 2. In addition, Fig. A.8 show a comparison between distributions of values obtained with OSTF using different sources as input: when PT is target muscle, better performances can be obtained when raw monopolar signals are used as input (Wilcoxon signed rank test with $p < 0.01$ or $p < 0.05$ according to the cases). No statistically significant differences has been detected in FCR for the presented test.

Results of the experiment with objective the evaluation of OSTF performances using a training set made up of contractions at different temporal length are reported in Fig. A.9. They demonstrates that OSTF has better performances when compared with SD and DD filters, regardless by the temporal length of concatenated contractions (Wilcoxon signed rank test with $p < 0.01$ or $p < 0.05$ according to the cases), with the following exceptions that do not provide statistically significant differences (all belonging to FCR, *No Middle* configuration): OSTF w M - 125 ms and OSTF w DD - 500 and 1000 ms both compared with SD. A paired comparison between distributions obtained with contractions at different length is available at Fig. A.10. Results show that in most of the cases statistically significant differences regard the first two distributions with the reaming ones in each group of boxplots. No other common trends can be appreciated from available data. Referring to Fig. A.11, it is possible to assert that in most of the cases is preferable to use three columns of electrodes instead of two (Wilcoxon signed rank test with $p < 0.01$ or $p < 0.05$ according to the cases). No statistically significant differences has been recorded in FCR distributions when OSTF w M has been used. A paired comparison between OSTF distribution obtained with different sources is available Fig. A.10. OSTF used with raw monopolar has lower estimation error if compared with OSTF applied on SD signals (Wilcoxon signed rank test with $p < 0.01$ or $p < 0.05$ according to the cases). Statistically significant differences can be appreciated in PT when ARV - *No Middle* configuration are studied. In addition, a common trend can be appreciated when FCR is analysed and contraction with length 500, 1000 and 2000 ms are considered. More specifically is possible to appreciate that in most of the cases OSTF applied to SD produce a lower average

error than the case in which DD signals are used (Wilcoxon signed rank test with $p < 0.05$).

The fourth experiment has been conducted with the aim to evaluate OSTF performances when only two selective contractions has been used as training set. Three different sources (raw monopolar, SD and DD signals) and three configuration (3,4 or 5 electrodes per muscle) has been studied. Results are reported in Fig. A.13, where it is possible to appreciate that for PT the OSTF performs better than SD and DD both for ARV and PSD estimation (Wilcoxon signed rank test with $p < 0.01$), with the exception of OSTF w DD - 5, where no statistically significant differences has been detected (both in SD and DD comparison). On the other hand, when FCR has been chosen as target muscle and ARV as parameter to study, OSTF provides better performances than SD and DD (Wilcoxon signed rank test with $p < 0.01$ or $p < 0.05$ according to the cases), with the exception OSTF w DD - 3 and 4 in *No Middle* configuration. Indeed, in those case no statistically significant differences can be appreciated when compared to SD. If PSD need to be studied and FCR has been chosen as target muscle is preferable to use OSTF in most of the cases (Wilcoxon signed rank test with $p < 0.01$ or $p < 0.05$ according to the cases). No statistically significant differences can be appreciated in the following cases: OSTF w M - 3 and 5 compared with DD (*External* configuration), OSTF with M - 3 compared with SD and DD and OSTF w DD - 4 compared with SD. A paired comparison between error distributions (Fig. A.10) does not show a clear evidence of which combination of rows provides better performances between possibilities. Fig. A.15 demonstrates that in most of the cases is preferable to use more columns of electrodes (Wilcoxon signed rank test with $p < 0.01$ or $p < 0.05$ according to the cases). OSTF applied to different sources produce surrogates whose estimation error do not show significant statistically differences in the majority of the cases (referring to Fig. A.16). In addition a paired comparison with results of test one has been executed, in order to evaluate if more selective contractions at different force level improve OSTF performances or not (Fig. A.17). In most of the cases is preferable to use conditions of test one (Wilcoxon signed rank test with $p < 0.01$ or $p < 0.05$ according to the cases). Indeed, by doing that, a lower average estimation error is obtained.

The last experiment has the aim to evaluate if OSTF can provide a not biased CV estimation, since the method works properly in simulation conditions [25]. Unfortunately, CV estimation has been critical in this experimental study. Reasons of those results can be different, for example, because of the small dimensions of studied muscles a perfect alignment to muscular fibres was complex. Moreover the presence of IZ in the set of electrodes chosen as input to OSTF can generate surrogates that do not propagate in the same direction as the ones obtained with a different set of channels.

In conclusion, OSTF can be considered as a good substitute to traditional spatial filters in estimation of amplitude and spectral indexes when data corrupted by

crosstalk are analysed. It can be applied to different type of signals and set of electrodes, from small to big ones. The training phase, considered as the most important phase in OSTF application, can be conducted with few epochs of signals, each at different force level, enabling, for example, the application of this method to subjects that can not hold contraction at high force levels for long time.

As limitation, the method works properly when subject perform selective contractions; that could not be trivial depending on muscles involved. Moreover, this method can be applied to muscles that are anatomically located one close to the other. For example, it can not be applied to EMG recorded on bicep and triceps, because the presence of other muscles between them could be sources of crosstalk that can not be classified properly. In addition, significant differences between validation set and training-test sets could produce error in crosstalk reduction, generating wrong surrogates. For example, if a spike (due to a source interference) has been recorded and included as signal for OSTF, the method will emphasize it non considering the remaining signal. Moreover, because of noisy data, statistical variability and sample of limited dimension, some statistically significant differences can not be appreciated.

Future studies can be conducted with more subjects as volunteers avoiding the issues presented before and with the objective to evaluate OSTF performances in dynamic contractions.

Appendix A

Results of Statistical Analysis

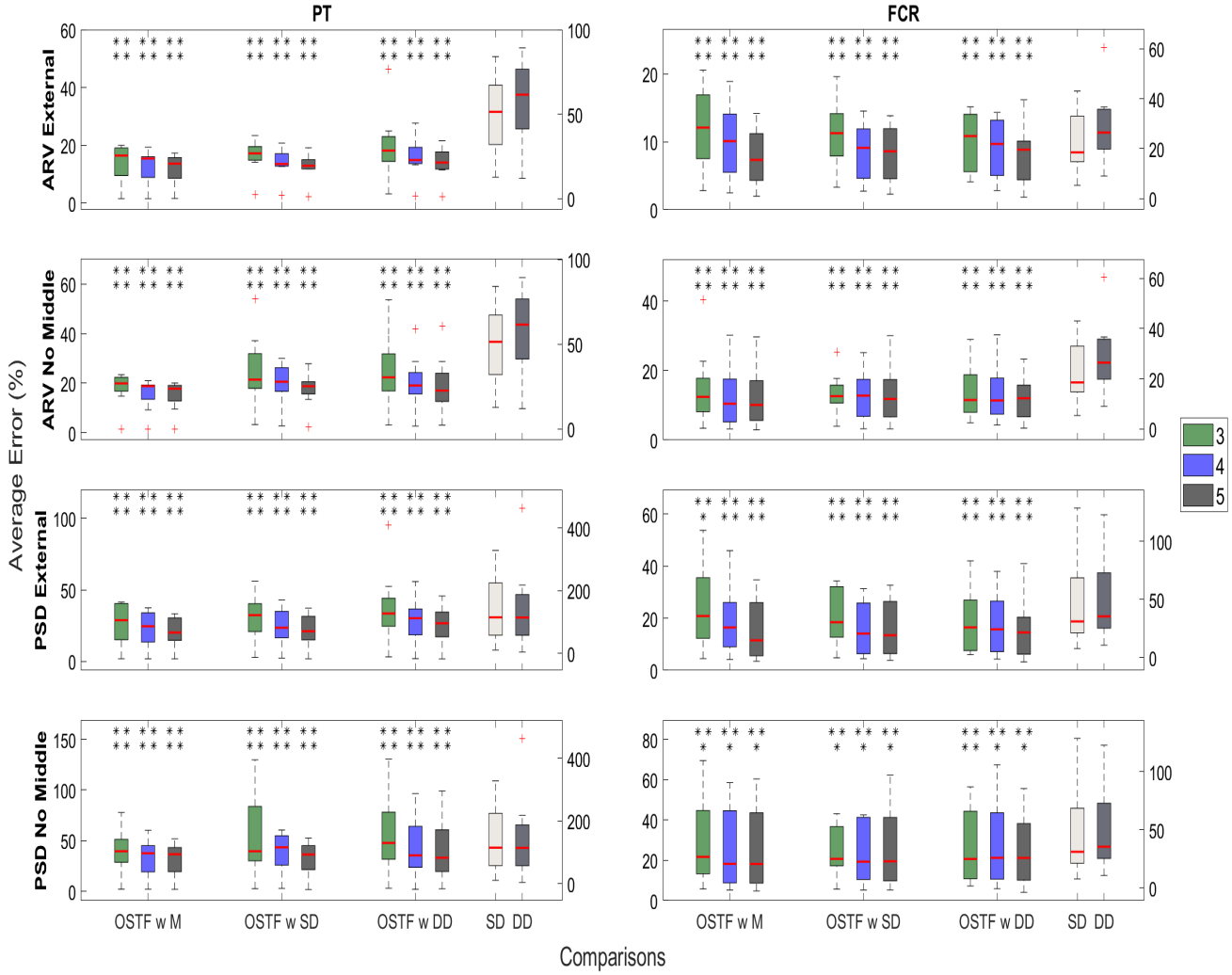

Figure A.1: *Paired comparison between distributions of average estimation errors obtained with OSTF using a different spatial dimension and traditional filters (SD and DD). The markers on boxplots identifies statistically significant differences with SD (bottom) and DD (top). (* $p < 0.05$, ** $p < 0.01$)*

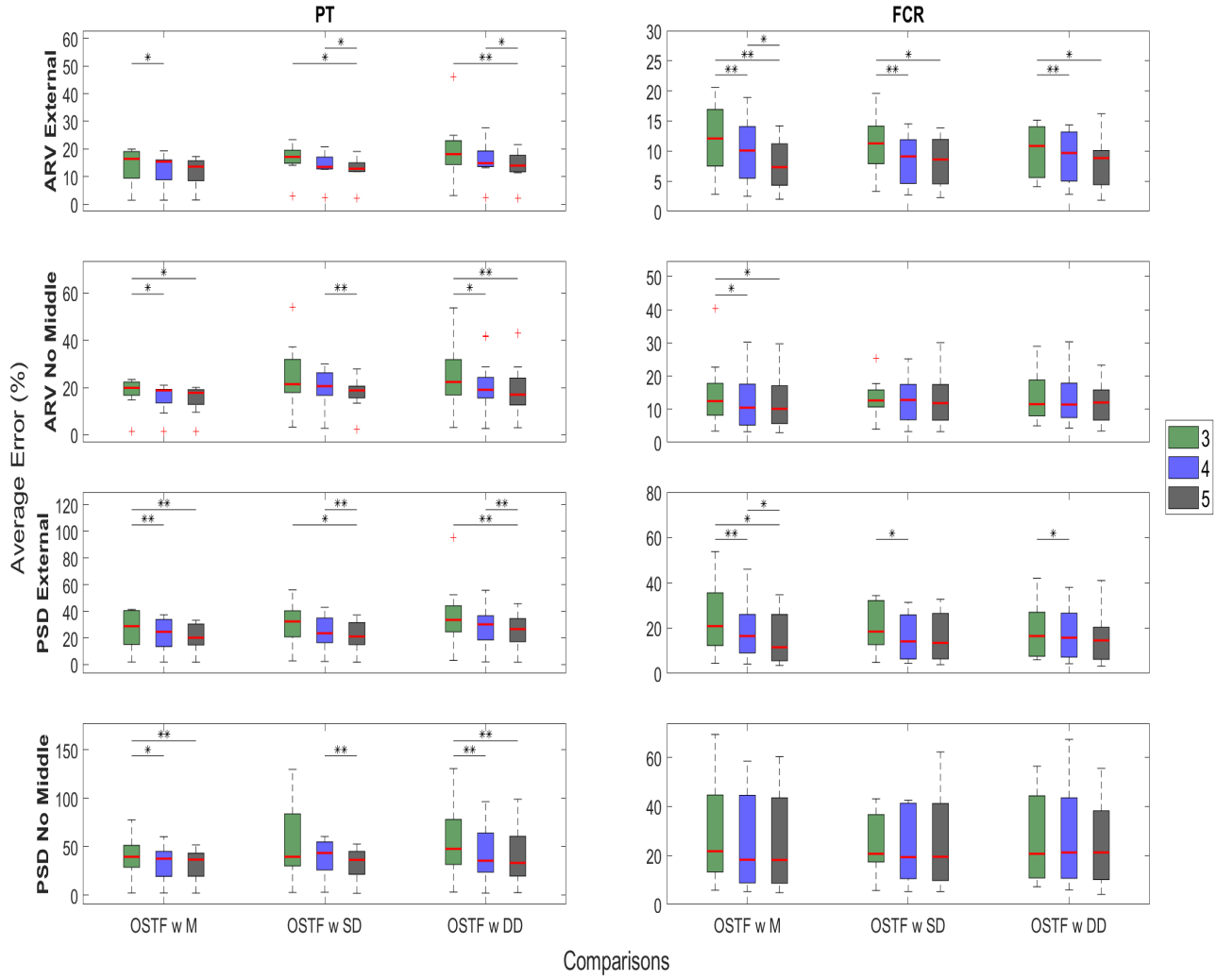

Figure A.2: *Paired comparison between distributions of average estimation errors obtained with OSTF using a different spatial dimension and same sources as input. (* $p < 0.05$, ** $p < 0.01$)*

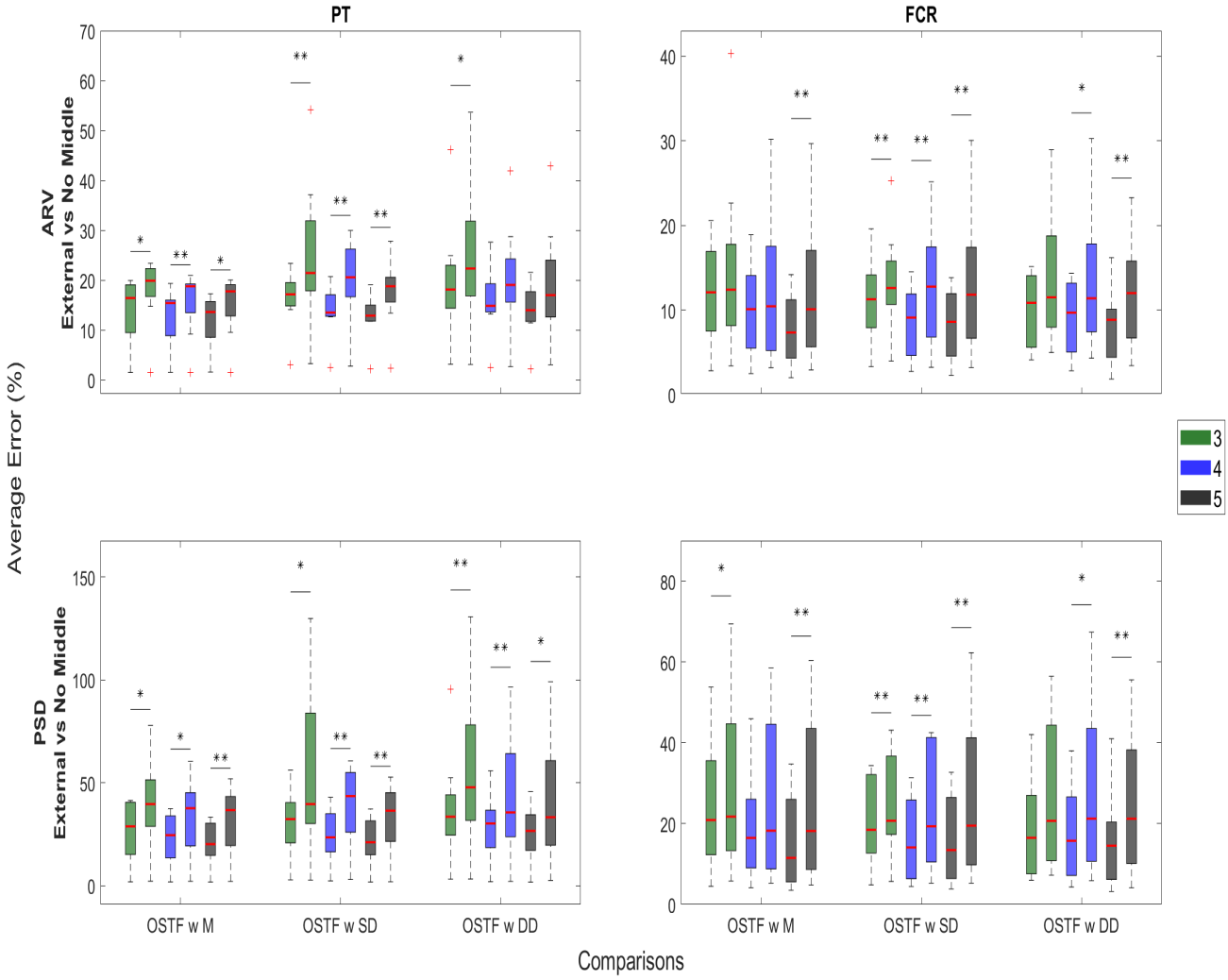

Figure A.3: *Paired comparison between distributions of average estimation errors obtained with OSTF using two or three columns; different spatial dimensions has been taken into account too. (* $p < 0.05$, ** $p < 0.01$)*

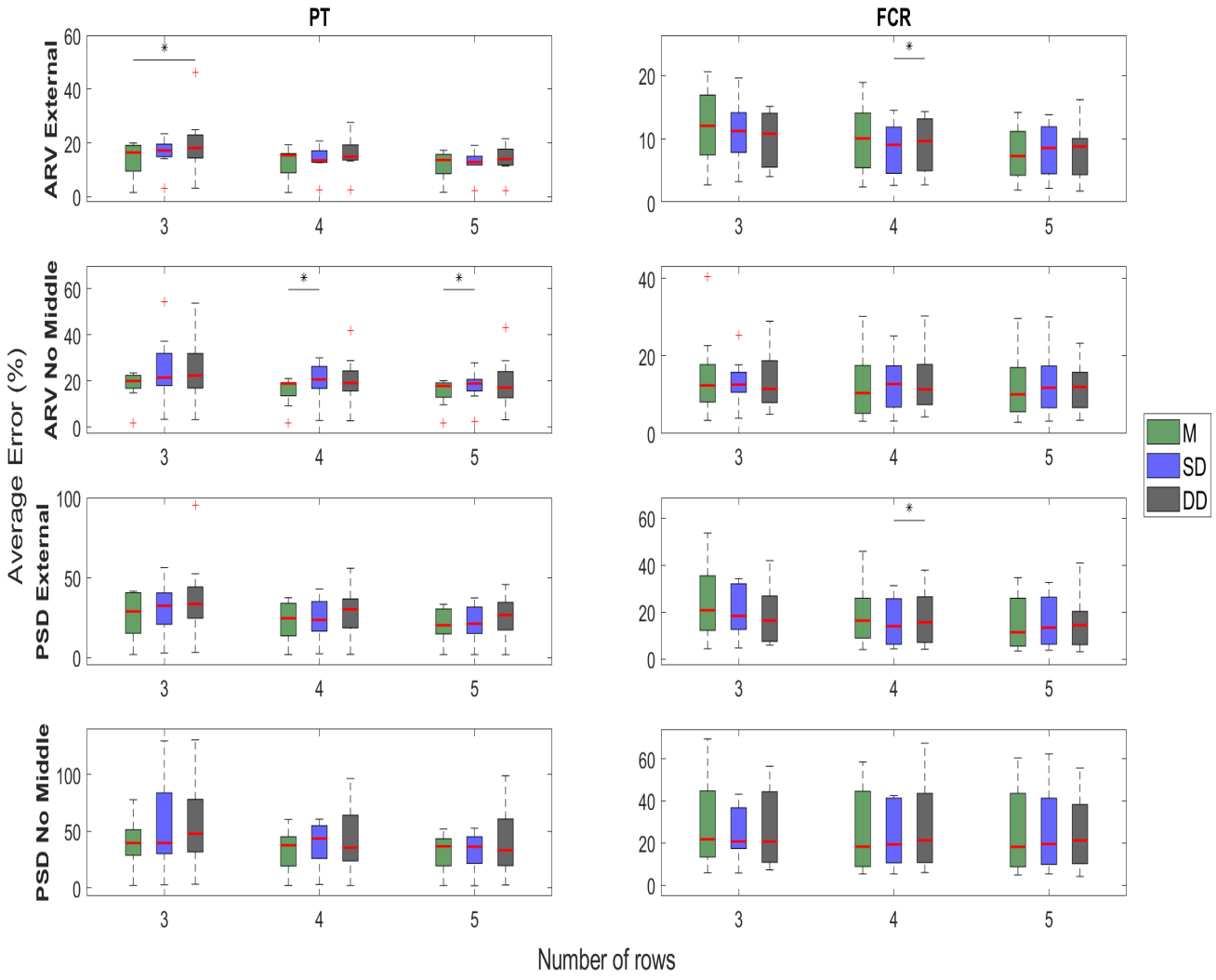

Figure A.4: *Paired comparison between distributions of average estimation errors obtained with OSTF using different sources. (* $p < 0.05$, ** $p < 0.01$)*

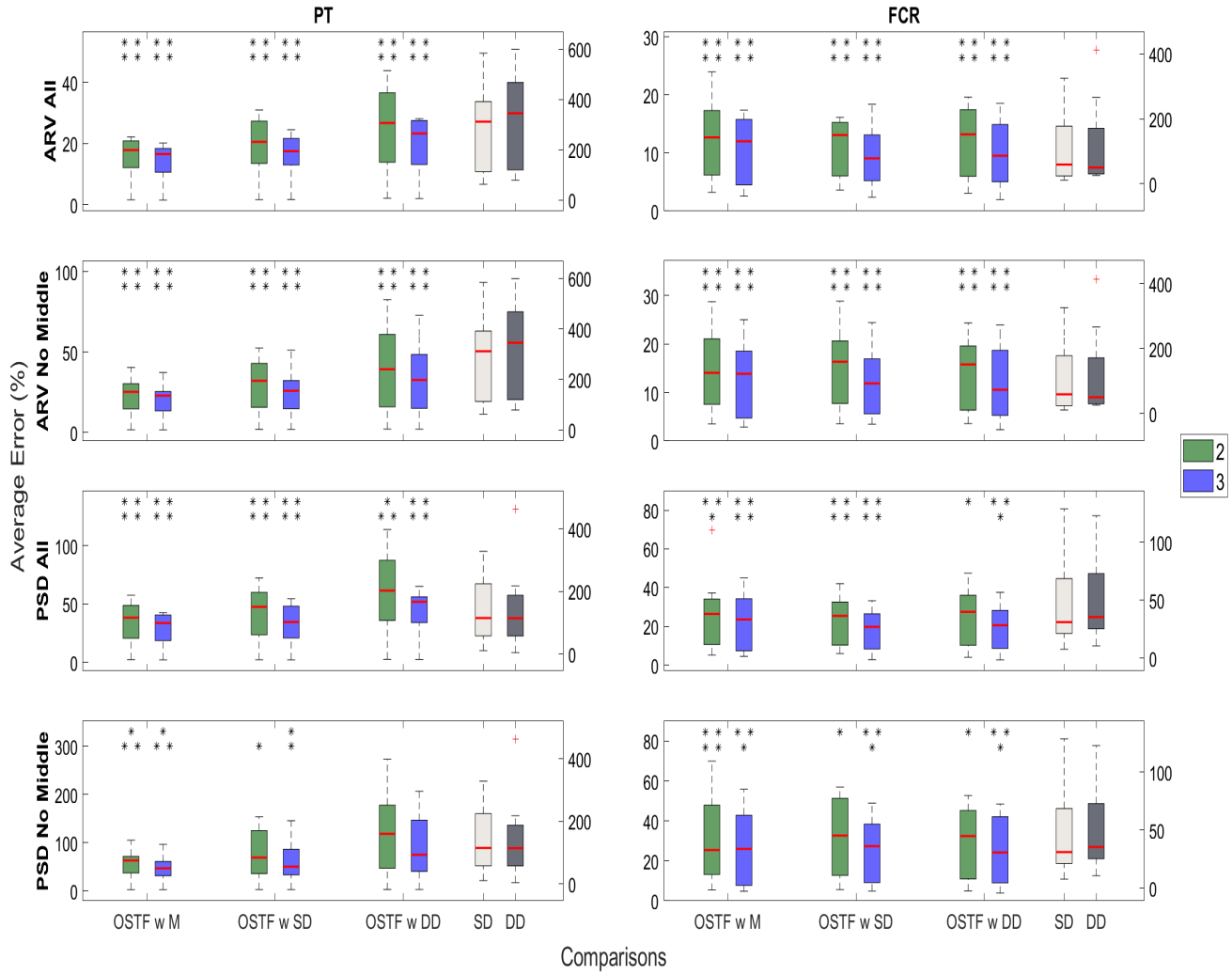

Figure A.5: *Paired comparison between distributions of average estimation errors obtained with OSTF using a different spatial dimension and traditional filters (SD and DD). Bigger electrodes has been simulated. The markers on boxplots identifies statistically significant differences with SD (bottom) and DD (top). (* $p < 0.05$, ** $p < 0.01$)*

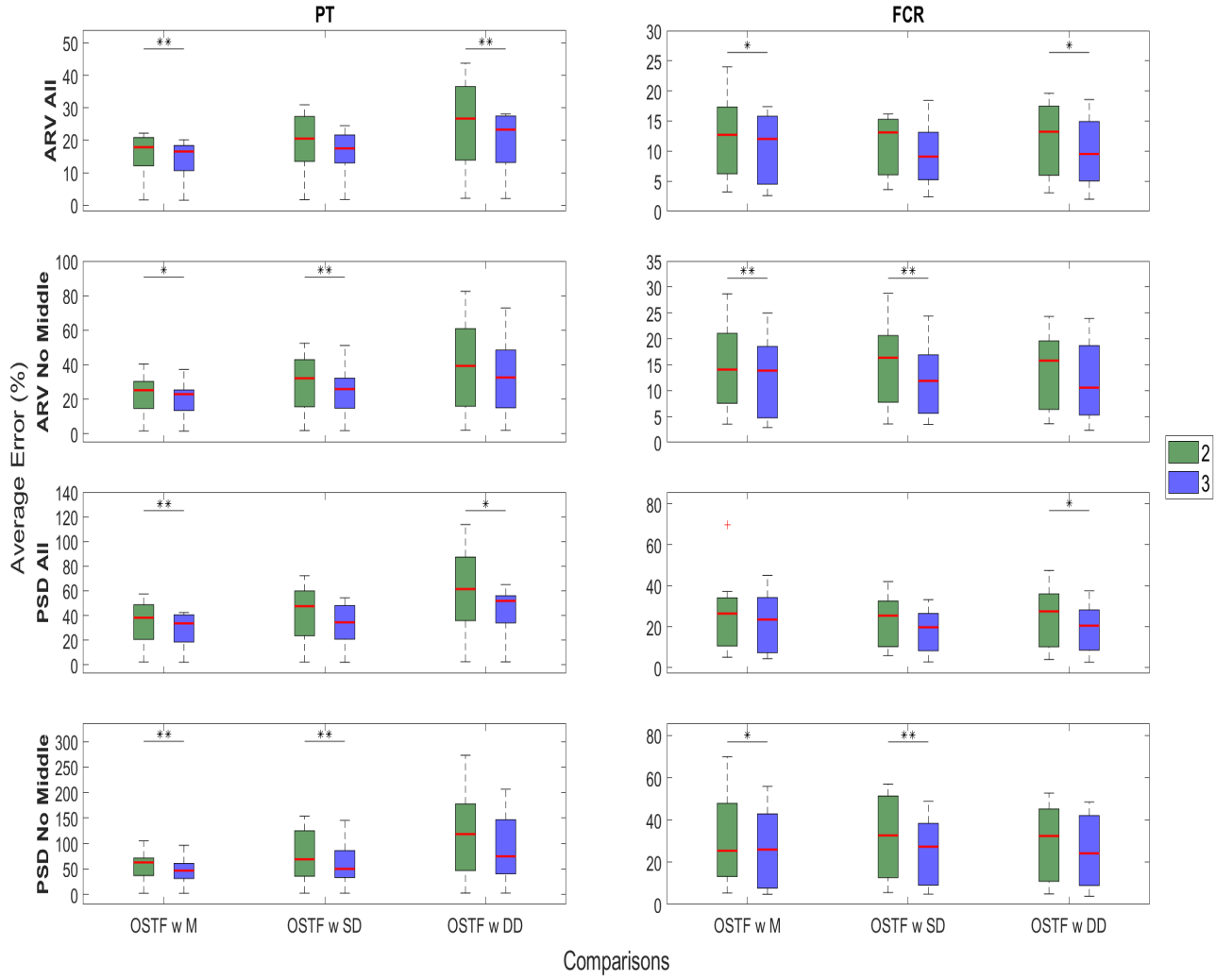

Figure A.6: *Paired comparison between distributions of average estimation errors obtained with OSTF using a different spatial dimension and same sources as input. Bigger electrodes has been simulated. (* $p < 0.05$, ** $p < 0.01$)*

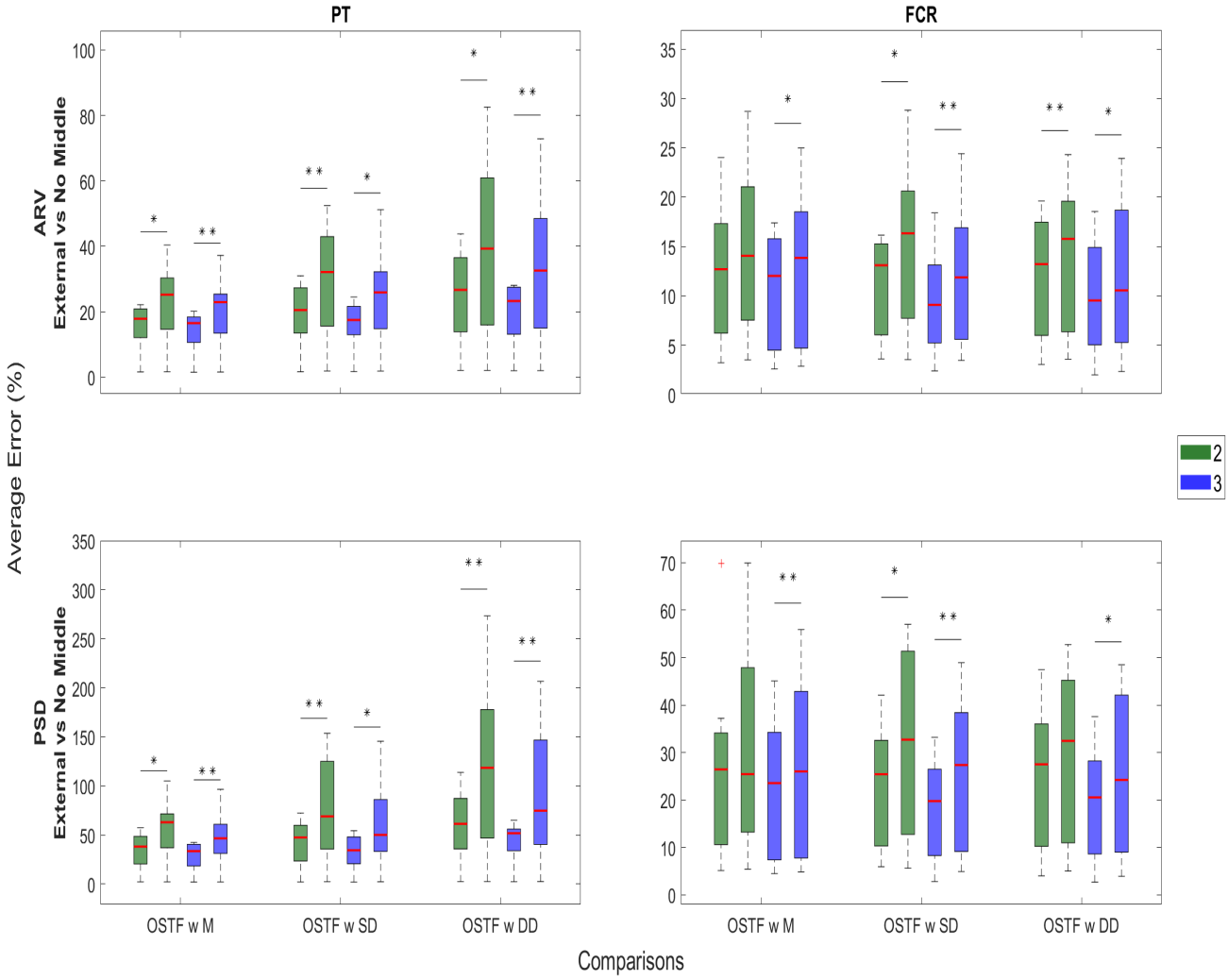

Figure A.7: *Paired comparison between distributions of average estimation errors obtained using two or three columns; different spatial dimensions has been taken into account too. Bigger electrodes has been simulated. (* $p < 0.05$, ** $p < 0.01$)*

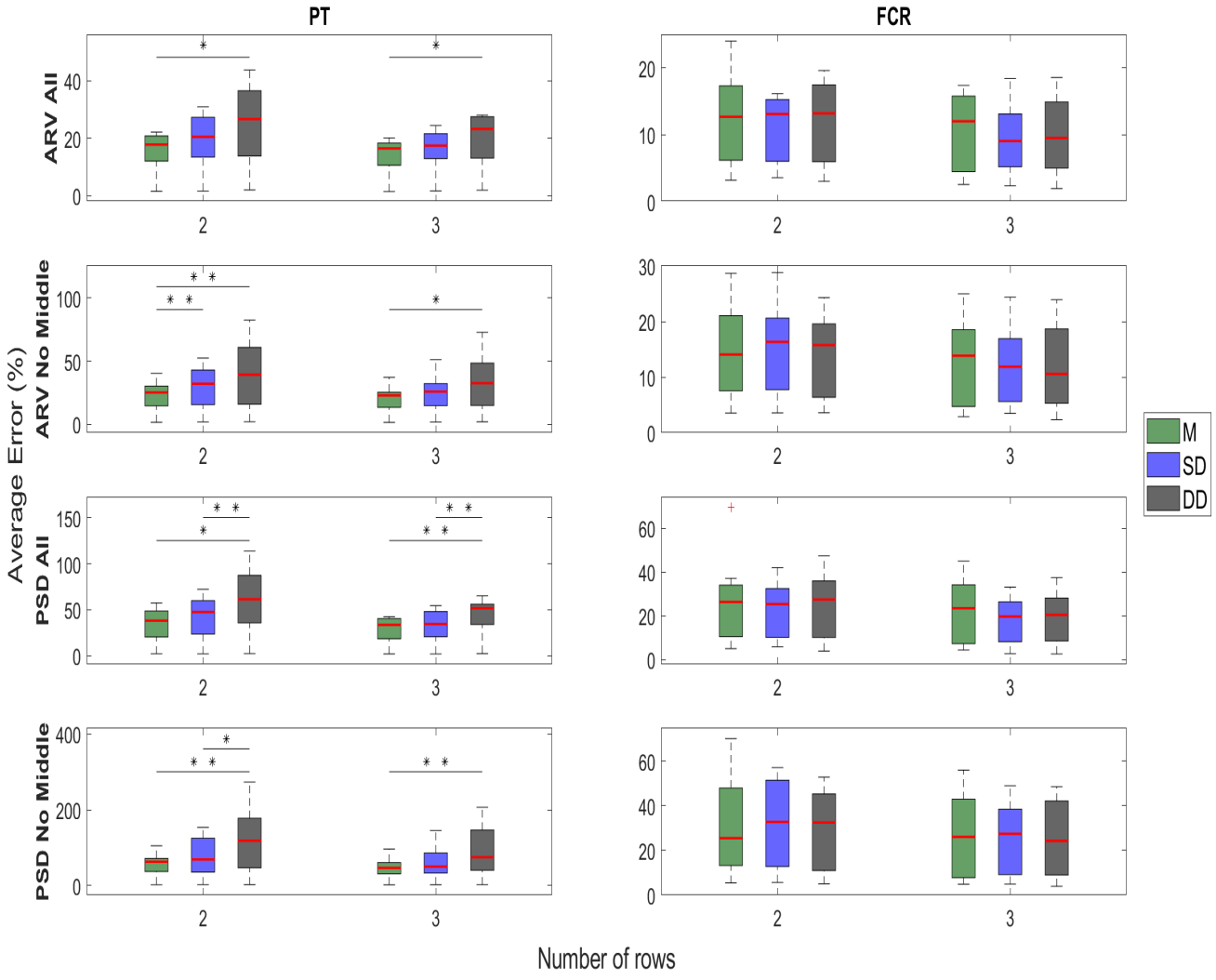

Figure A.8: *Paired comparison between distributions of average estimation errors obtained with OSTF using different sources. Bigger electrodes has been simulated. (* $p < 0.05$, ** $p < 0.01$)*

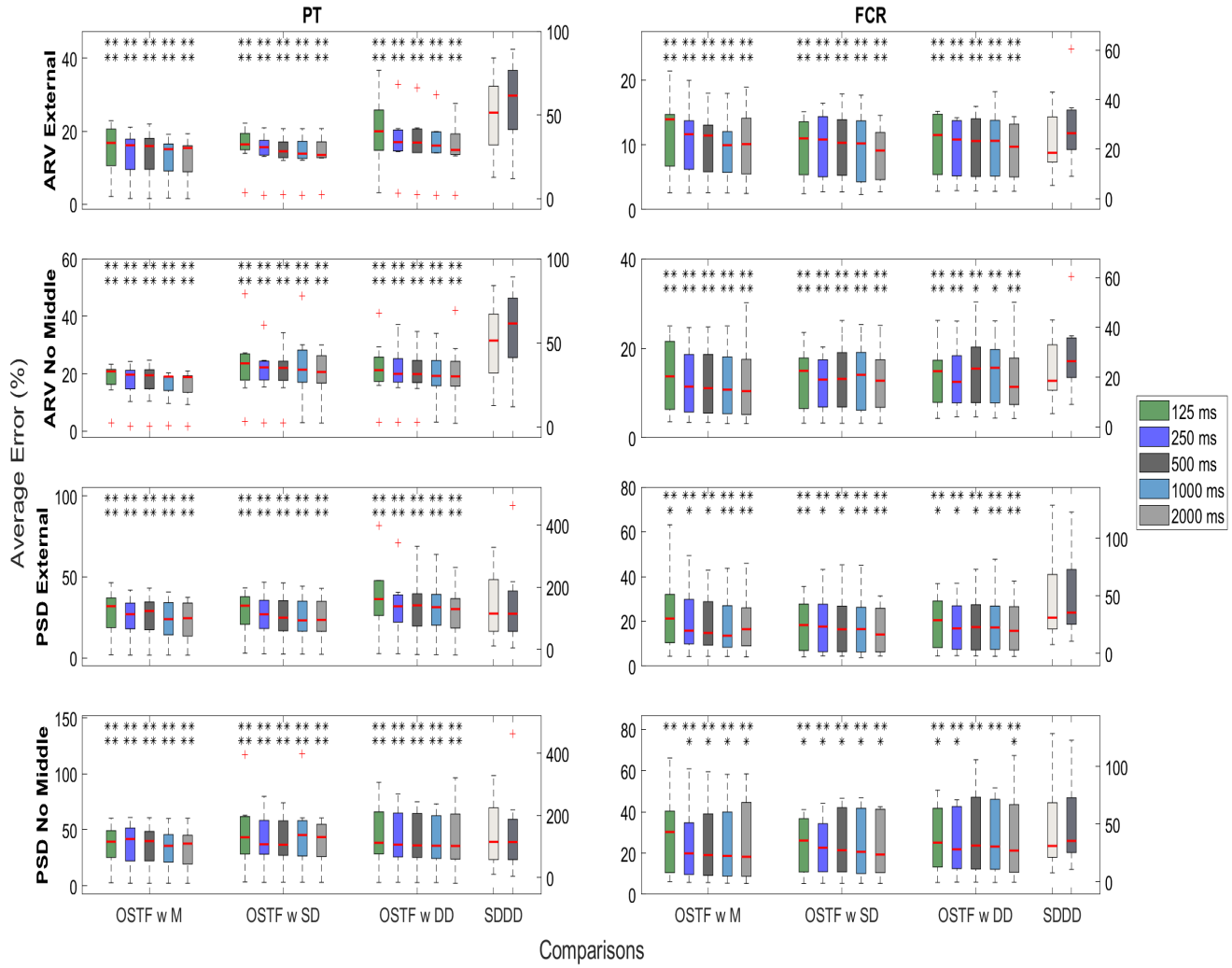

Figure A.9: *Paired comparison between distributions of average estimation errors obtained with OSTF trained through concatenated contractions of different temporal length and traditional spatial filters (SD and DD). The markers on boxplots identifies statistically significant differences with SD (bottom) and DD (top). (* $p < 0.05$, ** $p < 0.01$)*

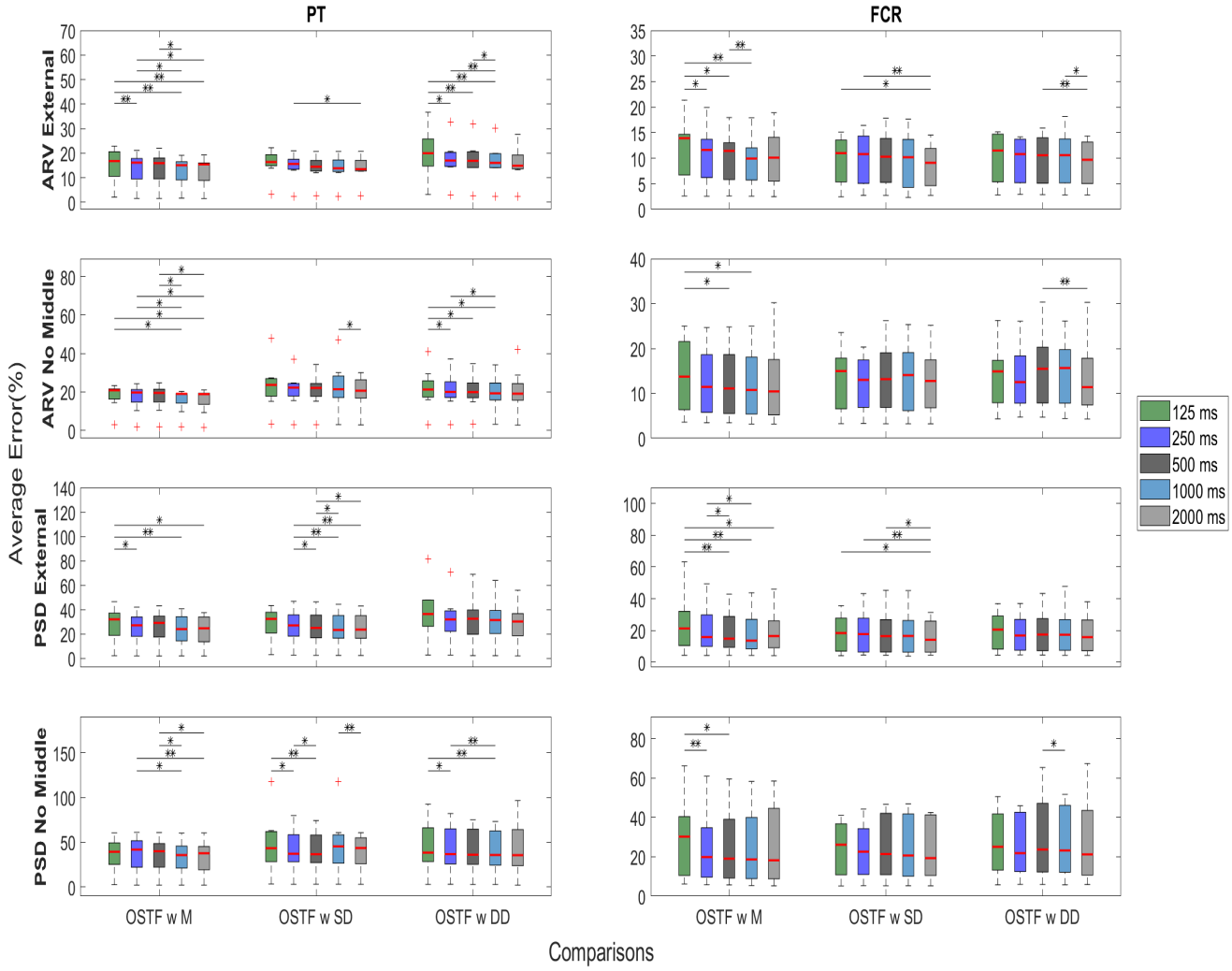

Figure A.10: *Paired comparison between distributions of average estimation errors obtained with OSTF trained through concatenated contractions of different temporal length and same sources as input. (* $p < 0.05$, ** $p < 0.01$)*

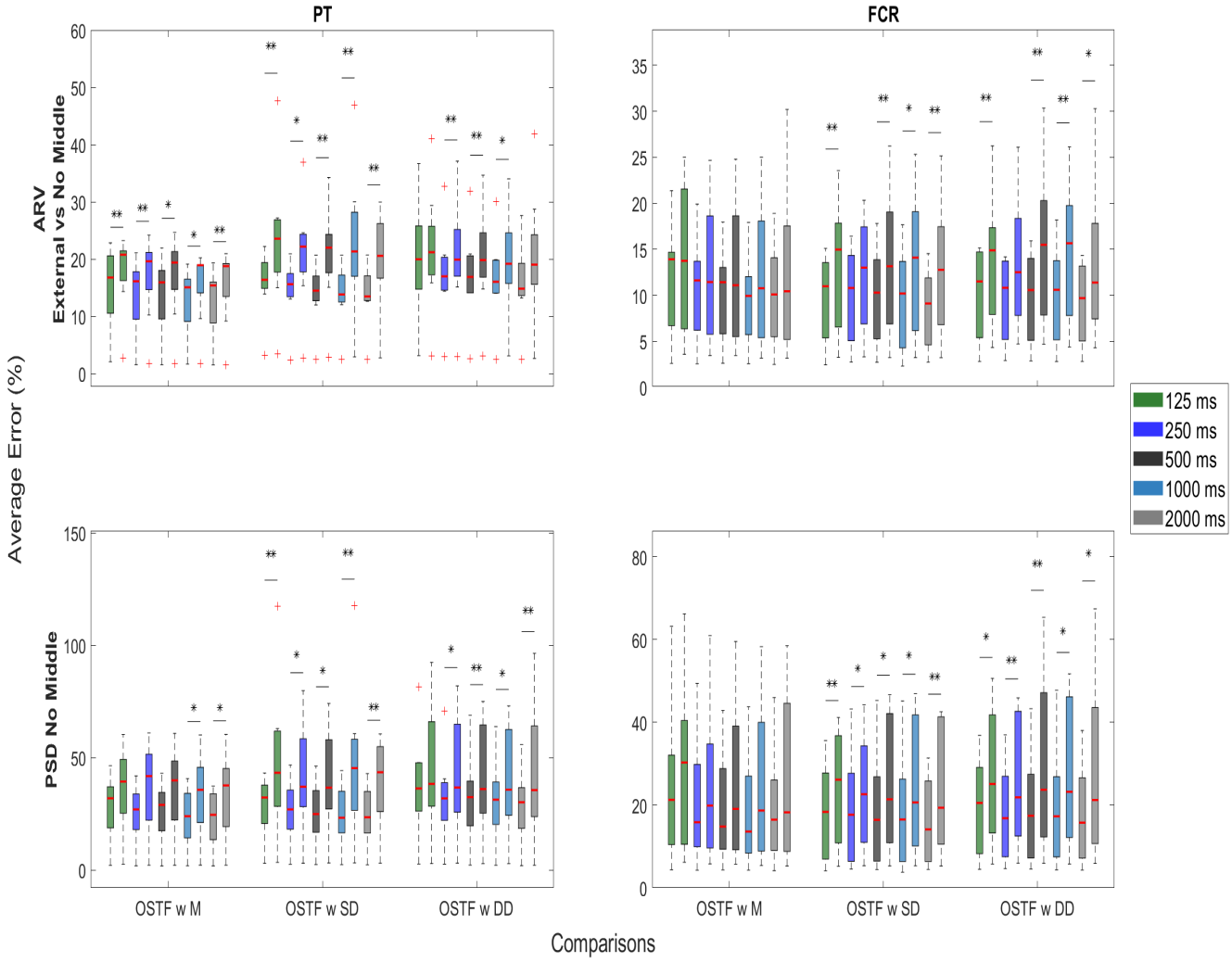

Figure A.11: *Paired comparison between distributions of average estimation errors obtained with two or three columns of electrodes both using OSTF trained through concatenated contractions of different temporal length. (* $p < 0.05$, ** $p < 0.01$)*

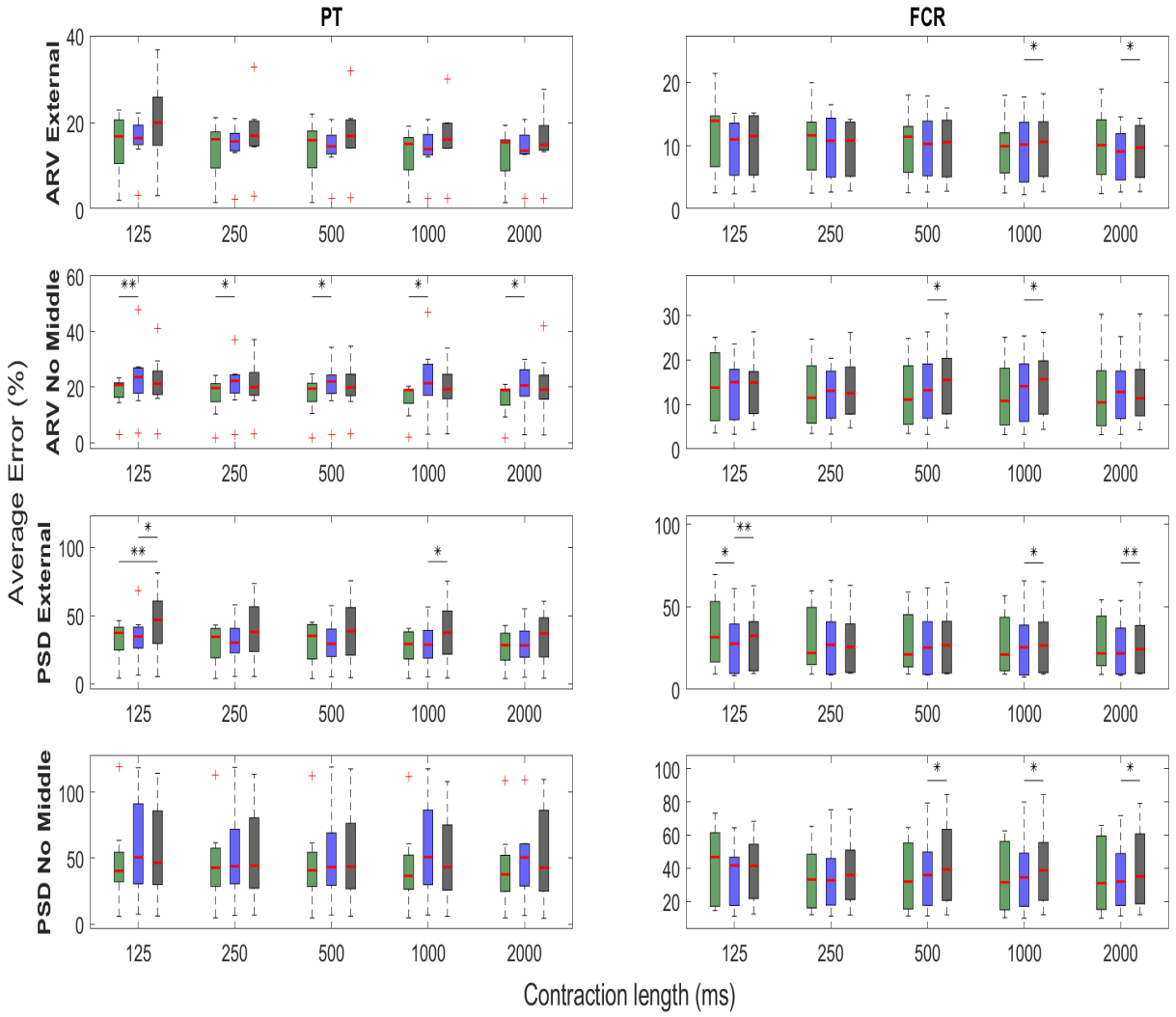

Figure A.12: *Paired comparison between distributions of average estimation errors obtained with OSTF using three different sources and trained through concatenated contractions of different temporal length. (* $p < 0.05$, ** $p < 0.01$)*

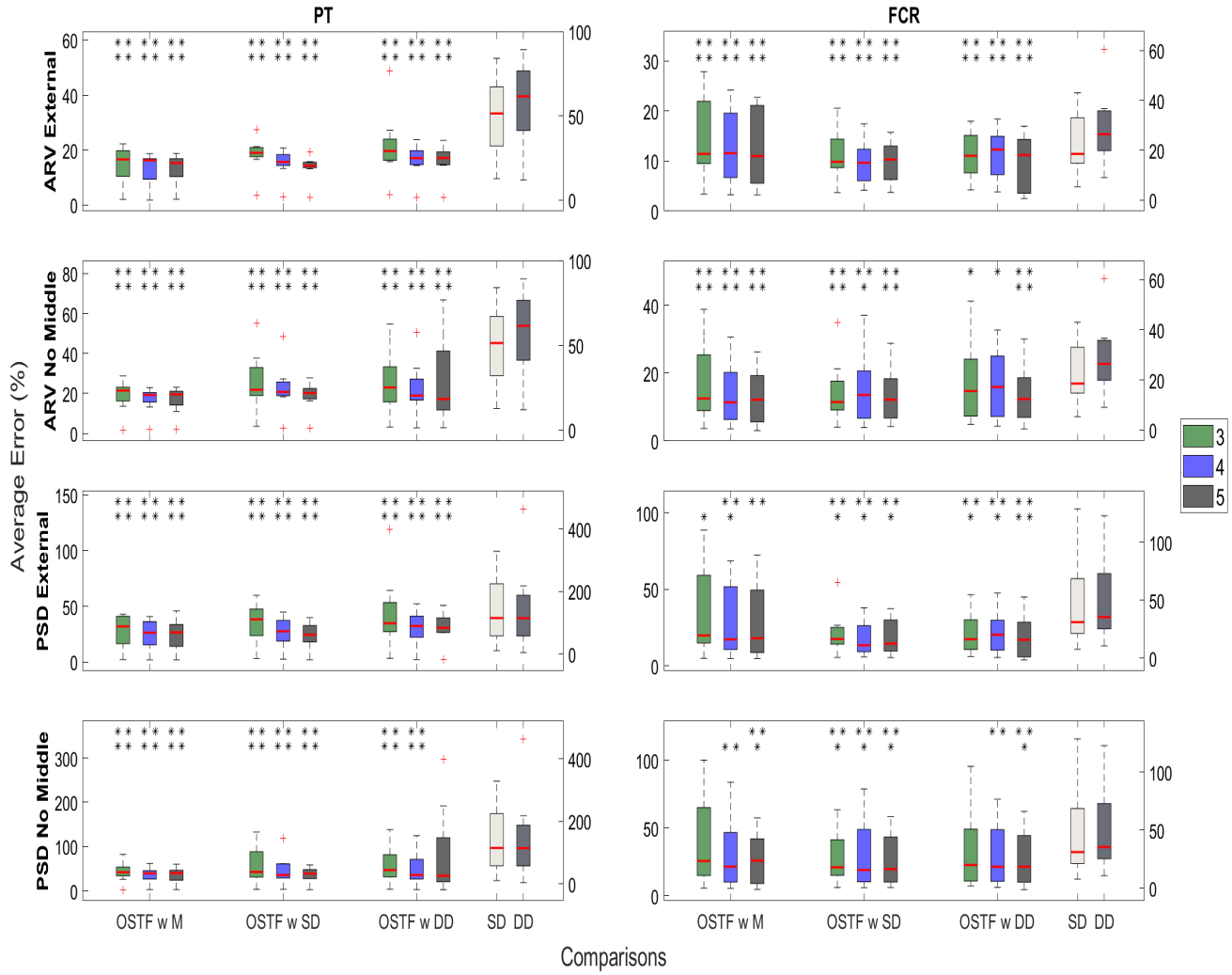

Figure A.13: *Paired comparison between distributions of average estimation errors obtained with OSTF (trained with two selective contractions) using a different spatial dimension and traditional filters (SD and DD). Training set is made up of only two selective contractions. The markers on boxplots identifies statistically significant differences with SD (bottom) and DD (top). (* $p < 0.05$, ** $p < 0.01$)*

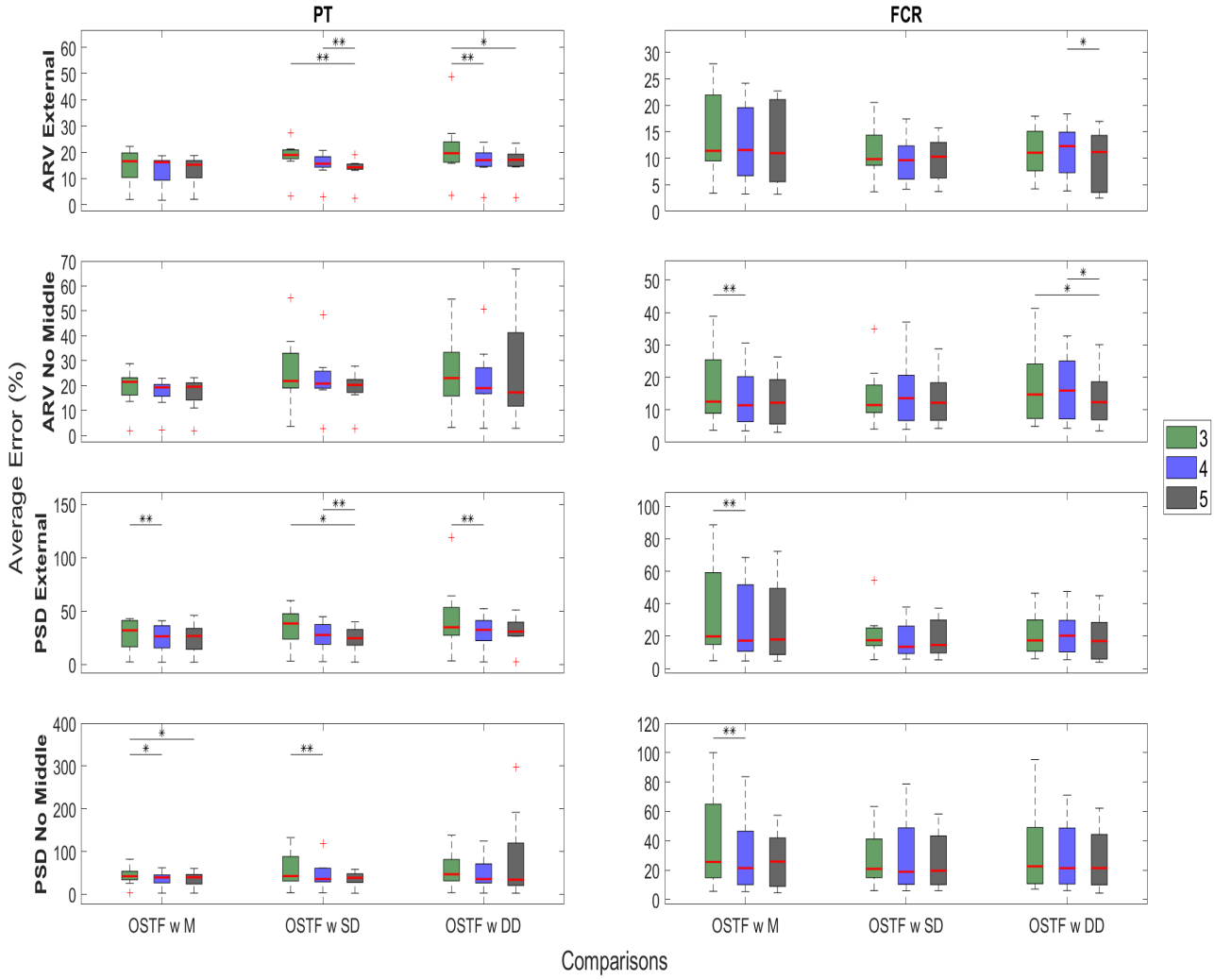

Figure A.14: *Paired comparison between distributions of average estimation errors obtained with OSTF (trained with two selective contractions) using a different spatial dimension and same sources as input. (* $p < 0.05$, ** $p < 0.01$)*

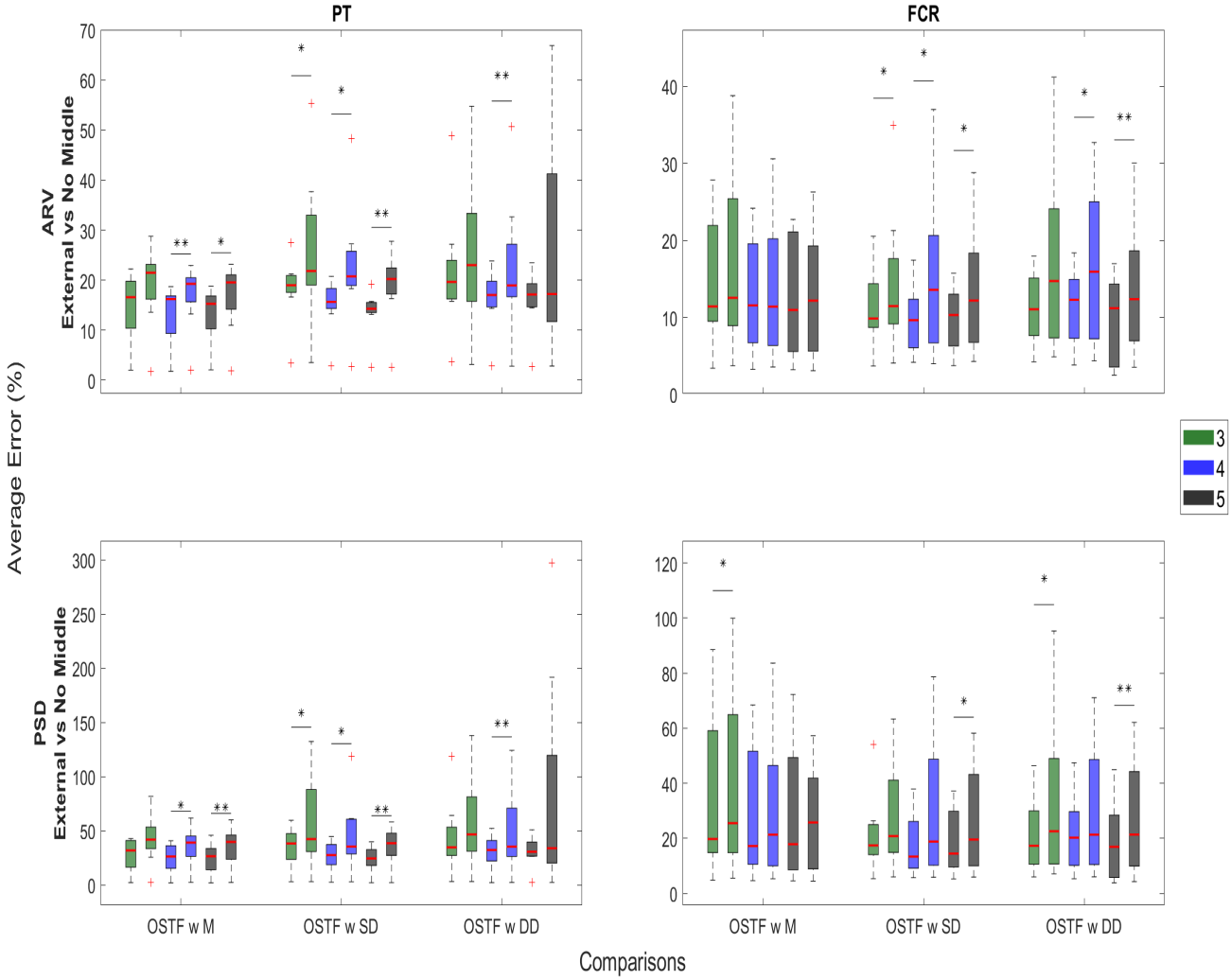

Figure A.15: *Paired comparison between distributions of average estimation errors obtained with OSTF (trained with two selective contractions) using two or three columns; different spatial dimensions has been taken into account too. (* $p < 0.05$, ** $p < 0.01$)*

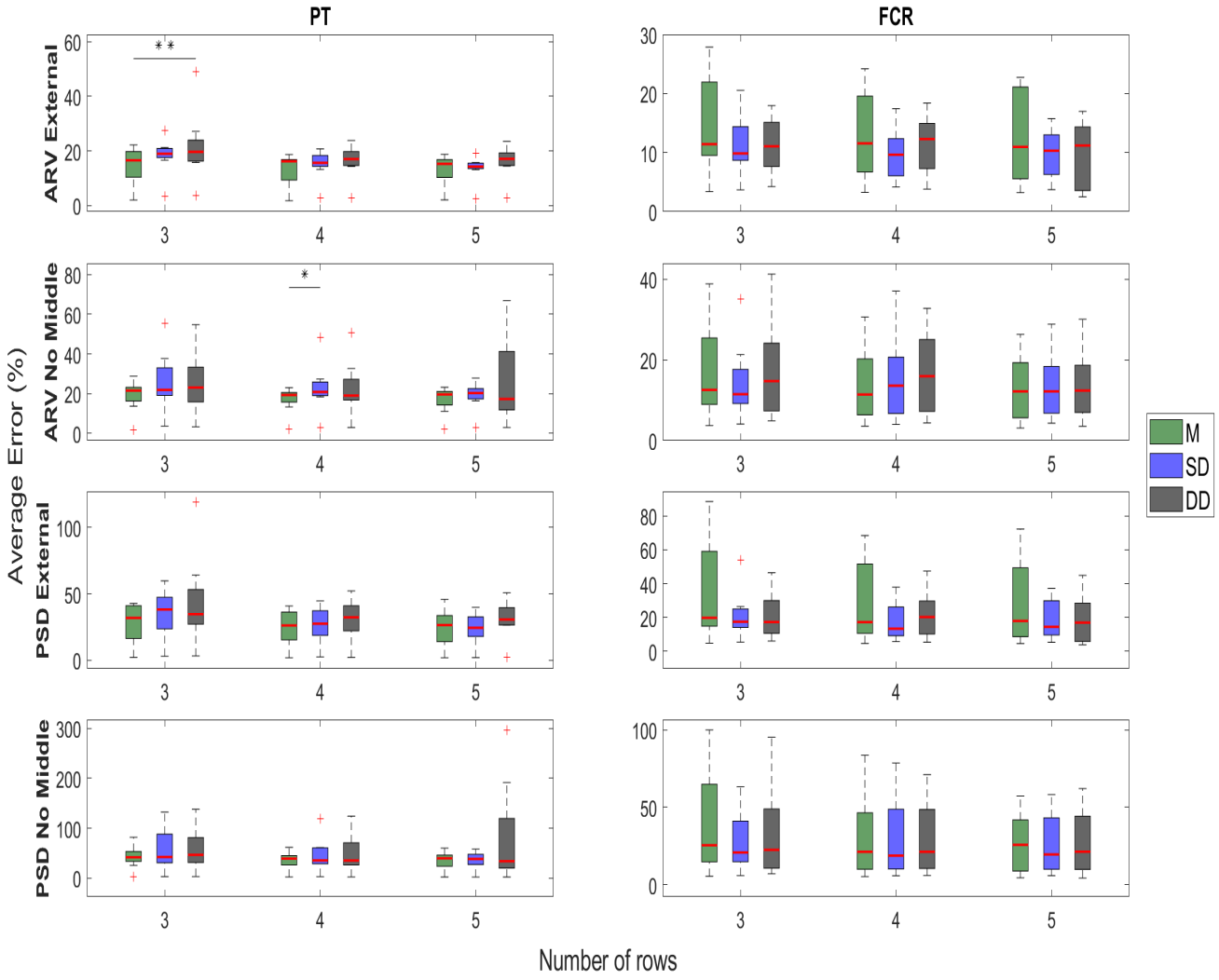

Figure A.16: *Paired comparison between distributions of average estimation errors obtained with OSTF (trained with two selective contractions) using different sources. (* $p < 0.05$, ** $p < 0.01$)*

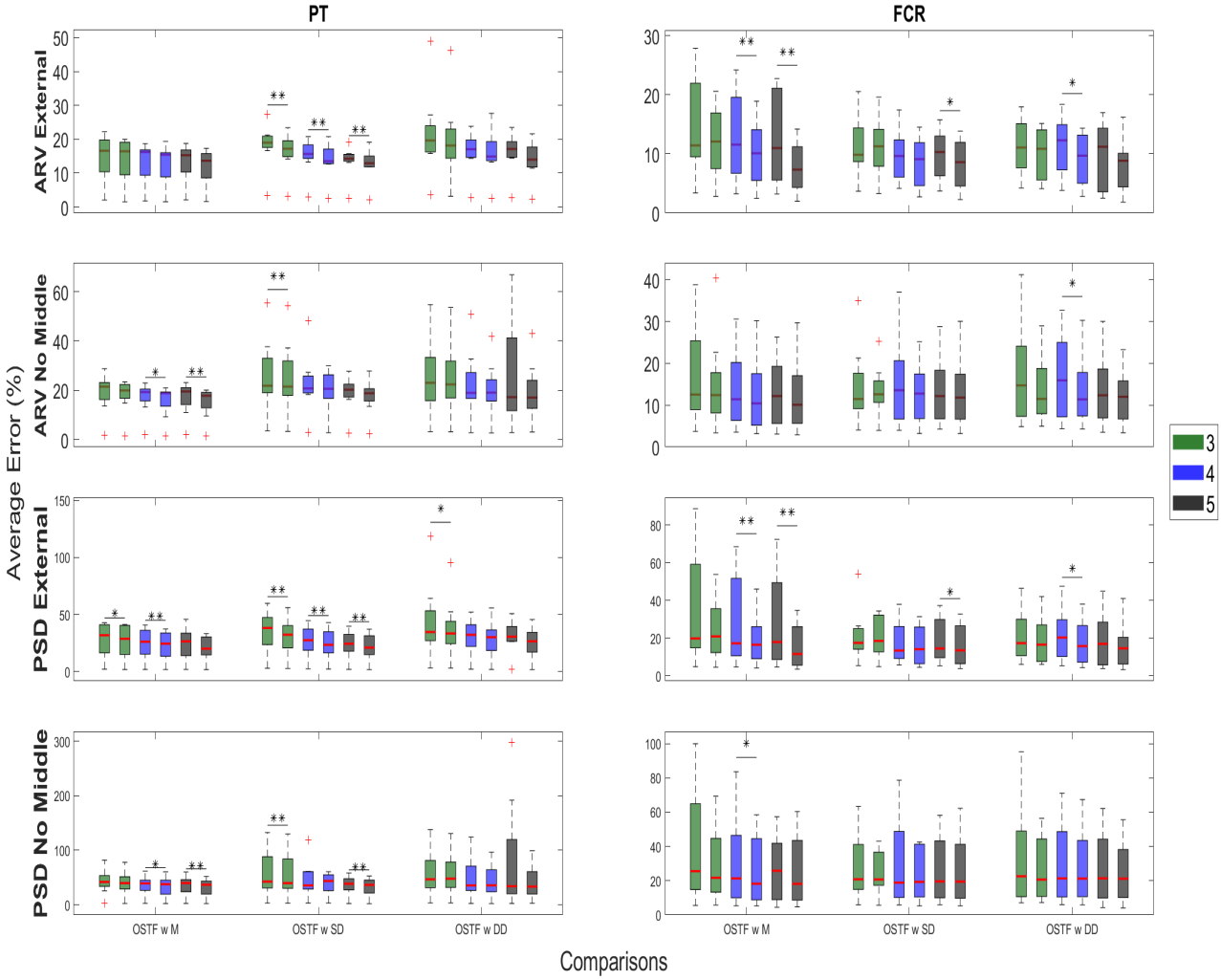

Figure A.17: *Paired comparison between distributions of average estimation errors obtained with OSTF trained through only two selective contractions and OSTF whose training is made up of multiple selective contractions. (* $p < 0.05$, ** $p < 0.01$)*

References

[1] Scalon V C. and Sanders T. *Essentials of Anatomy an Physiolog*, pages 138–47. F.A. DAVIDS COMPANY, 2007.

[2] Mesin L. *Neuromuscular System Engineering*, pages 2–9. IL MIO LIBRO, 2019.

[3] Makoto E. *Calcium-Induced Calcium Release in Skeletal Muscle*. Physiological Reviews, 89:1153–76, 2008.

[4] Henneman E, Somjen G, and Carpenter DO. *Functional significance of cell size in spinal motoneurons*. J Neurophysiol, 28:560–80, 1965.

[5] Merletti R and Parker PA. *Functional significance of cell size in spinal motoneurons*. IEEE Press Series in Biomedical Engineering, First ed. John Wiley Sons, Inc.,Hogoken, New Jersey, 2004.

[6] Fuglevand AJ, Winter DA, and Patla AE. *Models of recruitment and rate coding organization in motor-unit pools*. J Neurophysiol, 70(6):2470–88, 1993.

[7] Mesin L. *Neuromuscular System Engineering*, pages 10–11. IL MIO LIBRO, 2019.

[8] Plotkin D L, Roberts M D., Haun C T., and Schoenfeld B J. *Muscle Fiber Type Transitions with Exercise Training: Shifting Perspectives*. Sports, 9(9), 2021.

[9] Miller M S., Debold E P., and Toth M J. *Muscle Anatomy, Physiology, and Biochemistry*, chapter 5. Elsevier, 2021.

[10] Muscolino J E. *Kinesiology, The Skeletal System and Muscle Function*, pages 450–71. ELSEVIER, 2011.

[11] De Stefano A, Burridge JH, Yule VT, and Allen R. *Effect of gait cycle selection on EMG analysis during walking in adults and children with gait pathology*. Gait Posture, 20(1):92–101, 2004.

[12] Agostini V, Ghislieri M, Rosati S, Balestra G, and Knaflitz M. *Surface Electromyography Applied to Gait Analysis: How to Improve Its Impact in Clinics?* Front Neurol, 11:994, 2020.

[13] Mesin L. *Neuromuscular System Engineering*, pages 55–63. IL MIO LIBRO, 2019.

[14] Mesin L. *Neuromuscular System Engineering*, pages 76–83. IL MIO LIBRO, 2019.

[15] Mesin L. *Neuromuscular System Engineering*, pages 89–90. IL MIO LIBRO, 2019.

[16] Basmajian J and De Luca CJ. Muscle alive: Their function revelated by electromyography. *Williams and Wilkins*, 5th ed., 1985.

[17] De Luca CJ. Physiology and mathematics of myoelectric signals. *IEEE Trans. Biomed. Eng.*, 26:313–25, 1979.

[18] Van Boxtel A and Schomaker LR. Influence of motor unit firing statistics on the median frequency of the emg power spectrum. *Eur J Appl Physiol Occup Physiol*, 52(2):207–13, 1984.

[19] Le fever R and De Luca CJ. The contribution of individual motor units to the emg power spectrum. *in Oric. 29th Ann Conf. Eng. Med. Biol*, 1976.

[20] Mesin L. *Introduction to biomedical signal processing*, pages 72–78. IL MIO LIBRO, 2017.

[21] Mesin L. Separation of interference surface electromyogram into propagating and non-propagating components. *Biomedical Signal Processing and Control*, 52:238–47, 2019.

[22] Mesin L. *Neuromuscular System Engineering*, pages 110–25. IL MIO LIBRO, 2019.

[23] Lindstrom L and Magnusson R. Interpretation of myoelectric power spectra: A model and its applications. *Proc IEEE*, 65:653–62, 1977.

[24] Mesin L. *Crosstalk in surface electromyogram: literature review and some insights.* Phys Eng Sci Med, 43(2):481–92, 2020.

[25] Mesin L. *Optimal spatio-temporal filter for the reduction of crosstalk in surface electromyogram.* J Neural Eng, 15(1), 2018.

[26] Jiang N, Englehart KB, and Parker PA. *Extracting simultaneous and proportional neural control information for multiple-DOF prostheses from the surface electromyographic signal.* IEEE Trans Biomed Eng., 56(4):1070–80, 2009.

[27] Mesin L. *Neuromuscular System Engineering*, pages 63–73. IL MIO LIBRO, 2019.

[28] Farina D, C Févotte, C Doncarli, and Merletti R. *Blind separation of linear instantaneous mixtures of nonstationary surface myoelectric signals.* IEEE Trans Biomed Eng, 51:1555–67, 2004.

[29] Fletcher R. *Practical Methods of Optimization, Second Edition.* John Wiley and Sons, 2000.

[30] Arduino. Uno rev3. https://store.arduino.cc/products/arduino-uno-rev3, 2022.

[31] MATLAB. *version 9.8.0 (R2020a).* The MathWorks Inc., Natick, Massachusetts, 2022.

[32] Giacoboni N. Basic custom arduino library for hx711. http://www.mathworks.com/matlabcentral/fileexchange/66641-basic-custom-arduino-library-for-hx711, 2022.

[33] Merriam-Webster. Statistics, 2022. https://www.merriam-webster.com/dictionary/statistics.

[34] Iliya Valchanov. What is a distribution in statistics?, 2017. https://365datascience.com/tutorials/statistics-tutorials/distribution-in-statistics.

[35] Mesin L. *Introduction to biomedical signal processing*, pages 170–71. IL MIO LIBRO, 2017.

[36] Mesin L. *Introduction to biomedical signal processing*, pages 178–80. IL MIO LIBRO, 2017.

[37] Pereira C and Wechsler S. On the concept of p -value. *Brazilian Journal of Probability and Statistics*, 7:159–77, 12 1993.

[38] Mesin L. *Introduction to biomedical signal processing*, pages 181–85. IL MIO LIBRO, 2017.

[39] Uchechi H and Akwiwu E. Parametric and nonparametric statistics. *Sokoto Journal of Medical Laboratory Science*, 4:5–15, 07 2019.

[40] Kruskal W H and Wallis W A. Use of ranks in one-criterion variance analysis. *Journal of the American Statistical Association*, 47(260):583–621, 1952.

[41] Corder G.W. and Foreman D.I. *Nonparametric statistics: A Step-by-Step Approach*, pages 117–20. Wiley, 2014.

[42] https://it.mathworks.com/help/stats/kruskalwallis.html.

[43] Corder G.W. and Foreman D.I. *Nonparametric statistics: A Step-by-Step Approach*, pages 40–41. Wiley, 2014.